

Rice University

**Marine Gas Hydrate: response to change of seafloor
temperature, ocean sulfate concentration, and
compositional effect**

by
Guangsheng GU

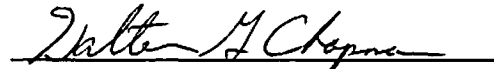
A THESIS SUBMITTED
IN PARTIAL FULFILLMENT OF
THE REQUIREMENTS FOR THE DEGREE

Doctor of Philosophy

Approved, THESIS COMMITTEE:



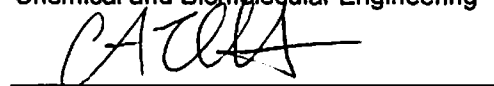
George J. Hirasaki, Chair
A. J. Hartsook Professor in
Chemical and Biomolecular Engineering



Walter G. Chapman, co-chair
William W. Akers Professor in
Chemical and Biomolecular Engineering



Sibani Lisa Biswal,
Associate Professor in
Chemical and Biomolecular Engineering



Colin A. Zelt,
Professor in Earth Science

HOUSTON, TX
October 2013

Abstract

The global inventory of carbon in gas hydrate at present day is comparable to that in oil & coal reserve, therefore, gas hydrate could have played an important role in earth carbon cycle, e.g., during the Paleocene Eocene Thermal Maximum (PETM) event. However, ocean floor temperatures were ~6°C higher than today, so the hydrate abundance under warmer conditions was a question to be clarified. By using numeric simulations, this work showed that gas hydrate abundance is not only affected by ocean floor temperature, but, more essentially, greatly dominated by the organic carbon buried into sediment. During PETM, higher organic carbon contents due to less dissolved oxygen at seafloor and increased methanogenesis rates, both resulted from higher ocean temperatures, enhanced hydrate accumulation. Therefore, though hydrate stability zone would be thinner and shallower than present-day, depending on water depth and sedimentation rate, gas hydrate abundance could be still higher in some marine sediment columns than present-day value. The quantity of carbon stored in marine gas hydrates during PETM may have been similar to that of present-day.

The ocean sulfate concentration is as another factor affecting hydrate abundance. From seafloor to sulfate-methane transition (SMT) zone, sulfate consumes a certain portion of organic carbon. Via numerical models, this work proposed and demonstrated that the organic carbon remaining at SMT,

should be regarded as the real organic carbon content available for methanogenesis, which contributes to gas hydrate inventory. This work also revealed that lower ocean sulfate is favorable for higher gas hydrate inventory because it consumes less organic carbon in a shallow zone of sediment from seafloor to SMT.

By using an example mixed gas system, this work showed that a transition zone which contains both solid hydrates and free gas can span over a thick zone (~300m). The gradual change of seismic impedance across the transition zone diminishes the strength of the Bottom Simulating Reflector (BSR). The results provide a possible mechanism for enigmatic weak-to-absent BSR in prolific hydrocarbon basins across the world.

Key words: gas hydrate, numeric simulation, Paleocene Eocene Thermal Maximum (PETM), partial differential equation (PDE), seismic response, digital signal processing, methane, thermodynamics, multi-phase flow

Acknowledgement

I would like to gratefully thank my advisor Dr. George J. Hirasaki. His guidance, broad knowledge, and generous financial support, made the completion of my thesis possible. I am grateful for my co-advisor Dr. Walter G. Chapman for his time, effort, and deep knowledge which support my thesis work, most importantly for his patience on discussion with me when I had difficulties in research.

Thank Dr. Colin Zelt for serving in my committee, and for helping me on geophysical exploration especially on seismology which is very important for my research. His favorite support on my project helped me a lot on my work.

I would like to thank Dr. Gerald Dickens for fruitful discussions on marine hydrate systems and geochemistry. His great ideas and intuition always excited me, and helped me on complex situations.

Thank Dr. Sibani Lisa Biswal for serving in my committee, and provided valuable inputs and comments on thesis and defense.

Thank Dr. Bandan Dugan, Dr. Gaurav Bhatnagar, Dr. Sayantan Chatterjee, Dr. Priyank Jaiswal, Dr. Hugh Daigle, Dr. Frederick S Colwell and colleagues for fruitful discussions. I appreciate many other faculties, staffs, colleagues, and friends in the department and throughout Rice University, for their favorable and valuable help.

I gratefully thank my family, my late parents, my sisters and brother, and my wife for their favorable support. Especially thank my wife's support under hard time both for me and for her.

Guangsheng GU

List of Illustrations

Figure 1. 1 Methane Hydrate: molecular structure and sample.....	1
Figure 1. 2. Existence of Natural Methane Hydrate from analysis of phase diagram: both in permafrost location and in marine sediments.	2
Figure 1. 3. Discovered presence of Gas Hydrate around the world.....	2
Figure 1. 4. Natural Hydrate Amount (left pyramid), Comparing to Conventional Natural Gas Resource for USA (right pyramid).....	4
Figure 2. 1. Paleocene Eocene Thermal Maximum (PETM, previously called Late Paleocene Thermal Maximum, LPTM) Event. (Zachos, 2001).....	7
Figure 2. 2. Isotope Compositions of Some Materials	8
Figure 2. 3. Schematic figure of isotopic ratio change in ocean DIC of the PETM event	8
Figure 2. 4. Required amount of carbon for PETM excursion event (revised from Jones et al., 2012). The only possible option to meet the amount required is the carbon from biogenic methane.	10
Figure 2. 5. Hypothesis: dissociation of large amount of hydrate caused PETM $\delta^{13}\text{C}$ negative shift (Revised from G. Dickens, 2003).....	11
Figure 2. 6. The changes caused by seafloor temperature increase.	12
Figure 2. 7. 1-D scenario of methane hydrate accumulation in marine sediments. (Revised from Bhatnagar, 2007).	13
Figure 2. 8. Reactions about organic carbon, sulfate, and methane, from ocean bottom to deep sediment. SRZ: sulfate reduction zone; SMT: sulfate / methane transition zone.	14
Figure 4.1. 1. Microbe Metabolic Rate Constant.....	27
Figure 4.1. 2. Reaction Rate Constant Model applied in this work. The vertical axis is $\lambda(T)/\lambda(\bar{T})$, where \bar{T} is average temperature in GHSZ.	28
Figure 4.2. 1. Schematic representation of the global thermohaline circulation. Surface currents are shown in red, deep waters in light blue and bottom waters in dark blue. The main deep water formation sites are shown in orange. (Rahmstorf, 2006).	29
Figure 4.2. 2. Oxygen Solubility in Sea Surface, under 1 atm.....	30
Figure 4.2. 3. Present oxygen concentration in 2.0 km deep ocean.	31
Figure 4.2. 4. Contour plot for seafloor organic concentration α_0	32
Figure 4.2. 5. Change of α_0 , $D_{sf}=1.0$ km.....	33
Figure 4.2. 6. Change of α_0 , $D_{sf}=2.0$ km.....	34
Figure 4.2. 7. Change of α_0 , $D_{sf}=3.0$ km.....	34

Figure 4.3. 1. Temperature Profile beneath Seafloor.	37
Figure 4.3. 2. Porosity Profile beneath Seafloor.	38
Figure 4.3.1. 1. In-situ Reaction Rate Constant Profile.....	39
Figure 4.3.1. 2. Hydrate Volume Fraction Profile.	40
Figure 4.3.1. 3 Total Hydrate Amount (per unit seafloor area) vs Seafloor Temperature.	41
Figure 4.3.1. 4 Average Sh and Average Volume Fraction vs Seafloor Temperature.	42
Figure 4.3.1. 5 Normalized Organic Concentration Profile.	43
Figure 4.3.1. 6 Hydrate Saturation Profile.....	44
Figure 4.3.1. 7 Gas Phase Saturation Profile.	45
Figure 4.3.1. 8 Normalized Methane Concentration in Pore Water Profile, and Normalized Methane Solubility Profile.	46
Figure 4.3.1. 9 In-situ Methane Production Rate Profile.....	47
Figure 4.4. 1 Contour Plot for $k = V_{h,9C} / V_{h,3C}$	63
Figure 4.4. 2 Contour Plot for $k = V_{h,9C} / V_{h,3C}$	64
Figure 4.4. 3 Contour Plot for $k = V_{h,9C} / V_{h,3C} \cdot D_{sf} = 1.0$ km.....	66
Figure 4.4. 4 Contour Plot for $k = V_{h,9C} / V_{h,3C} \cdot D_{sf} = 2.0$ km.....	68
Figure 4.4. 5 Contour Plot for $k = V_{h,9C} / V_{h,3C} \cdot D_{sf} = 3.0$ km.....	70
Figure 5. 1 (a). Schematic figure of sulfate and methane hydrate system (b). Schematic profiles of sulfate, POC, and methane concentrations in methane hydrate system. Left: normalized depth $0 < \tilde{z} < 2$; Right: zoomed in. Normalized depth $\tilde{z} = z/L_t$, $L_t = 450$ mbsf for Blake Ridge. Blue curve: POC (α); Red curve: $[SO_4]^{2-}$; Green curve: $[CH_4]$; dotted black curve: CH_4 solubility. $\alpha_{0, meth}$ --- the organic carbon content available for methanogenesis; α_{SMT} --- the organic carbon content at bottom of SMT. At low $DaPOC$, $\alpha_{0, meth} \approx 1$	75
Figure 5. 2 Record of Ocean Sulfate Concentration.....	76
Figure 5. 3 Interaction of sulfate with POC and methane at high $DaPOC$	78
Figure 5. 4 Base case: Blake Ridge, site 997.....	84
Figure 5. 5 Base case: Blake Ridge, site 997 (zoomed in).....	85
Figure 5. 6. Transient Processes, $DaPOC = 30$, $C_{s, crit} = 0.1$ mM is shown as a black	

dash line in $[\text{SO}_4]^{2-}$ profile. (from $\tilde{t} = 0.2$ to steady state).....	86
Figure 5. 7. Effect of Da_{POC} (zoomed in). “POC” means the region for POC reaction.	
The black horizontal dash line is refers to the bottom of SMT zone.....	90
Figure 5. 80. Effect of Pe_7/Da (ratio of sedimentation flux / methane production rate)	
.....	91
Figure 5. 9. Effect of Da_{AOM} (indicator of reaction rate between sulfate and methane)	
.....	92
Figure 5. 10. Effect of Da_{AOM} (zoomed in).....	93
Figure 5. 11. Effect of Organic Carbon Content at Seafloor (β).....	94
Figure 5. 12. Effect of Ocean Sulfate Concentration (C_{so}), at steady state, with $Da_{\text{POC}} = 30$ (standard value).....	96
Figure 5. 13. Effect of Ocean Sulfate Concentration (C_{so}), at steady state, with $Da_{\text{POC}} = 30$ (standard value). zoomed in. “POC” means the region for POC reaction..	97
Figure 5. 146. Effect of Ocean Sulfate Concentration (C_{so}), with $Da_{\text{POC}} = 3000$ (high value).....	98
Figure 5. 1915. Effect of Ocean Sulfate Concentration (C_{so}), with $Da_{\text{POC}} = 30$ (standard value), $C_{\text{s,crit}} = 0.1$ mM.....	102
Figure 5. 160. Effect of Ocean Sulfate Concentration (C_{so}), with $Da_{\text{POC}} = 30$ (standard value), $C_{\text{s,crit}}=1$ mM.	103
Figure 5. 171 Effect of Ocean Sulfate Concentration (C_{so}), with $Da_{\text{POC}} = 30$ (standard value), $C_{\text{s,crit}}=10$ mM.....	104
Figure 6. 1. The Incipient Hydrate Formation Pressure of a $\text{CH}_4\text{-C}_3\text{H}_8\text{-H}_2\text{O}$ System. Data were obtained using CSM Gem v1.0, showing the equilibrium conditions at which hydrate starts to form. C_3 fraction: water-free molar fraction of C_3H_8 , $x_{\text{C}_3\text{H}_8}^{\text{wf}}$. Black dot curve: seafloor. Black dash-dot curve: geotherm. Red dash curve: sl hydrate equilibrium condition; Solid curves: sll hydrate equilibrium conditions at different values of $x_{\text{C}_3\text{H}_8}^{\text{wf}}$. L_{10} , L_{t1} , L_{t5} : thicknesses of GHSZ at $x_{\text{C}_3\text{H}_8}^{\text{wf}} = 0, 0.01, 0.05$, respectively. Seafloor temperature $T_{\text{sf}} = 276.15$ K, seafloor pressure $P_{\text{sf}}=5.0$ MPa, and geothermal gradient $G= 0.04$ K/m.	113
Figure 6. 2. Phase Diagram and Sediment Zones in a $\text{CH}_4\text{-C}_3\text{H}_8\text{-H}_2\text{O}$ System, assuming $x_{\text{C}_3\text{H}_8}^{\text{wf}} = 0.05$ everywhere. Black dot curve: seafloor. Black dash-dot curve: geotherm. Red dash curve: sl hydrate equilibrium condition; Red solid curve: sll hydrate equilibrium condition at $x_{\text{C}_3\text{H}_8}^{\text{wf}} = 0.05$. Region A, B, C: phase regions. Zone A, B, C: zones in sediment according to corresponding phase regions. M_1, M_2, M_3, M_4 : point of interest for different zones in sediment. $T_{\text{sf}}, P_{\text{sf}}$, and G are same with Figure 6.1.....	115
Figure 6. 3. Saturation Profiles of an example of the $\text{CH}_4\text{-C}_3\text{H}_8\text{-H}_2\text{O}$ System.	

Conditions: water-free propane molar fraction is 0.05 and overall composition is the same everywhere: $x_{CH_4}=0.019$, $x_{C_3H_8}=0.001$, $x_{H_2O}=0.98$; T_{sf} , P_{sf} , and G are same with Figure 6.1. Assume: The overall composition is the same in the spatial domain. There are 3 zones of sediments in the domain. Zone A: $Aq + Hydrate (=sl + sll)$; Zone B: $Aq + sll + V$; Zone C: $Aq + V$. Dash-dot line N_1N_2 and N_3N_4 , are boundaries for $S_g=0$ and $S_h=0$ in the sediment, respectively. Red solid curve and blue solid curve are saturation profiles for All Hydrate ($=sl + sll$), and for Vapor, respectively. Pressure is marked on the right side. 116

Figure 6. 4. Profiles of normalized acoustic properties in an example $CH_4-C_3H_8-H_2O$ System. Conditions are the same as Figure 6.3. Impedance $Z = \rho V_p$. Data are normalized so that those at seafloor are 1. L_{tran} : the thickness of the whole transition zone in which hydrate and gas phase coexist. L_{STZ} : the thickness of the significant transition zone in which 99% of impedance variation from top of the transition zone has been achieved. 118

Figure 6. 5. Impulse response of a step change V_p system (BSR)..... 120

Figure 6. 6. Impulse Response of a system with a transition zone 121

Figure 6. 7. A sample Ricker wavelet, $f_{peak}=30$ Hz 122

Figure 6. 8. Seismic Response from Step BSR and Gradual Transition Zone..... 123

Figure 6. 9. Amplitude Ratio as a Function of L_{stz}/λ 124

Table of Contents

MARINE GAS HYDRATE: RESPONSE TO CHANGE OF SEAFLOOR TEMPERATURE, OCEAN SULFATE CONCENTRATION, AND COMPOSITIONAL EFFECT	I
ABSTRACT	II
ACKNOWLEDGEMENT	IV
LIST OF ILLUSTRATIONS	V
TABLE OF CONTENTS.....	IX
CHAPTER 1. INTRODUCTION TO METHANE HYDRATE	1
AND THESIS FRAME	1
1.1. <i>Methane hydrate and its existence in natural environments.....</i>	<i>1</i>
CHAPTER 2. PETM EVENT AND ROLE OF MARINE METHANE HYDRATE.....	6
2.1. <i>PETM Event</i>	<i>6</i>
2.2. <i>Hypothesis of methane hydrate as the candidate for PETM $\delta^{13}C$ event and the challenge for this hypothesis.....</i>	<i>11</i>
2.3. <i>Typical 1-D scenario of methane hydrate accumulation in marine sediments.....</i>	<i>13</i>
2.4. <i>Possible solutions for abundant hydrate inventory before PETM.....</i>	<i>14</i>
CHAPTER 3. NUMERICAL MODEL ABOUT HYDRATE INVENTORY DUE TO HIGHER ORGANIC CARBON INPUT AND REACTION RATE CONSTANT	15
3.1. ASSUMPTIONS	15
3.2. NUMERICAL MODEL.....	16
3.3. DESCRIPTION ON EFFECTS OF T_{SF} INCREASE	22
3.4. CASES AND SCENERIES TO BE STUDIED.....	22
CHAPTER 4. HYDRATE INVENTORY DUE TO LOW OCEAN OXYGEN CONCENTRATION AND HIGH REACTION RATE CONSTANT	26
4.1. CHANGE OF REACTION RATE CONSTANT.....	26
4.2. CHANGE OF SEAFLOOR ORGANIC CONCENTRATION α_0	28
4.3. HYDRATE PROFILE CHANGE, SEAFLOOR DEPTH $D_{SF} = 2.0$ KM.....	35
4.4. CONTOUR PLOTS FOR REMAINING RATIO OF TOTAL HYDRATE AMOUNT K	62
4.5. CONCLUSIONS	72
CHAPTER 5: OCEAN SULFATE AS A FACTOR AFFECTING ORGANIC CARBON AND ITS INTERACTION WITH METHANE AND HYDRATE.....	74
5. 1. INTRODUCTION	74
5.2. GENERIC REACTIONS AND MODEL	78
5.3. MATHEMATIC MODEL: COMPONENT MASS BALANCES.....	79
5.4. BASE CASE: BLAKE RIDGE	84
5.5. TRANSIENT PROCESSES	85
5.6. STEADY STATE RESULTS DEPENDING ON SEVERAL IMPORTANT PARAMETERS	88

5.7. EFFECT OF OCEAN SULFATE CONCENTRATION (C_{s0})	95
5.8. EFFECT OF CRITICAL SULFATE CONCENTRATION ($C_{s,CRIT}$)	101
5.9. CONCLUSION	105
CHAPTER 6. GAS HYDRATE AND FREE GAS DISTRIBUTION IN MARINE SEDIMENT FOR A MIXED METHANE - PROPANE SYSTEM AND THE ASSOCIATED WEAK SEISMIC RESPONSE.....	107
6.1. INTRODUCTION.....	107
6.2. PHASE DIAGRAMS FOR SYSTEMS WITH MULTIPLE GAS COMPONENTS	110
6.3. ACOUSTIC PROPERTIES AND SYNTHETIC SEISMIC RESPONSE.....	117
6.4. DISCUSSION.....	124
6.5. CONCLUSION	126
CHAPTER 7. FUTURE WORK	128
BIBLIOGRAPHY.....	130
LIST OF SYMBOLS	137

Chapter 1. Introduction to methane hydrate and thesis frame

1.1. Methane hydrate and its existence in natural environments

Methane hydrate, a type of ice-like solid material, with methane molecules captured in the cages of water molecules, is widely distributed around the world. Figure 1.1 indicates a cage structure of structure I (sI) hydrate and sample of gas hydrate. Hydrate is stable only at high pressure and low temperature, so can exist in deep ocean sediment or at permafrost regions (Figure 1.2), and has been discovered in many locations around the world (Figure 1.3).

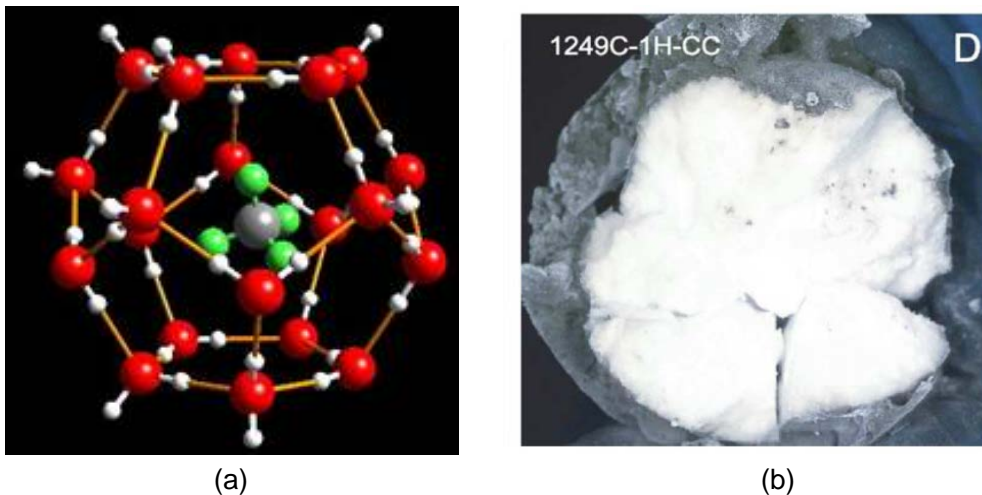


Figure 1. 1 Methane Hydrate: molecular structure and sample.

(a): methane hydrate molecular structure, credit: USGS; (b) methane hydrate sample from ocean sediment drilling core, credit: Trehu & Torres 2004.

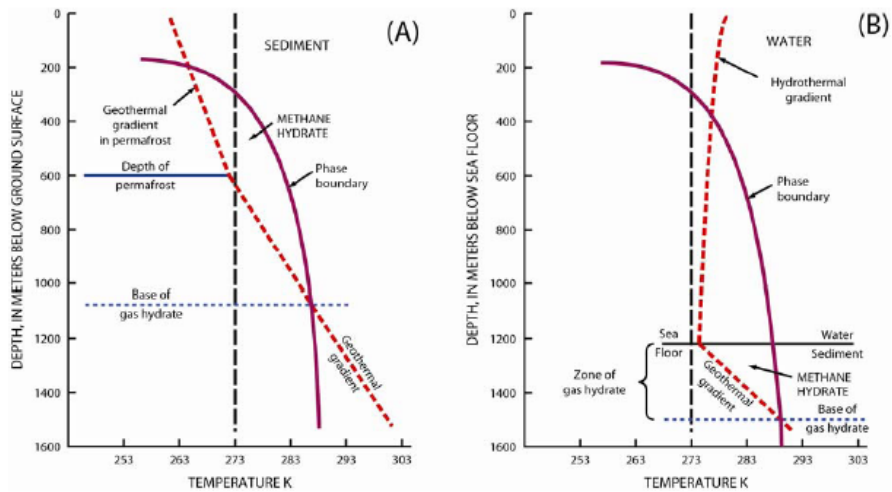


Figure 1. Methane hydrate phase diagram for a (A) onshore arctic permafrost location and a (B) offshore marine location.

Figure 1. 2. Existence of Natural Methane Hydrate from analysis of phase diagram: both in permafrost location and in marine sediments.

(T.S. Collett, USGS, Proceedings of Offshore Technology Conference (OTC), 2008).

It shows the phase boundary and stability zone, in both onshore permafrost locations, and for offshore marine locations. Zone of gas hydrates indicate the gas hydrate stability zone (GHSZ).

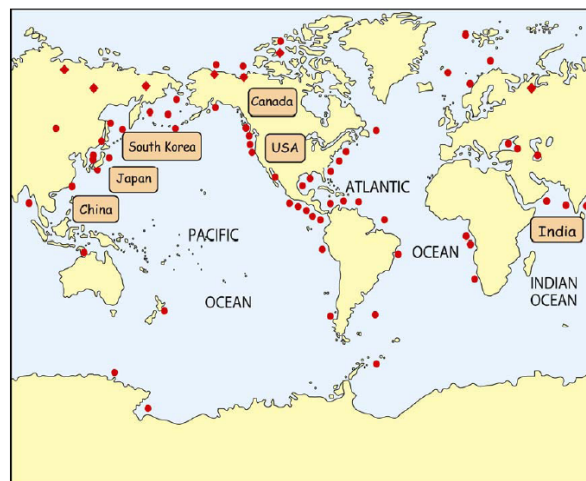


Figure 1. 3. Discovered presence of Gas Hydrate around the world.

(T.S. Collett, USGS, report on OTC08, 2008).

Gas hydrate has been widely studied because of the following reasons:

(1) Gas hydrate may be a promising future energy resource. Gas hydrate is

stable under high pressure and low temperature. All around the world, in most of ocean area with water depth deeper than hundreds of meters and seafloor temperatures near 4°C, there is often an appropriate marine sediment zone, in which gas hydrate can be stable. Due to large seafloor area of around the world, there is possibly large amount of hydrate in deep marine sediments. Similarly, some hydrate exists in permafrost regions. In many locations, gas hydrate samples have been discovered (Figure 1.3).

(2) Hydrate has acted as a cement in sediment if hydrate saturations are appropriate, therefore, the dissociation of marine hydrate may cause instability of seafloor sediment, and induce geo hazard;

(3) The huge amount of methane hydrate is considered as one of the largest reservoirs in global carbon cycling, which is very important in geo-chemical research; the dissociation of huge amount of methane hydrate due to temperature change, may induce important feedback to climate change. For example, during Paleocene – Eocene Thermal Maximum (PETM), gas hydrate may have acted as a big thermal-sensitive carbon capacitor for the carbon release event.

(4) The gas hydrate system affects distribution of chemical compounds in marine sediment greatly. So it is important to understand and explain the interaction of gas hydrate and chemical compounds in sediment, for example, sulfate, calcium, *etc.*

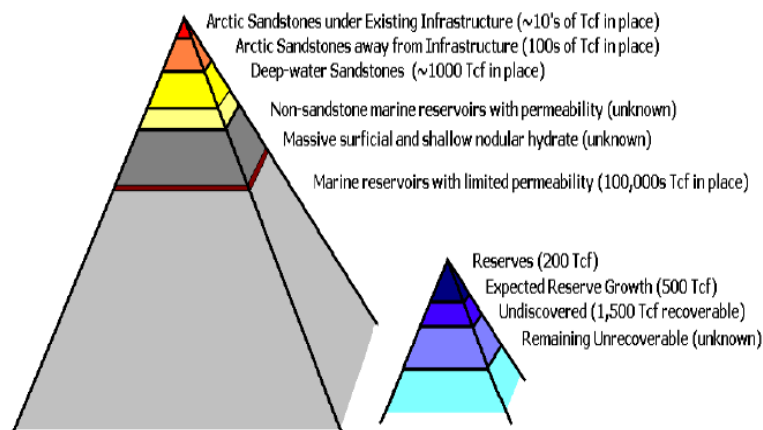


Figure 1. 4. Natural Hydrate Amount (left pyramid), Comparing to Conventional Natural Gas Resource for USA (right pyramid).

(E.D. Sloan, report on OTC08, 2008).

This figure shows possible high end of global gas hydrate amount. It shows relative ratio of estimated hydrate amount in different locations or situations.

Due to the difficulty of detection and sampling, there is still much unknown on marine hydrates. However, since the amount of marine hydrate might be very huge, there is a need to detect and try to exploit it. Currently, there are several major questions on marine hydrates (Sloan, et al, 2008):

- (1) How to remotely detect marine hydrate;
- (2) Estimate the total amount of marine hydrate;
- (3) Find and demonstrate the capability of economically recoverable hydrate provinces;
- (4) Estimate the impact of hydrate on climate and environments.
- (5) The role of gas hydrate in earth history, for example, during Paleocene Eocene Thermal Maximum (PETM).

Both the detection of marine hydrate is the first step and estimation of hydrate amount would be very important. This work focused on marine hydrate inventory study, effects on climate, and detection.

This thesis is organized as below:

Chapter 1: Introduction

Chapter 2 – 4: Demonstrating the amount of gas hydrate during PETM, at warmer ocean and seafloor temperatures, could be similar with that at present day. Major reasons are: (1) The organic carbon depositing on seafloor was higher than present day value, due to less oxygen concentration in ocean at warmer ocean conditions; (2) The methanogenesis rate constant was faster than present day because of higher temperatures.

Chapter 5: Showing the interaction among sulfate, methane, and particulate organic carbon (POC). Low ocean sulfate during PETM can contribute to high amount of gas hydrate, compared with present day conditions.

Chapter 6: Showing that multiple gas components in gas hydrate systems can induce different hydrate / free gas distribution and possible weak seismic response.

Chapter 2. PETM Event and Role of Marine Methane Hydrate

2.1. PETM Event

Paleocene-Eocene Thermal Maximum (PETM), or called Late Paleocene Thermal Maximum (LPTM), was a short warm interval in geo-history, at ~ 55 Ma (million years ago), lasting for ~ 20,000 yrs (years). During PETM, a rapid seafloor temperature spike occurred. Seafloor Temperature T_{sf} rose by 4~8 °C. Soon after T_{sf} rose, a large negative excursion (~-3 ‰) of $\delta^{13}\text{C}$ isotope ratio occurred. There was an intense perturbation on the global bio-system: e.g., numerous benthic lives (such as foraminifera) disappeared due to anoxia in deep-seas; major turnover of mammalian species happened.

The $\delta^{13}\text{C}$ isotope ratio is defined as:

$$\left(\delta^{13}\text{C}\right)_{sample} = \frac{\left(^{13}\text{C}/^{12}\text{C}\right)_{sample} - \left(^{13}\text{C}/^{12}\text{C}\right)_{std}}{\left(^{13}\text{C}/^{12}\text{C}\right)_{std}} \times 1000\text{‰} \quad (2-1)$$

The common reference for $\delta^{13}\text{C}$, the PDB Marine Carbonate Standard, was obtained from a Cretaceous marine fossil, *Belemnitella americana*, from the PeeDee formation. This material has a higher $^{13}\text{C}/^{12}\text{C}$ ratio than nearly all other natural carbon-based substances; for convenience it is assigned a $\delta^{13}\text{C}$ value of zero, giving almost all other naturally-occurring samples negative

delta values.

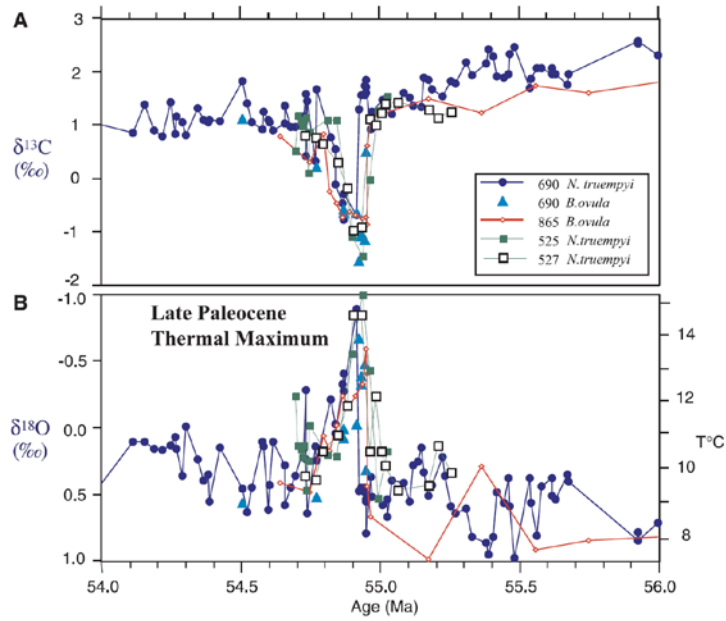


Figure 2. 1. Paleocene Eocene Thermal Maximum (PETM, previously called Late Paleocene Thermal Maximum, LPTM) Event. (Zachos, 2001).

Table 2.1. PDB as a Reference of $\delta^{13}\text{C}$

	^{13}C , %	^{12}C , %	$^{13}\text{C}/^{12}\text{C}$	$\delta^{13}\text{C}$
PDB	1.11123	98.8888	0.0112372	$\equiv 0$

Isotope compositions of some materials, are shown below in Figure 2.2:

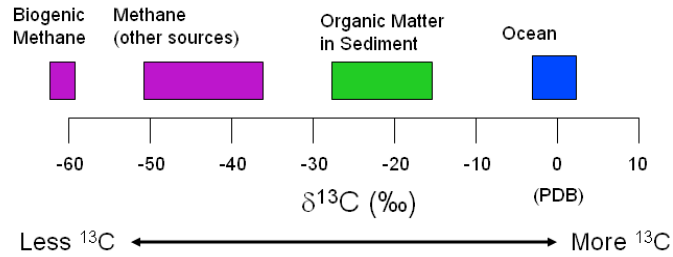


Figure 2. 2. Isotope Compositions of Some Materials (Revised from G. Dickens, 2007).

During PETM, the isotopic ratio $\delta^{13}\text{C}$ in ocean dissolved inorganic carbon (DIC) decreased significantly, due to some certain injection of a significant amount of carbon from some not-well explained $\delta^{13}\text{C}$ - depleted source (Figure 2.3). Before PETM, the $\delta^{13}\text{C}$ in ocean DIC was $\sim 1\text{‰}$; after a rapid injection of $\delta^{13}\text{C}$ depleted carbon from some certain unknown source, the $\delta^{13}\text{C}$ in ocean decreases to -2‰ , or decreased by around 3‰ . The ocean DIC was in the amount of around 38000 GtC .

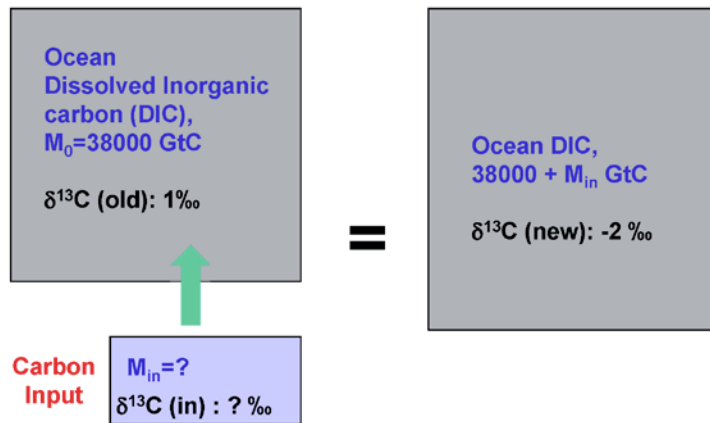


Figure 2. 3. Schematic figure of isotopic ratio change in ocean DIC of the PETM event

Denote the unknown injection carbon source was at the amount of $M_{in} \text{ GtC}$, with unknown $\delta^{13}\text{C}$ value of δ_{in} . The conservative relationship between amount M_{in} and δ_{in} can be described as:

$$M_0\delta_0 + M_{in}\delta_{in} = M_n\delta_n \quad (2-2)$$

and the total mass of carbon amount is conservative:

$$M_0 + M_{in} = M_n \quad (2-3)$$

by rearrangement, equations (2-2) and (2-3) become:

$$M_{in}\delta_{in} = M_n\delta_n - M_0\delta_0 \quad (2-4)$$

$$M_{in}\delta_{in} = (M_0 + M_{in})\delta_n - M_0\delta_0 \quad (2-5)$$

$$M_{in}(\delta_{in} - \delta_n) = M_0\delta_n - M_0\delta_0 \quad (2-6)$$

$$M_{in} = \frac{M_0(\delta_n - \delta_0)}{\delta_{in} - \delta_n} \quad (2-7)$$

where

M_0 , GtC: amount of carbon in ocean DIC before PETM event (old), = 38000

M_n , GtC: amount of carbon in ocean DIC after PETM event (new)

M_{in} : amount of carbon injected into ocean during PETM event

δ_0 : $\delta^{13}\text{C}$ in ocean DIC before PETM event (old), = 1‰

δ_n : $\delta^{13}\text{C}$ in ocean DIC after PETM event (new), = -2‰

δ_{in} : $\delta^{13}\text{C}$ of the carbon source injected into ocean during PETM event

So the relationship between M_{in} and δ_{in} is a hyperbolic function.

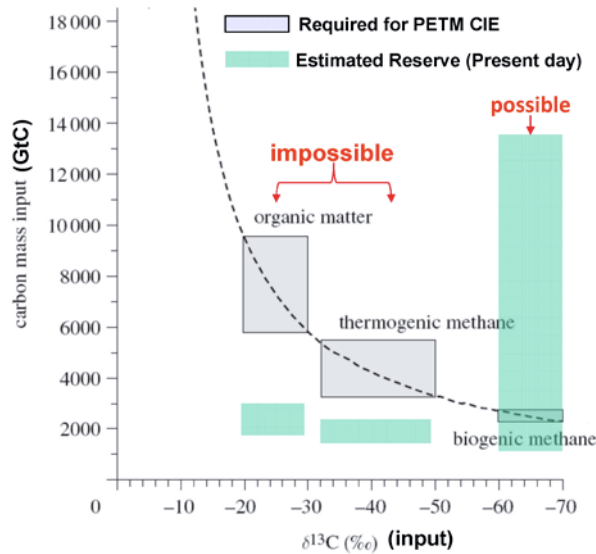


Figure 2. 4. Required amount of carbon for PETM excursion event (revised from Jones et al., 2012). The only possible option to meet the amount required is the carbon from biogenic methane.

Figure 2.4 shows the relationship between the amount of carbon injected into ocean M_{in} and the $\delta^{13}\text{C}$ of the carbon source injected into ocean during PETM event, with consideration of several sources evaluated by several papers. Organic matter (such as peat, coal, etc.), thermogenic methane (such as methane in natural gas), and biogenic methane (from methanogenesis, especially that stored in methane hydrate), have been evaluated. However, compared to their global inventories at present day, neither of organic matter, or thermogenic methane can be sufficient to cause the PETM carbon source event, the only possible option is methane hydrate.

2.2. Hypothesis of methane hydrate as the candidate for PETM $\delta^{13}\text{C}$ event and the challenge for this hypothesis

The major reason that methane hydrate is the only possible candidate, is that the isotope ratio of carbon methane hydrate is much lower than that in ocean or that in sediment, due to the fractioning during methanogenesis reaction. The $\delta^{13}\text{C}$ – depleted methane from biogenic process, i.e., the methanogenesis, is stored in the forms of methane hydrate and free gas. When large amount of methane hydrate dissociates, a large negative excursion of $\delta^{13}\text{C}$ value would happen in ocean. Therefore, a hypothesis was proposed that the large $\delta^{13}\text{C}$ negative shift during PETM, was due to large amount of methane hydrate dissociation (G. Dickens, 1995; 1997; 2008). This hypothesis is the most possible explanation to PETM isotope ratio decrease, with many evidences reported.

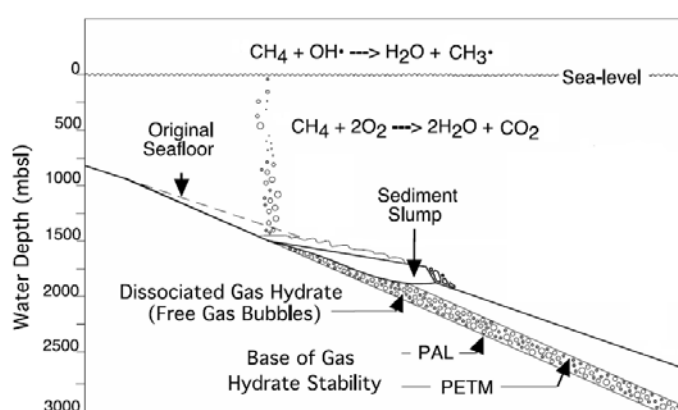


Figure 2. 5. Hypothesis: dissociation of large amount of hydrate caused PETM $\delta^{13}\text{C}$ negative shift (Revised from G. Dickens, 2003).

However, there still remains a question: just before PETM, the seafloor

temperature was very high (~ 8-10 °C). Whether there was enough Methane Hydrate pre-reserved to cause the $\delta^{13}\text{C}$ shift in PETM, becomes a problem.

As Figure 2.6 shows, when seafloor temperature rises, the Gas Hydrate Stability Zone (GHSZ), in which the hydrate is thermodynamically stable, will shrink. As shown in the following figure. And because of the thickness of GHSZ, L_t decreases, the diffusion loss is increased, therefore, the average hydrate saturation may decrease. These will result a decreased total hydrate amount. How to resolve this issue is one of the major purposes of this thesis.

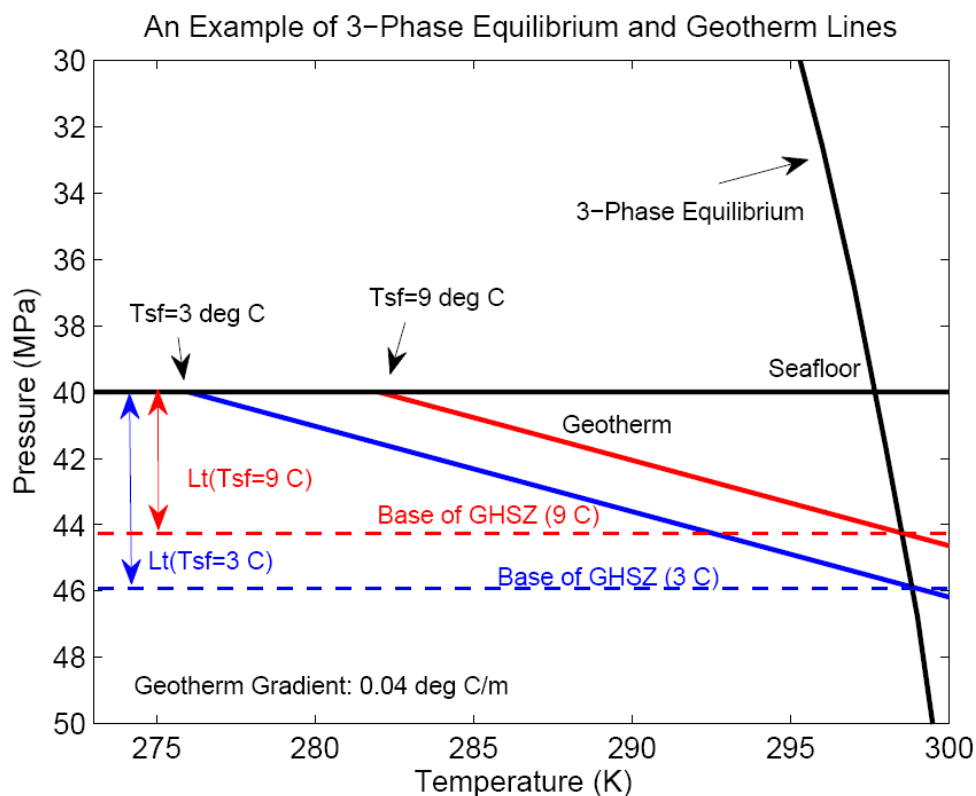


Figure 2. 6. The changes caused by seafloor temperature increase.

2.3. Typical 1-D scenario of methane hydrate accumulation in marine sediments

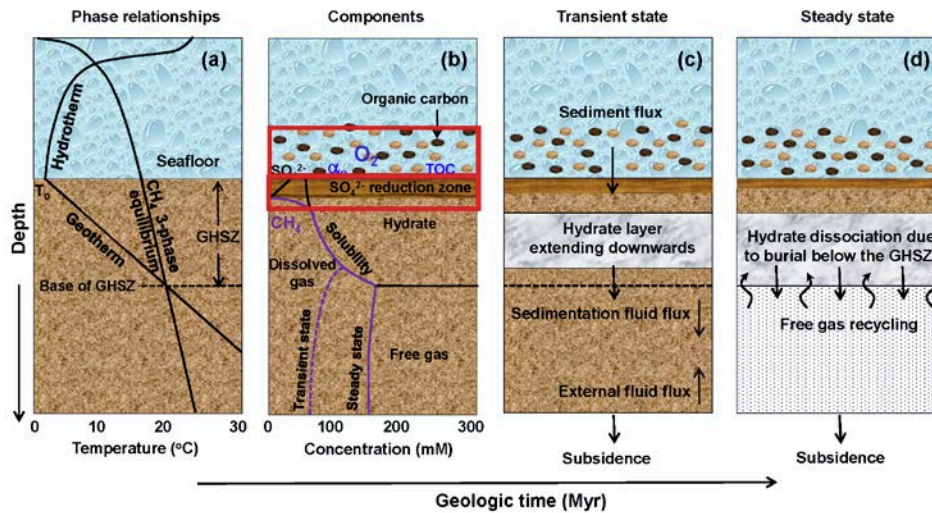


Figure 2. 7. 1-D scenario of methane hydrate accumulation in marine sediments. (Revised from Bhatnagar, 2007).

Figure 2.7 shows a 1-D scenario of methane hydrate accumulation in marine sediments across geological time scale. Before buried into sediment and becoming available for methanogenesis in deep sediment, organic carbon in ocean must pass through two oxidation zones as shown in Figure 2.8: (1) oxygen-containing water zone above the seafloor, or simply named as oxygen water zone (OWZ) in this work; (2) sulfate-containing zone in shallow sediment, which is also called sulfate reduction zone (SRZ). Most of the organic carbon in ocean, will be oxidized by oxygen in OWZ, and the rest will become total organic carbon (TOC) in sediment at seafloor; after organic carbon passes through OWZ, some portion will be consumed due to the reaction with sulfate or the organoclastic reaction.

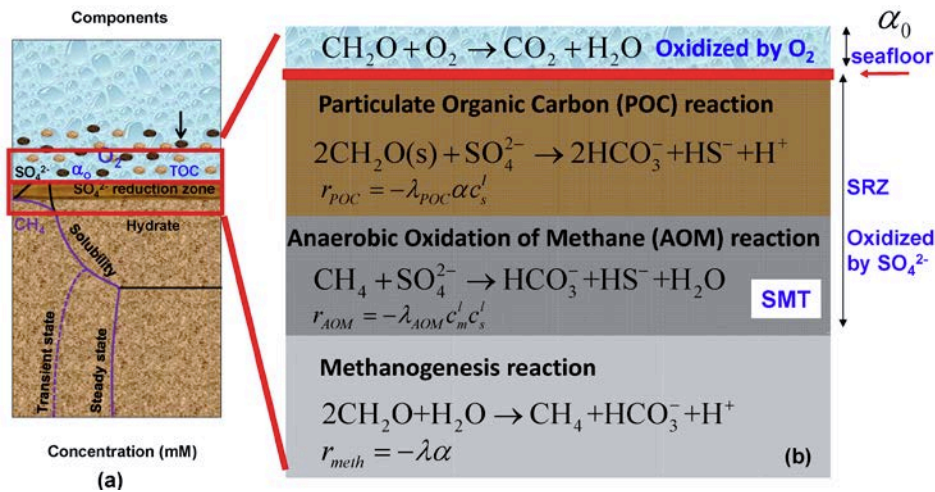


Figure 2. 8. Reactions about organic carbon, sulfate, and methane, from ocean bottom to deep sediment. SRZ: sulfate reduction zone; SMT: sulfate / methane transition zone.

2.4. Possible solutions for abundant hydrate inventory before PETM

Several previous works concluded that hydrate inventory could not be as high as that at present day at warm conditions before PETM. However, these were based on the model, with the same total organic carbon (TOC) in seafloor sediment as the input, and using the constant biogenic reaction rate constant. But this might not be true. Because (1) the TOC may have been higher than present day due to low oxygen concentration in the whole ocean because of higher ocean temperatures; (2) ocean sulfate concentration was lower than present day, which may cause less consumption of organic carbon by sulfate than present day; (3) as Arrhenius law shows, reaction rate constant should increase with temperature. In this work, we examined the possibilities regarding these three factors.

Chapter 3. Numerical Model about Hydrate Inventory due to Higher Organic Carbon Input and Reaction Rate Constant

The schematic scenario is following Figure 2.7 and Figure 2.8. In Chapter 3-4 we examine the results due to assumptions that: (1) the TOC should have been higher than present day due to low oxygen concentration in the whole ocean because of higher ocean temperatures; (2) as Arrhenius law shows, methanogenesis reaction rate constant should increase with temperature.

The numerical model is revised from the 1-D hydrate accumulation model in Bhatnagar's paper (Bhatnagar, 2007). The main difference in our new model, is that we focus on the processes in which the temperature at seafloor is changed.

3.1. Assumptions

Different from models in present literature studying hydrate accumulation, the following effects are considered:

- (1) The methanogenesis reaction rate constant is changing with temperature, while in literature, the rate constant is constant.
- (2) The seafloor organic concentration is increasing due to the decrease of global seafloor oxygen concentration; the global seafloor oxygen concentration decrease is caused by the solubility decrease at sources of

global deep ocean flows (e.g. Antarctic sea surface or Greenland sea surface, as the sources); the solubility decrease is due to the sea surface temperature rise.

3.2. Numerical Model

Since the derivation of the model has been described in Bhatnagar's paper and PhD dissertation (Bhatnagar, 2008), so here I will simply describe the model.

3.2.1. Porosity profile in sediment

Porosity in the sediment is decaying due to effective stress (Bear, 1988). A simple 1-D porosity derived by Bhatnagar is applied. To simplify the situation, the reference frame is fixed at the seafloor. The following assumptions are further made:

- (1) Densities of water and sediments are constant;
- (2) Sedimentation rate is constant and equal to the subsidence rate;
- (3) Porosity profile is independent of time;
- (4) No external upward fluid flow;
- (5) Fluid and solid velocities become equal as a minimum porosity is achieved;
- (6) Generation of water through diagenetic reactions is neglected.

The depth co-ordinate system is positive at downward direction.

The porosity change due to sedimentation and compaction caused by hydrostatic pressure is:

$$\begin{aligned}\phi &= \phi_{\infty} + (\phi_0 - \phi_{\infty}) \exp(-\sigma_e / \sigma_{\phi}) \\ &= \phi_{\infty} + (\phi_0 - \phi_{\infty}) \exp[(\sigma_v - p) / \sigma_{\phi}]\end{aligned}\quad (3-1)$$

$$\Rightarrow -\sigma_{\phi} \left(\frac{\phi_0 - \phi_{\infty}}{\phi - \phi_{\infty}} \right) \frac{\partial}{\partial z} \left(\frac{\phi - \phi_{\infty}}{\phi_0 - \phi_{\infty}} \right) = (\rho_s - \rho_f)(1 - \phi)g \quad (3-2)$$

where ϕ_0 --- porosity of sediments at seafloor

ϕ_{∞} --- minimum porosity which can be achieved

σ_e --- effective stress, = $\sigma_v - p$

σ_v --- overburden, caused by pressure difference between mineral

and fluid densities

σ_{ϕ} --- characteristic constant with unit of pressure

p --- hydrostatic pressure

To make Eq. (3-2) normalized, define:

$$\tilde{\phi} = (\phi - \phi_{\infty}) / (1 - \phi_{\infty}), \quad (3-3)$$

$$\eta = (\phi_0 - \phi_{\infty}) / (1 - \phi_{\infty}), \quad (3-4)$$

$$\gamma = (1 - \phi_{\infty}) / \phi_{\infty} \quad (3-5)$$

$$L_{\phi} = \frac{\sigma_{\phi}}{(1 - \phi_{\infty})(\rho_s - \rho_f)g} \quad (3-6)$$

L_{ϕ} is a characteristic length indicating the effect of compression. The higher σ_{ϕ} is, the larger L_{ϕ} will be, and the $|d\phi/dz|$ along the depth (downward) is smaller. Here is an example of how long the typically length scale of L_{ϕ} is :

for $(\rho_s - \rho_f = 2.56 - 1.03) = 1.53 \text{ g/cm}^3$, if $\sigma_\phi = 5.4 \text{ MPa}$, then $L_\phi = 400 \text{ m}$.

$$\tilde{z} = \frac{z}{L_\phi} = \frac{z}{\sigma_\phi / [(1 - \phi_\infty)(\rho_s - \rho_f)g]} \quad (3-7)$$

$$\Rightarrow \frac{1}{\tilde{\phi}} \frac{\partial \tilde{\phi}}{\partial \tilde{z}} = -(1 - \tilde{\phi}), \quad \text{B.C.: at } \tilde{z} = 0, \tilde{\phi} = \eta \quad (3-8)$$

$$\Rightarrow \tilde{\phi} = \frac{\eta}{\eta + (1 - \eta)e^{\tilde{z}}} \quad (3-9)$$

3.2.2. Sediment Balance

From the mass balance for sediment, with the porosity – depth relationship, a sediment balance equation can be obtained (Berner, 1980; Davie and Buffett; 2001).

$$\frac{\partial((1 - \phi)\rho_s)}{\partial t} + \nabla \cdot ((1 - \phi)\rho_s v_s) = 0 \quad (3-10)$$

where v_s --- sediment velocity.

Assume in steady state, the sediment flux is invariant along depth, then it equals the product of sedimentation rate (\dot{S}) at seafloor and $(1 - \phi_0)$. Denote the sediment flux as:

$$U_s = v_s(z)(1 - \phi(z)) = [(1 - \phi)v_s]_{z=0} = \dot{S}(1 - \phi_0). \quad (3-11)$$

3.2.3. Organic Material Balance

Assume:

- (1) sedimentation rate and the amount of degradable organic carbon at the seafloor (α_0) remain constant over time;
- (2) microbial methanogenesis begins at the seafloor;
- (3) solid organic material moves downwards with sediment at constant

velocity of v_s ;

(4) sediment density is not altered by microbial degradation of organic carbon.

Via the mass balance, organic material balance (Berner, 1980; Davie and Buffett, 2001; Bhatnagar, 2007) can be expressed as:

$$\frac{\partial}{\partial t}(\rho_s \alpha(1-\phi)) + \frac{\partial}{\partial z}(\rho_s v_s \alpha(1-\phi)) = -\rho_s \lambda \alpha(1-\phi) \quad (3-12)$$

$$\begin{cases} I.C.: \alpha(z,0) = 0 \\ B.C.: \alpha(0,t) = \alpha_0 \end{cases} \quad (3-13)$$

where λ --- 1st-order reaction rate constant

α --- organic material concentration available to methanogens, which is a fraction of Total Organic Carbon (TOC). α is expressed as a mass fraction of total sediment.

α_0 --- organic material concentration at seafloor

Define dimensionless variables:

$$\tilde{z} = \frac{z}{L_t} \quad (3-14)$$

$$\tilde{U}_s = \frac{U_s}{U_{f, sed}} = \frac{\gamma U_{f, sed}}{U_{f, sed}} = \gamma \quad (3-15)$$

$$Pe_1 = \frac{U_{f, sed} L_t}{D_m} \quad (3-16)$$

Define In-situ Damkholer number:

$$Da(z) = \frac{\lambda(z) L_t^2}{D_m} \quad (3-17)$$

$$\tilde{\alpha} = \alpha / \alpha_0 \quad (3-18)$$

where L_t --- Thickness of GHSZ.

$$\Rightarrow \frac{\partial}{\partial \tilde{t}} (\tilde{\alpha}(1-\tilde{\phi})) + Pe_1 \frac{\partial}{\partial \tilde{z}} \left(\frac{1+\gamma}{\gamma} \tilde{U}_s \tilde{\alpha} \right) = -Da(1-\tilde{\phi})\tilde{\alpha} \quad (3-19)$$

The I.C. and B.C. are:

$$\begin{cases} I.C.: \tilde{\alpha}(\tilde{z}, 0) = 0 \\ B.C.: \tilde{\alpha}(0, \tilde{t}) = 1 \end{cases} \quad (3-20)$$

Define a dimensionless parameter:

$$N_{t\phi} = L_t / L_\phi \quad (3-21)$$

we have

$$\tilde{\phi} = \frac{\eta}{\eta + (1-\eta)e^{N_{t\phi}\tilde{z}}} \quad (3-22)$$

Later we may use a Average In-situ Da number, or briefly called Average- Da , at $T_{sf} = 3^\circ\text{C}$, as an important parameter. It's defined as the In-situ Da number at mid point ($z=L_t/2$) when $T_{sf} = 3^\circ\text{C}$.

$$(\overline{Da})_0 = (\overline{Da})_{T_{sf}=3^\circ\text{C}, z=L_t/2} = \left(\frac{\lambda L_t^2}{D_m} \right)_{T_{sf}=3^\circ\text{C}, z=L_t/2} \quad (3-23)$$

where subscript "0" refers to case $T_{sf} = 3^\circ\text{C}$.

If the activation energy $E/R = 0$ (here the universal gas constant $R = 8.314$ J/K/mol), then the analytical solution to the organic mass balance equation is (Bhatnagar, 2007):

$$\tilde{\alpha}|_{\tilde{z}=1} = \left[\eta + (1-\eta)e^{N_{t\phi}} \right]^{-1/N_{t\phi}(1+\gamma)Pe_1/Da} \quad (3-24)$$

At steady state, Converted Amount of Organic Carbon within GHSZ = $(1-\tilde{\alpha}|_{\tilde{z}=1})\beta$. Pe_1 and $(1-\tilde{\alpha}|_{\tilde{z}=1})\beta$ can be combined together to determine

average hydrate saturation ($\langle S_h \rangle$).

Therefore, to consider the effect of changing parameters, we can plot contour plots of average saturation, or Total Hydrate Amount (defined in next chapter,

$$V_h = L_t \int_0^1 (S_h \phi) d\tilde{z}), \text{ in parameter space: } (N_{i\phi 0}, (Pe_1 / \bar{Da})_0).$$

3.2.4. Dimensionless Methane Balance (Bhatnagar, 2007)

$$\begin{aligned} & \frac{\partial}{\partial \tilde{t}} \left[\frac{1+\gamma\tilde{\phi}}{\gamma} (1-S_h-S_g) \tilde{c}_m^l + \frac{1+\gamma\tilde{\phi}}{\gamma} S_h \tilde{c}_m^h \tilde{\rho}_h + \frac{1+\gamma\tilde{\phi}}{\gamma} S_g \tilde{c}_m^g \tilde{\rho}_g \right] + \\ & \frac{1+\gamma}{\gamma} \frac{\partial}{\partial \tilde{z}} \left[(Pe_1 + |Pe_2|) \tilde{U}_f \tilde{c}_m^l + Pe_1 \tilde{U}_s \frac{1+\gamma\tilde{\phi}}{\gamma(1-\tilde{\phi})} S_h \tilde{c}_m^h \tilde{\rho}_h + Pe_1 \tilde{U}_s \frac{1+\gamma\tilde{\phi}}{\gamma(1-\tilde{\phi})} S_g \tilde{c}_m^g \tilde{\rho}_g \right] \\ & = \frac{\partial}{\partial \tilde{z}} \left[\frac{1+\gamma\tilde{\phi}}{\gamma} (1-S_h-S_g) \frac{\partial \tilde{c}_m^l}{\partial \tilde{z}} \right] + \left(\frac{M_{CH_4} \rho_s}{M_{org} \rho_f} \right) Da (1-\tilde{\phi}) \beta \tilde{\alpha} \end{aligned} \quad (3-25)$$

where

$$\tilde{c}_m^l = \frac{c_m^l}{c_{m,eqb}^l}, \quad \tilde{c}_m^h = \frac{c_m^h}{c_{m,eqb}^h}, \quad \tilde{c}_m^g = \frac{c_m^g}{c_{m,eqb}^g} \quad (3-26)$$

c_m^i ---- methane mass fraction in i -phase, $i=l, h, g$

$c_{m,eqb}^l$ ---- methane solubility at Base of GHSZ in *liquid*-phase

$$Pe_2 = \frac{U_{ext} L_t}{D_m} \quad (3-27)$$

Pe_2 is the 2nd Peclet number corresponding to the ratio of external flux to diffusion, and

$$\tilde{\rho}_h = \frac{\rho_h}{\rho_f}, \quad \tilde{\rho}_g = \frac{\rho_g}{\rho_f}, \quad \beta = \frac{\alpha_0}{c_{m,eqb}^l} \quad (3-28)$$

I.C. and B.C.:

$$I.C. \quad \tilde{c}_m^l(z, 0) = 0 \quad (3-29)$$

$$B.C. (1): \tilde{c}_m^l(0, t) = 0 \quad (3-30)$$

$$B.C. (2): \frac{\partial \tilde{c}_m^l}{\partial z}(D, \tilde{t}) = 0, \quad \text{if } |Pe_2| < |Pe_1| \quad (3-31)$$

$$\text{or } \tilde{c}_m^l(D, \tilde{t}) = \tilde{c}_{m,ext}, \quad \text{if } |Pe_2| > |Pe_1| \quad (3-32)$$

D refers to the bottom of the spatial domain.

3.3. Description on Effects of T_{sf} increase

When seafloor temperature, T_{sf} , increases, the following effects will happen:

(1) L_t will decrease;

(2) Pe_1 and $N_{t\phi}$ will decrease according to $Pe_1 = \frac{U_{f, sed} L_t}{D_m}$, $N_{t\phi} = L_t / L_\phi$;

(3) In-situ Damkohler number, $Da(z)$, will decrease due to decrease of L_t , but will increase if reaction rate constant, λ , is increasing, thus a comprehensive

result is that Da will follow this equation: $Da(z) = \frac{\lambda(z)L_t^2}{D_m}$.

(4) α_0 may increase according to further consideration on the decrease of seafloor oxygen concentration.

(5) Whether Total Hydrate Amount will increase or decrease, is a decided by all of the above factors.

3.4. Cases and Sceneries to Be Studied

Here scenery refers to a situation, in which E/R is specified, and the change of α_0 is also specified; and results in a parameter space of $(N_{t\phi_0}, (Pe_1 / \bar{D}a)_0)$

(note: subscript 0 means that the parameter value is defined at $T_{sf} = 3^{\circ}\text{C}$), will be searched, and contour plot of the result in such a parameter space, will be presented.

To compare results, *Base case0* and *Base scenery I*, using the same model as those in literature papers, are studied, in which $E/R=0$, and α_0 remains constant. Other cases and sceneries, using our new model, will be studied and compared with the base case and sceneries.

More than three special cases are studied in this work (in all of them, $Pe_2=0$):

(1) *Base case0*: $E/R=0$, and α_0 remains constant, $(Pe_1)_0=1$, $(\bar{D}a)_0=10$, $N_{i\phi 0}=1$, compare results when $T_{sf}=3, 6, 9, 12, 15$ degC;

(2) *Case I*: $E/R=13400$ mol*K, and α_0 varies according to Seafloor Organic Rain = $10 \mu\text{mol}/\text{cm}^2/\text{yr}$, $(Pe_1)_0=1$, $(\bar{D}a)_0=10$, $N_{i\phi 0}=1$, compare results when $T_{sf}=3, 6, 9, 12, 15$ degC;

(3) *Case II*: $E/R=13400$ mol*K, and α_0 varies according to Seafloor Organic Rain = $30 \mu\text{mol}/\text{cm}^2/\text{yr}$, $(Pe_1)_0=1$, $(\bar{D}a)_0=10$, $N_{i\phi 0}=1$, compare results when $T_{sf}=3, 6, 9, 12, 15$ degC.

The *Base case0* is studied as the base case, which is the same model with that in published literature papers; *Case I* and *II*, are special cases, using our new model, in which increased Total Hydrate Amounts are obtained.

More than three sceneries are studied in this work (in all of them, $Pe_2=0$):

(1) *Base scenery I*: $E/R=0$, and α_0 remains constant, $0.01 < (Pe_1 / \bar{D}a)_0 = (Pe_1 / \bar{D}a)_{T_{sf}=3C} < 10$, $0.2 < N_{i\phi 0} < 2$, only compare results when $T_{sf}=3^\circ\text{C}$ and 9°C ;

(2) *Base scenery II*: $E/R=13400 \text{ mol}\cdot\text{K}$, while α_0 still remains constant, $0.01 < (Pe_1 / \bar{D}a)_0 < 10$, $0.2 < N_{i\phi 0} < 2$, only compare results when $T_{sf}=3^\circ\text{C}$ and 9°C ;

(3) *Other sceneries*: $E/R=13400 \text{ mol}\cdot\text{K}$, α_0 is varying according to different seafloor depth, and different seafloor organic rain, $0.01 < (Pe_1 / \bar{D}a)_0 < 10$, $0.2 < N_{i\phi 0} < 2$, only compare results when $T_{sf}=3^\circ\text{C}$ and 9°C .

Such a parameter space can cover most of the situations in reality. In each scenery, results in the parameter space $0.01 < (Pe_1 / \bar{D}a)_0 < 10$, $0.2 < N_{i\phi 0} < 2$, are obtained, and a contour plot is presented.

Intervals of some parameters are listed in the table below.

Table 3.4.1. Dimensionless Groups and Physical Parameters Intervals

Dimensionless Groups	
$N_{i\varphi 0}^*$	0.2 ~ 2.0
Pe_2	0
$(Pe_1 / \bar{D}a)_0^*$	0.01 ~ 10
η	6/9
γ	9
Physical Parameters	
Seafloor Depth (D_{sf})	1.0 ~ 3.0 km
Seafloor Pressure (P_{sf})	10 ~ 30 MPa
Seafloor Temperature (T_{sf})	3 ~ 15 deg C
Geothermal Gradient (G)	0.04 deg C/m
α_0	0 ~ 5 %
ϕ_0	0.7
ϕ_∞	0.1
c_m^h (methane mass fraction in hydrate phase)	0.134
$\tilde{\rho}_h$ (= 0.958 / 1.03)	0.93
ρ_s / ρ_f (= 2.65 / 1.03)	2.57
\tilde{t}	4 (long enough to reach steady state)

*: subscript 0 means that the parameters are defined when $T_{sf}=3$ degC.

Chapter 4. Hydrate Inventory due to Low Ocean Oxygen Concentration and High Reaction Rate Constant

Following the numerical model described in Chapter 3, in this chapter we present the assumptions and the results about methane hydrate inventory before PETM due to (1) high organic carbon content at seafloor induced by low ocean oxygen concentration, and (2) higher reaction rate constant; both are linked with higher seafloor temperatures.

When seafloor temperature T_{sf} increases, assume:

- (1) Reaction rate constant is changed;
- (2) Seafloor organic concentration α_0 is changed, due to decrease of seafloor oxygen concentration;
- (3) Geothermal gradient G remains constant, temperature distribution reaches steady state;
- (4) Steady state results of hydrate distribution are evaluated in this work;
- (5) Porosity profile doesn't change;
- (6) Biogenic methane is only source for methane and methane hydrate;
- (7) Only pure methane hydrate is considered.

4.1. Change of Reaction Rate Constant

In published papers, the reaction rate constant is constant. However, this

might be too simplified in many cases. Microbe metabolic rate constant can vary by several order of magnitude with temperature change (Price and Sowers, 2004), as Figure 4.1.1 indicated. Therefore, in our work, a rate constant model in which rate constant is changeable, is applied, as Figure 4.1.2 shows. The Activation Energy is $E/R = 13400 \text{ mol}\cdot\text{K}$ (here universal gas constant $R = 8.314 \text{ J/K/mol}$), so we use the same energy in our model.

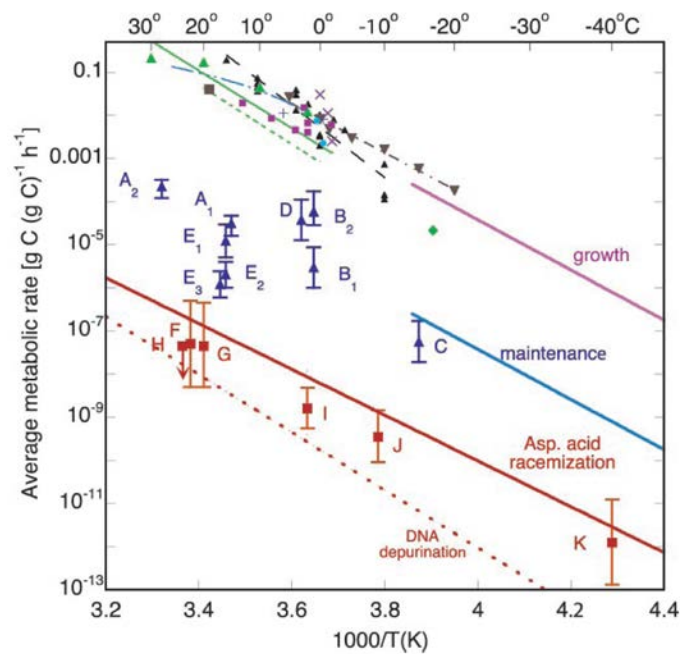


Figure 4.1. 1. Microbe Metabolic Rate Constant

(Price and Sowers, 2004). This figure indicates that, microbe metabolic rate constant $E/R=13400 \text{ mol}\cdot\text{K}$, $R = 8.314 \text{ J/K/mol}$ is the universal gas constant.

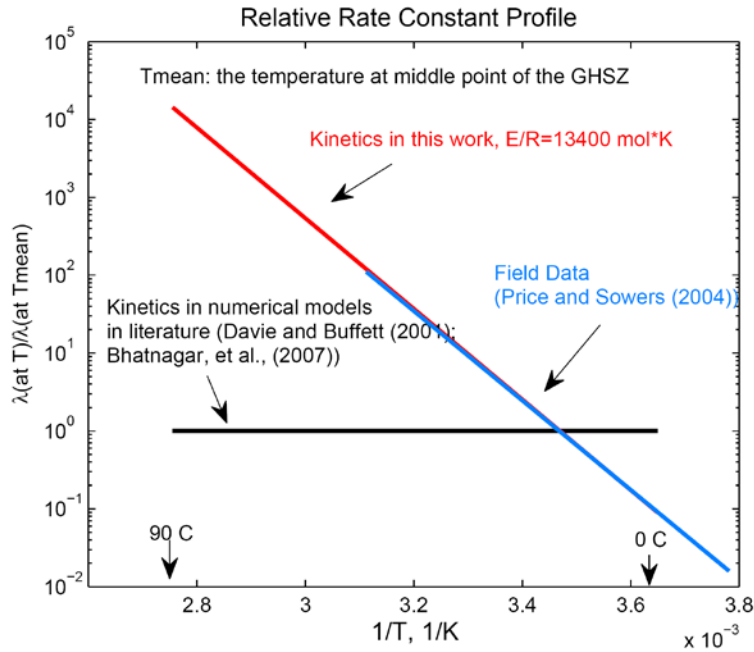


Figure 4.1. 2. Reaction Rate Constant Model applied in this work. The vertical axis is $\lambda(T)/\lambda(\bar{T})$, where \bar{T} is average temperature in GHSZ.

4.2. Change of Seafloor Organic Concentration α_0

The concentration of the remaining organic material at seafloor, is the Seafloor Organic Concentration, denoted by α_0 . The change of seafloor organic concentration when seafloor temperature increases, hasn't been considered in hydrate research models. However, this is highly possible and very important. Here we propose a simple estimation of its change.

In the global water system, the Greenland sea and Antarctic region act as two big sources for deep dense global ocean flow, as shown in the following figure (Rahmstorf, 2006). The periods for the global deep water flow, is around 4000 ~ 5000 yrs.

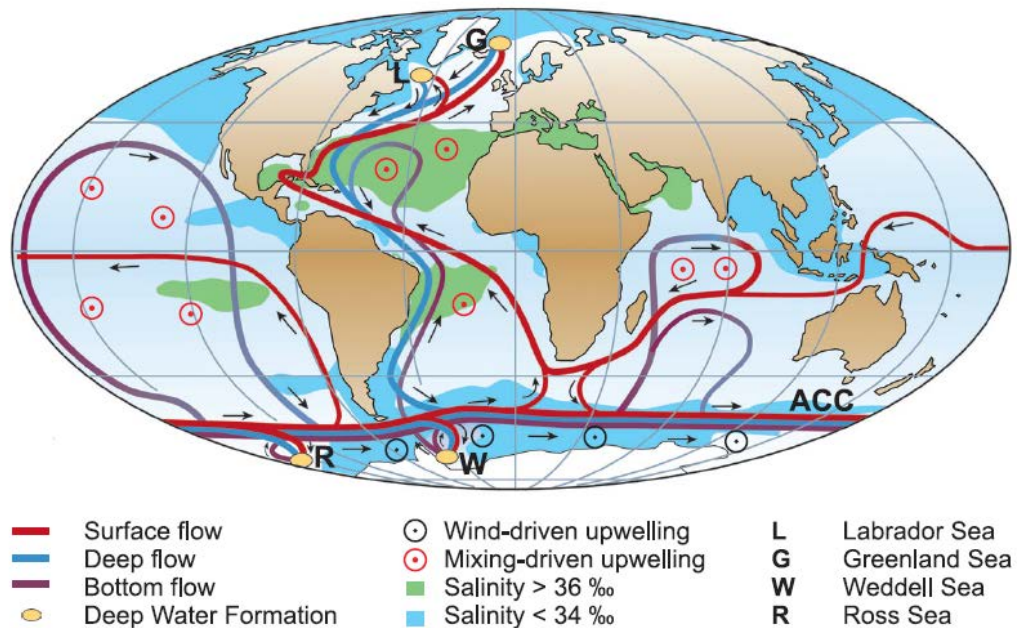


Figure 4.2. 1. Schematic representation of the global thermohaline circulation. Surface currents are shown in red, deep waters in light blue and bottom waters in dark blue. The main deep water formation sites are shown in orange. (Rahmstorf, 2006).

Therefore, when the sea-level temperatures in polar region increase, the global deep ocean water temperature will increase due to the global deep water flow. At the same time when polar ocean surface temperature increases, because the solubility of oxygen is dependent on temperature, polar ocean surface oxygen concentration will decrease due to the increased temperature, and consequently, following the global deep ocean flow, the oxygen concentration in deep oceans other than polar regions will decrease.

The next step, the seafloor organic concentration has strong relationship with the deep ocean oxygen concentration. The most of organic material in the

deep ocean is oxidized by oxygen in seawater, and the remaining part, will be berried into deep sediment, as the resource for methane production and so on. Therefore, much amount decrease of oxygen in deep ocean must decrease the oxidization effect on organic material. As a consequent, the amount of remaining organic material berried into sediment, or, Seafloor Organic Concentration will increase.

The seafloor organic concentration, α_0 , as a function of seafloor temperature, when considering the global oxygen concentration change, is obtained in the following steps.

Step 1: Obtain oxygen solubility change vs temperature, as the following figure shows.

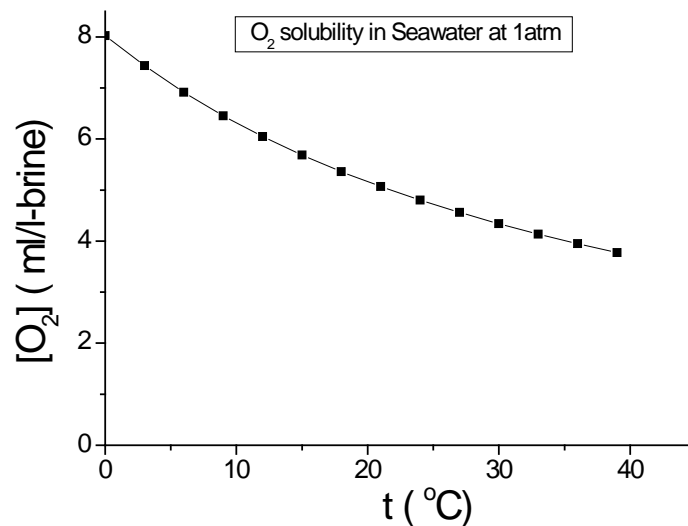


Figure 4.2. 2. Oxygen Solubility in Sea Surface, under 1 atm.

The current Antarctic region sea surface temperature is around 0 deg C, and

the [O₂] is around 8 ml/l-brine. Therefore, we can assume the [O₂] at the polar sea surface is always in equilibrium with atmosphere O₂ when, and of course, will decrease following the solubility curve. Denote the [O₂] at polar sea surface as $C_{ox,0}$. Please note that 0 deg C in polar ocean surface, corresponds to a typical seafloor temperature of $T_{sf}=3^{\circ}\text{C}$ at present.

Step 2: Find the present deep ocean [O₂] (e.g. at depth of $D_{sf} = 2\text{km}$), $C_{ox,d}$ as shown in the following figure.

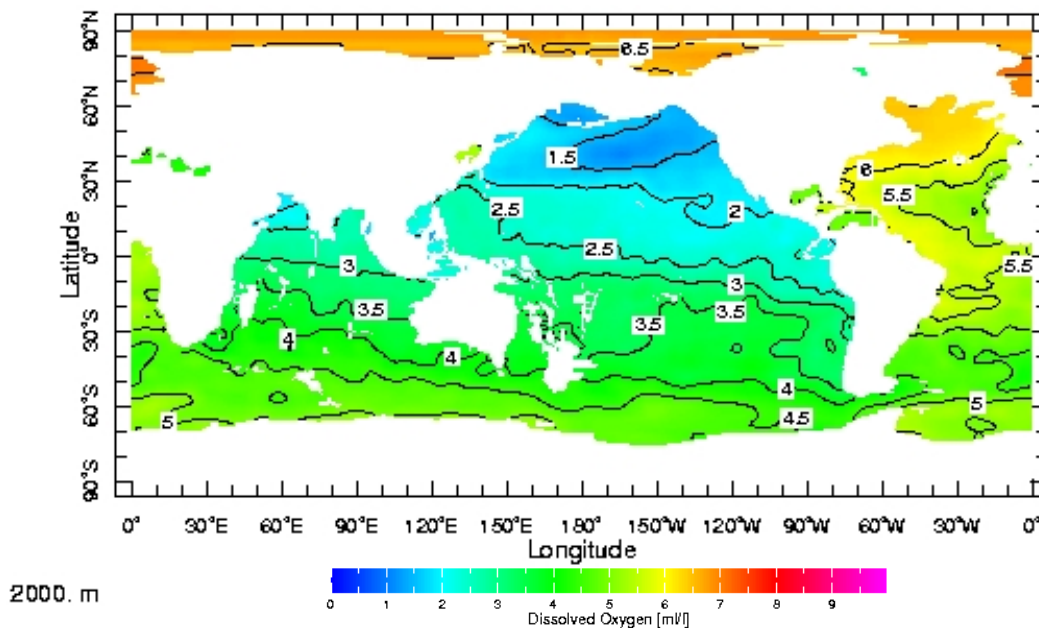


Figure 4.2. 3. Present oxygen concentration in 2.0 km deep ocean.

(From: <http://ingrid.lidgo.columbia.edu/SOURCES/.LEVITUS94/.ANNUAL/>)

Step 3: When the polar ocean surface [O₂] decreases by amount ΔC_{plr} due to temperature rise, the new polar ocean surface [O₂] is $C'_{ox,0} = C_{ox,0} - \Delta C_{plr}$.

Assume the deep ocean [O₂] in regions other than polar area, decrease by

the same amount ΔC_{plr} , until it reaches 0, or the new deep ocean [O₂] is:

$$C'_{ox,d} = C_{ox,d} - \Delta C_{plr} \quad (4-1)$$

Step 4: via a published model (Archer *et al.*, 2002) describing the relationship between $C'_{ox,d}$ and α_0 , get the new α_0 . The relationship can be described in a contour plot, as the following figure shows.

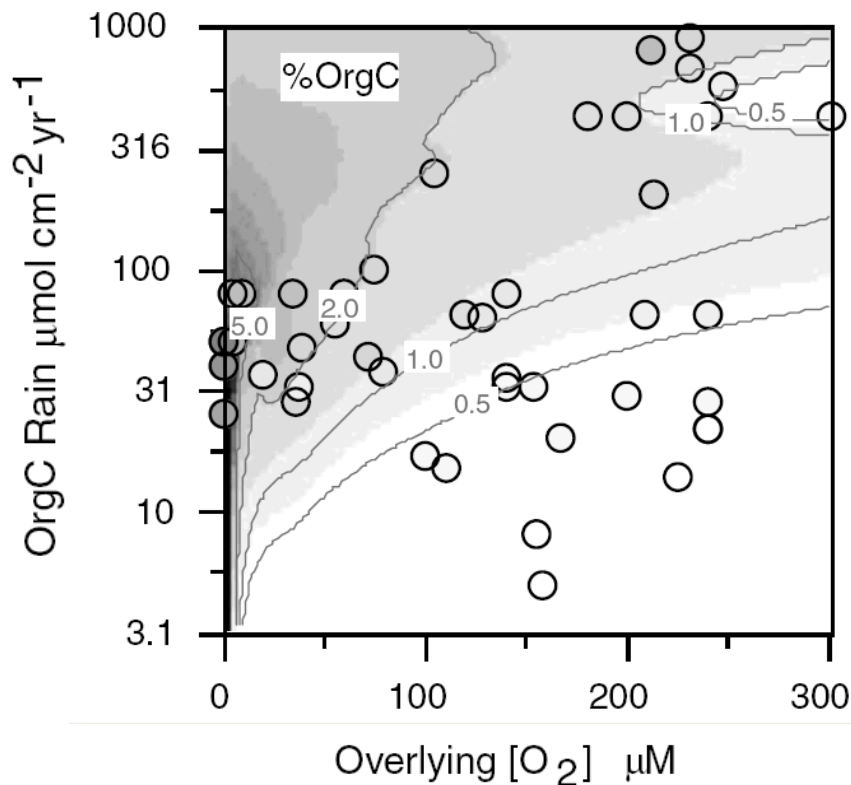


Figure 4.2. 4. Contour plot for seafloor organic concentration α_0 .

(Archer, *et al.*, 2002). 1ml/l-water=1 μ M (at 1atm).

Seafloor Depth, D_{sf} , which affecting the seafloor [O₂] is an important factor; and Organic Carbon Rain at seafloor, is another factor. Regarding that the lower limit of Organic Concentration when seafloor temperature < 2 deg C should be 0, and that the upper limit when seafloor temperature > 28 deg C is

also finite, the data can be fitted with Boltzmann functions:

$$\alpha_0 = A_2 + \frac{A_1 - A_2}{1 + \exp[(t_{sf} - x_0)/dx]} \quad (4-2)$$

where A_1 , A_2 , x_0 , dx are constant, as listed in the figures.

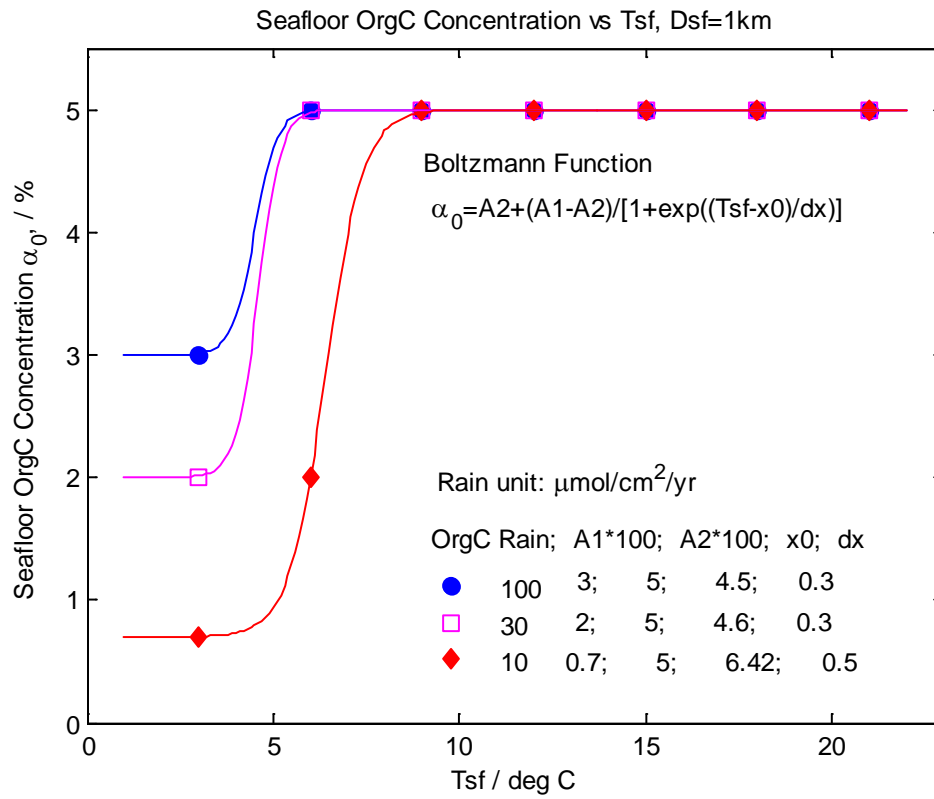


Figure 4.2. 5. Change of α_0 , $D_{sf}=1.0$ km.

The unit of Orgic Carbon Rain is $\mu\text{mol}/\text{cm}^2/\text{yr}$.

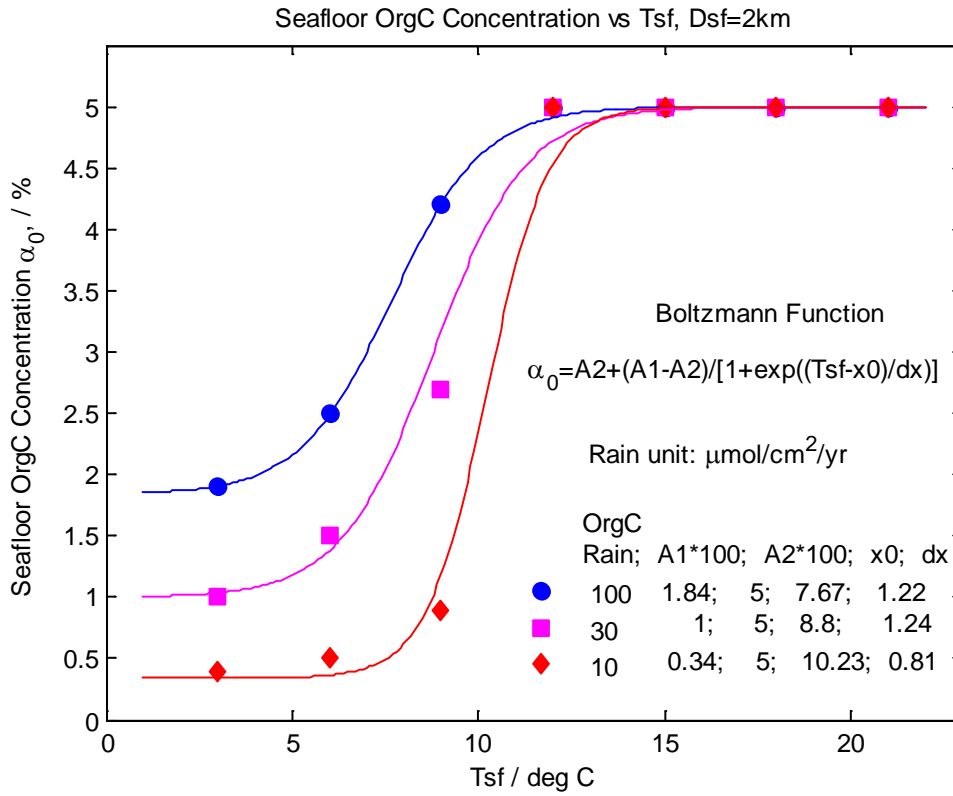


Figure 4.2. 6. Change of α_0 , $D_{sf}=2.0$ km

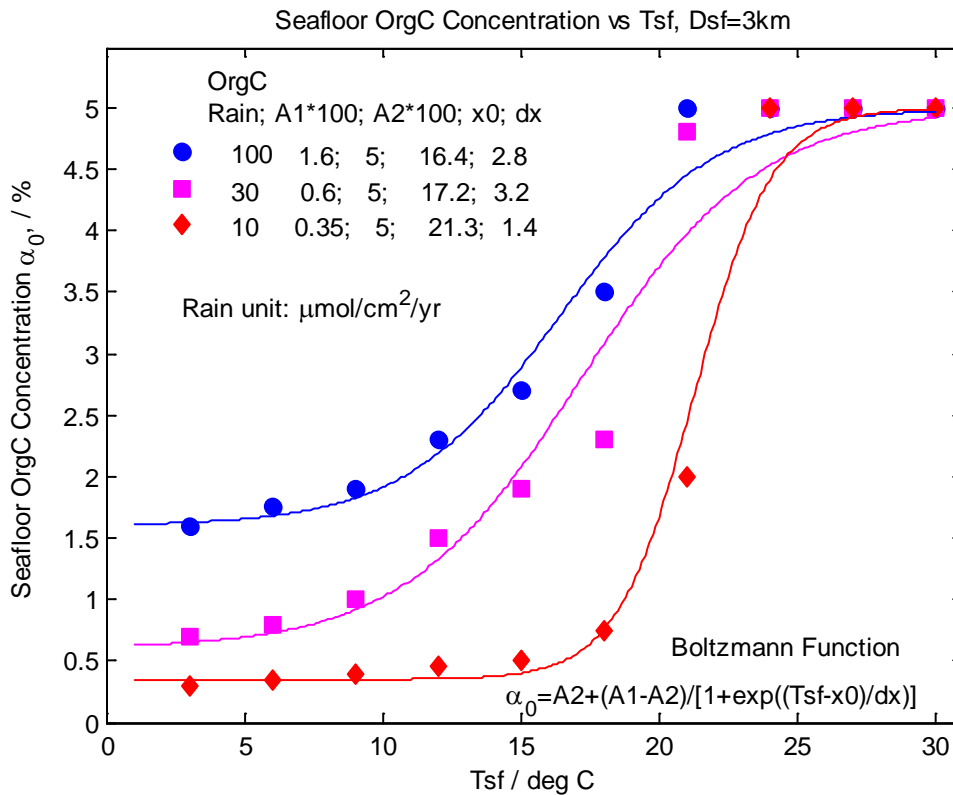


Figure 4.2. 7. Change of α_0 , $D_{sf}=3.0$ km

4.3. Hydrate Profile Change, Seafloor Depth $D_{sf} = 2.0$ km

The following terms are defined to describe the result.

Methane production rate (or Organic Reaction rate):

$$\begin{aligned} r &= dC_{Org}^{sed} / dt = \lambda C_{Org}^{sed} = \lambda C_{Org}^{matrix} (1 - \phi) \\ &= \lambda \alpha (1 - \phi) (\rho_s / M_{Org}) = \tilde{\alpha} Da (D_m / L_t^2) (1 - \phi) (\rho_s / M_{Org}) \beta c_{m,eq}^1 \end{aligned} \quad (4-3)$$

where C_{Org}^{sed} --- Average Organic Concentration in sediment (here sediment volume = pore + matrix)

C_{Org}^{matrix} --- Organic Concentration in matrix

unit of r is [mmol/(m³ sediment)/Myr], here sediment includes matrix and pore space. 1Myr= 1 million year.

Hydrate Volume Fraction:

$$\omega_i = S_i \phi, \quad i = h, \text{ or } g \quad (4-4)$$

where S_i --- Saturation of i -phase (hydrate or gas)

ϕ --- porosity.

Total Hydrate Amount (per unit seafloor area) as:

$$\begin{aligned} V_h &= \langle \omega_h \rangle L_t \\ &= L_t \int_0^1 \omega_h d\tilde{z} = L_t \int_0^1 (S_h \phi) d\tilde{z} \end{aligned} \quad (4-5)$$

where \tilde{z} is the normalized depth. The unit of V_h is m³/m². The physical meaning of V_h is the Total Hydrate Amount per unit seafloor area beneath the seafloor. To simply put, V_h will be called Total Hydrate Amount in the following pages.

Define Remaining Ratio of Total Hydrate Amount when T_{sf} increases, as:

$$k = V_{h,Tsf2} / V_{h,Tsf1} \quad (4-6)$$

where $V_{h,Tsfi}$ refers to Total Hydrate Amount at $T_{sf}=T_{sfi}$, $i=1,2,\dots$,

the most important case is

$$k = V_{h,9C} / V_{h,3C} \quad (4-7)$$

In the following figures, subscript 0 refers to parameters defined at $T_{sf}=3$ deg

C, or:

$$Pe_{1,0} / \bar{D}a_0 = (Pe_1 / \bar{D}a) \Big|_{Tsf=3C} \quad (4-8)$$

$$N_{i\phi 0} = L_{i,0} / L_\phi = (L_i \Big|_{Tsf=3C}) / L_\phi \quad (4-9)$$

where $\bar{D}a$ is the in-situ Damkholer number defined at mean temperature (mid-point temperature) in the GHSZ.

$$\bar{D}a = (\lambda \Big|_{\bar{T}}) \frac{L_t^2}{D_m} \quad (4-10)$$

The temperature and porosity profiles are shown in the following figures, assuming that the geothermal gradient remains constant.

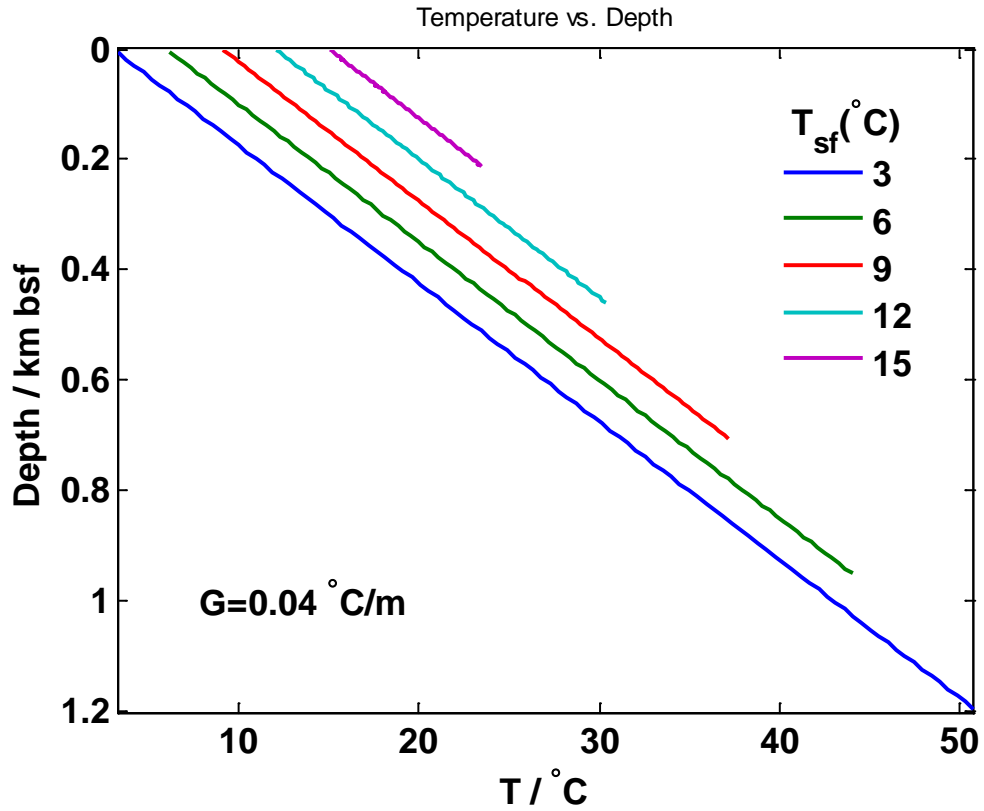


Figure 4.3. 1. Temperature Profile beneath Seafloor.

Different curves corresponds to different seafloor temperature. Assuming geothermal gradient G is constant. Thickness of GSHZ L_t , and dimensionless parameter $N_{t\phi}$ are listed.

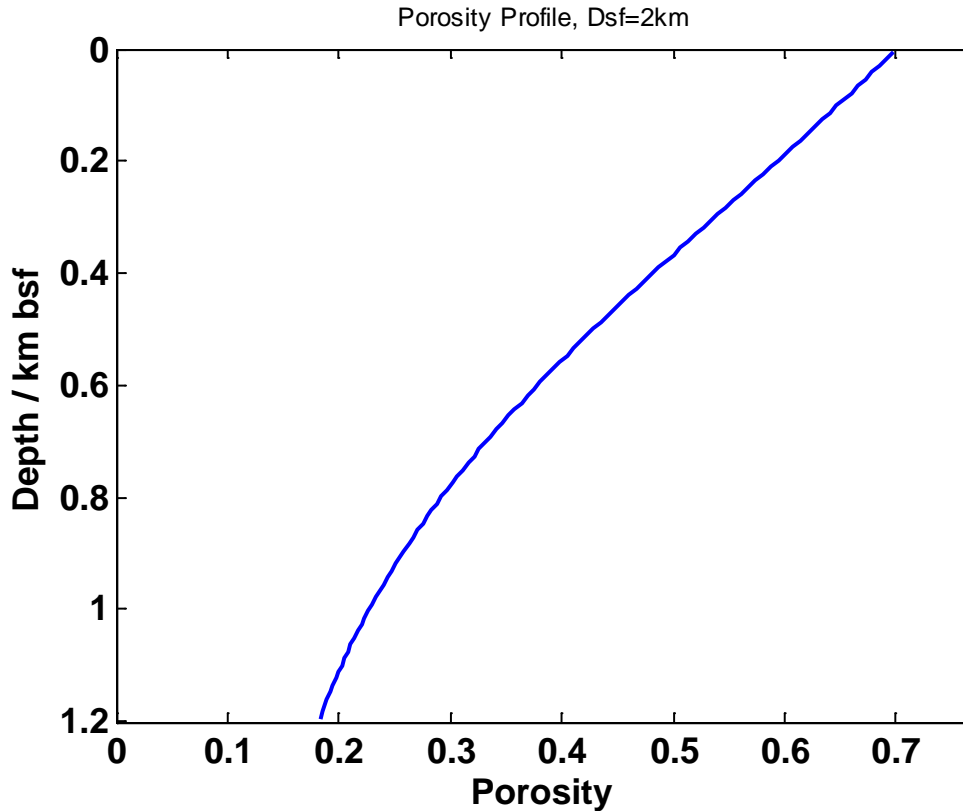


Figure 4.3. 2. Porosity Profile beneath Seafloor.

Assuming at $T_{sf}=3$ degC, $N_{t\phi}=1.0$.

The following are cases for different seafloor temperatures, in which with Remaining Ratios k (from $T_{sf} = 3^{\circ}\text{C}$ to $T_{sf} = 9^{\circ}\text{C}$) are greater than 1.0. For comparison, Case $E/R=0$ with constant seafloor organic concentration is studied as the *Base case0*.

4.3.1. Activation Energy $E/R = 0$, Seafloor Organic C Concentration doesn't Change (Base case0)

This case, $E/R=0$, and seafloor organic concentration remains constant, is the base case as is proposed in literature. The figures in this section, for this case are listed in the following, to be compared by our new models.

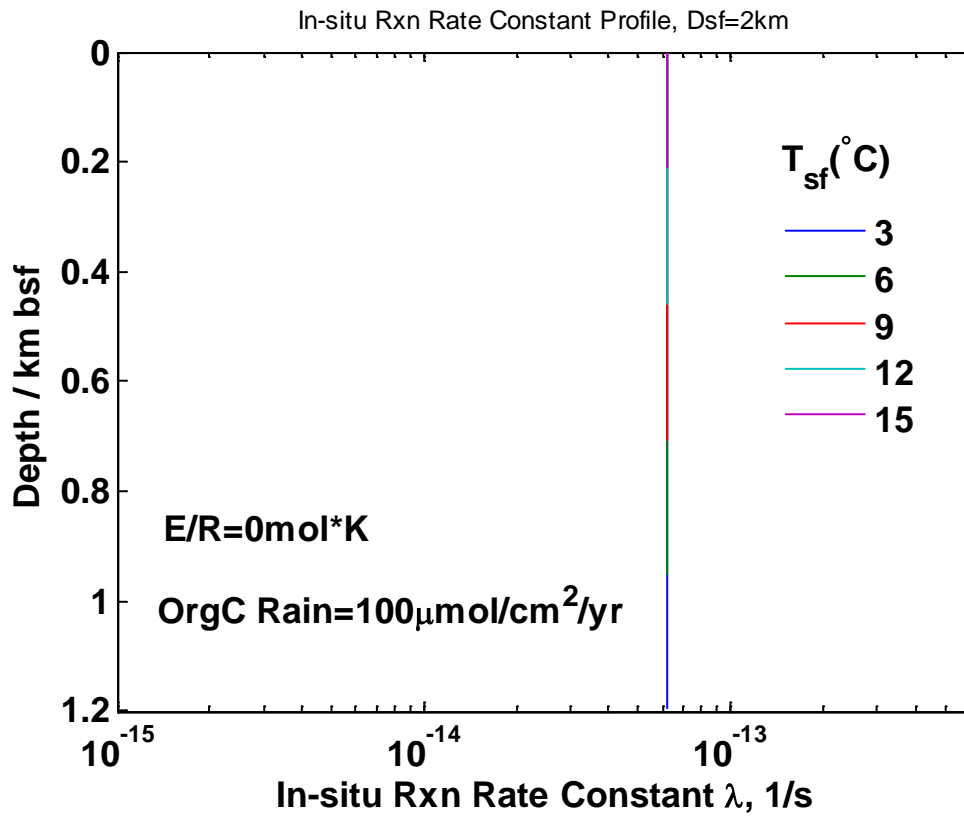


Figure 4.3.1. 1. In-situ Reaction Rate Constant Profile.

$E/R=0$ /s. Assuming that Average Da is 10 when $T_{sf}=3$ degC. Rate constant doesn't change with increase of T_{sf} .

The in-situ reaction rate constant λ (1/s), remains constant from seafloor to much lower positions, because $E/R=0$.

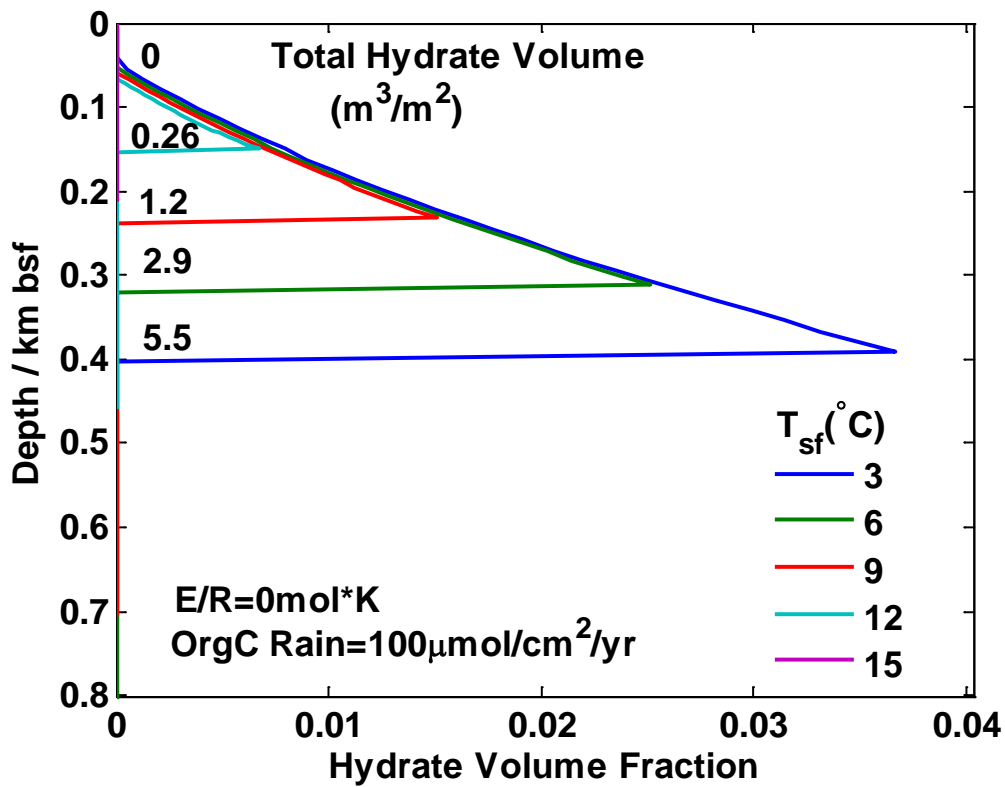


Figure 4.3.1. 2. Hydrate Volume Fraction Profile.

E/R=0, and α_0 Remains Constant. The Total Hydrate Amount (per unit seafloor area) are marked for each curve.

It can be found out that the hydrate volume fraction decreases very much from $T_{sf} = 3^\circ\text{C}$ to 9°C , the remaining Total Hydrate Amount at $T_{sf} = 9^\circ\text{C}$ is only 21% ($=1.2/5.5$) of that in $T_{sf} = 3^\circ\text{C}$.

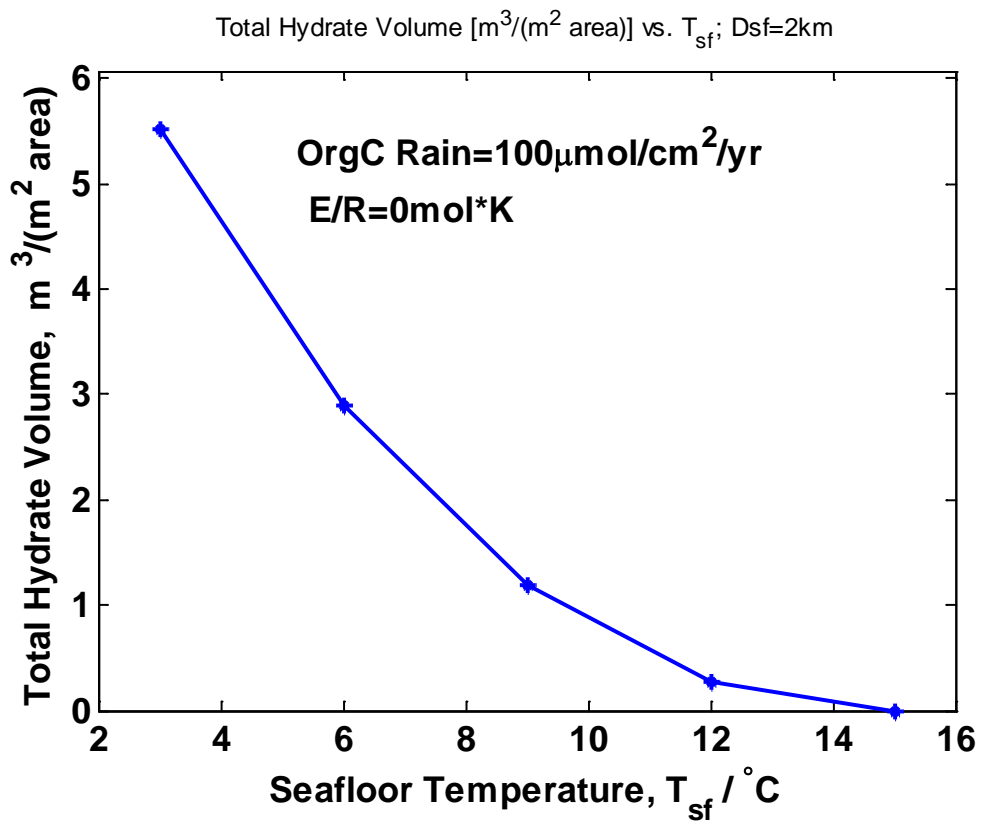


Figure 4.3.1. 3 Total Hydrate Amount (per unit seafloor area) vs Seafloor Temperature.

$E/R=0$, and α_0 Remain Constant. The parameters are listed for every seafloor temperature points calculated.

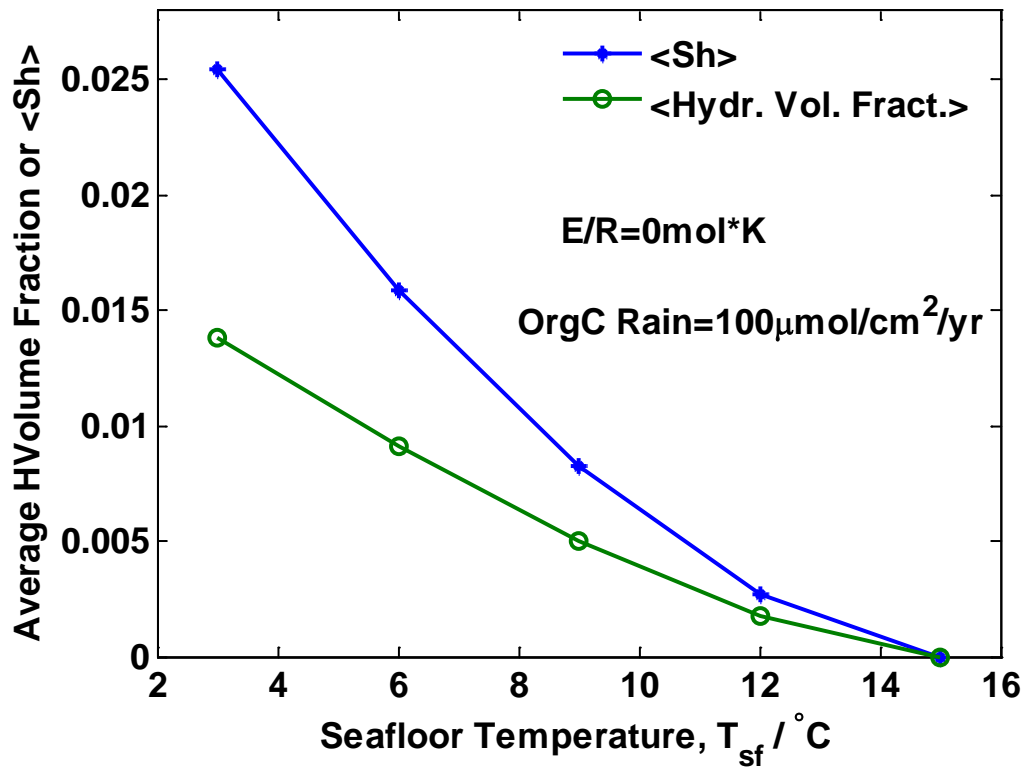


Figure 4.3.1. 4 Average Sh and Average Volume Fraction vs Seafloor Temperature.

$E/R=0$, and α_0 Remains Constant. The parameters are listed for every seafloor temperature points calculated.

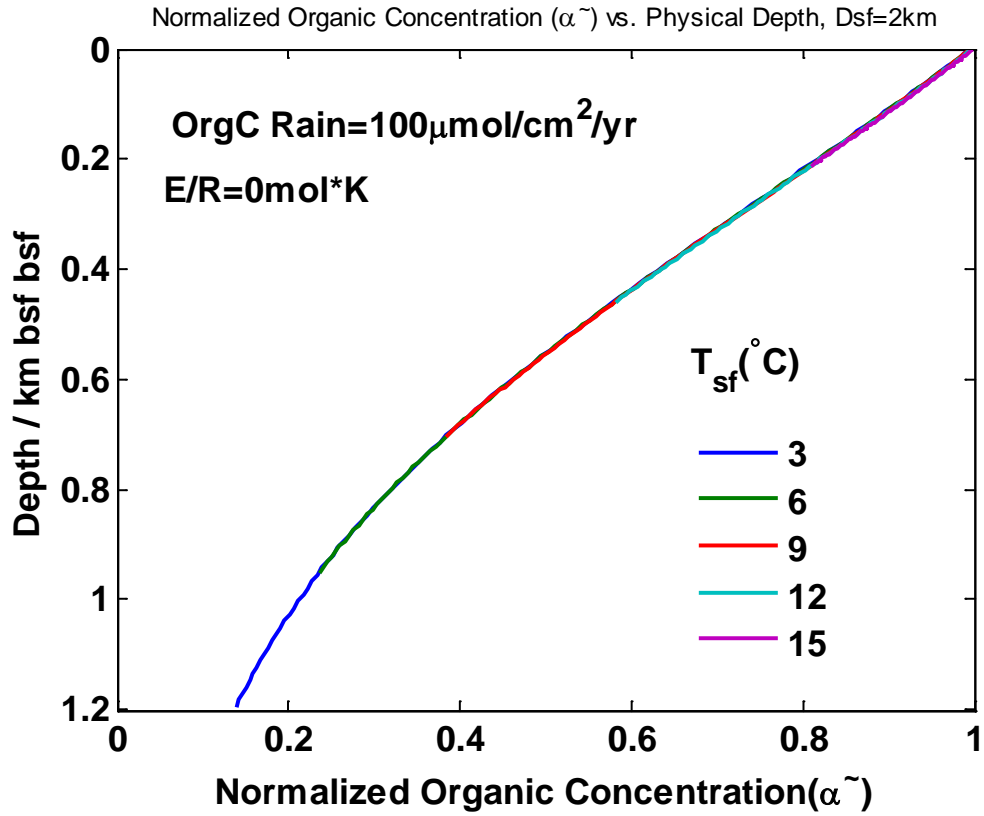


Figure 4.3.1. 5 Normalized Organic Concentration Profile.

E/R=0, and α_0 Remains Constant. Curves for different T_{sf} values are overlapping on each other, because the organic decay is dependent on $(1 + \gamma)N_{t\phi}Pe_1 / Da$, which remains constant, if E=0.

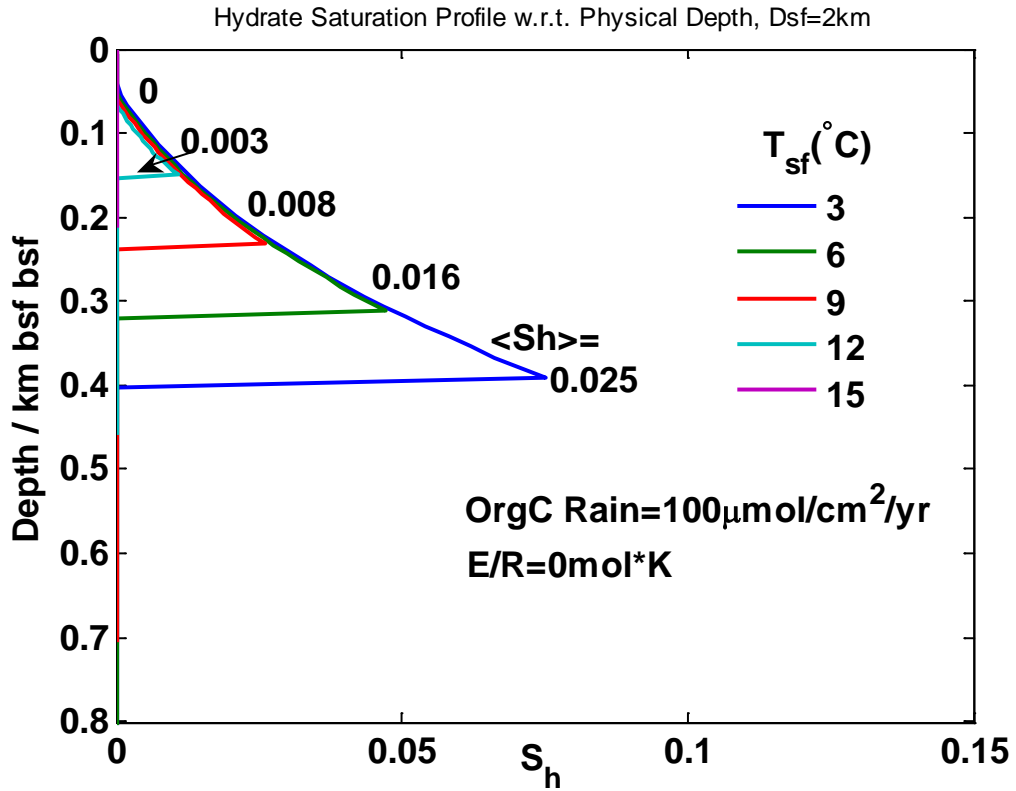


Figure 4.3.1. 6 Hydrate Saturation Profile.

$E/R=0$, and α_0 Remains Constant. The Average Hydrate Saturations (in the GHSZ) are marked for each curve.

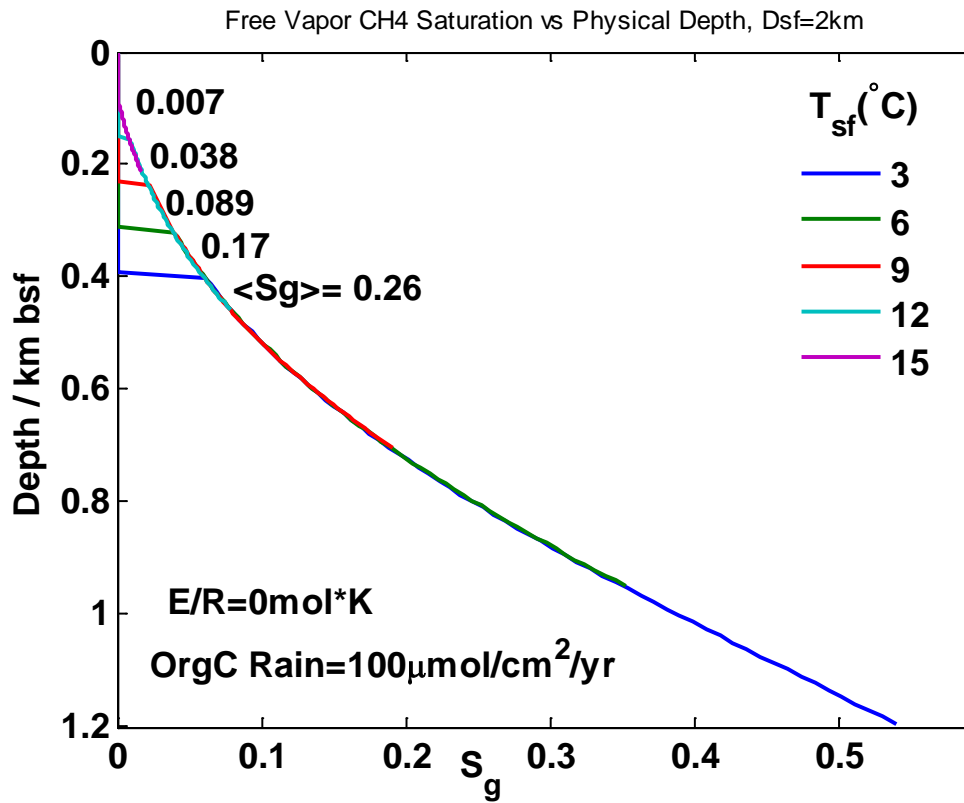


Figure 4.3.1. 7 Gas Phase Saturation Profile.

$E/R=0$, and α_0 Remains Constant.

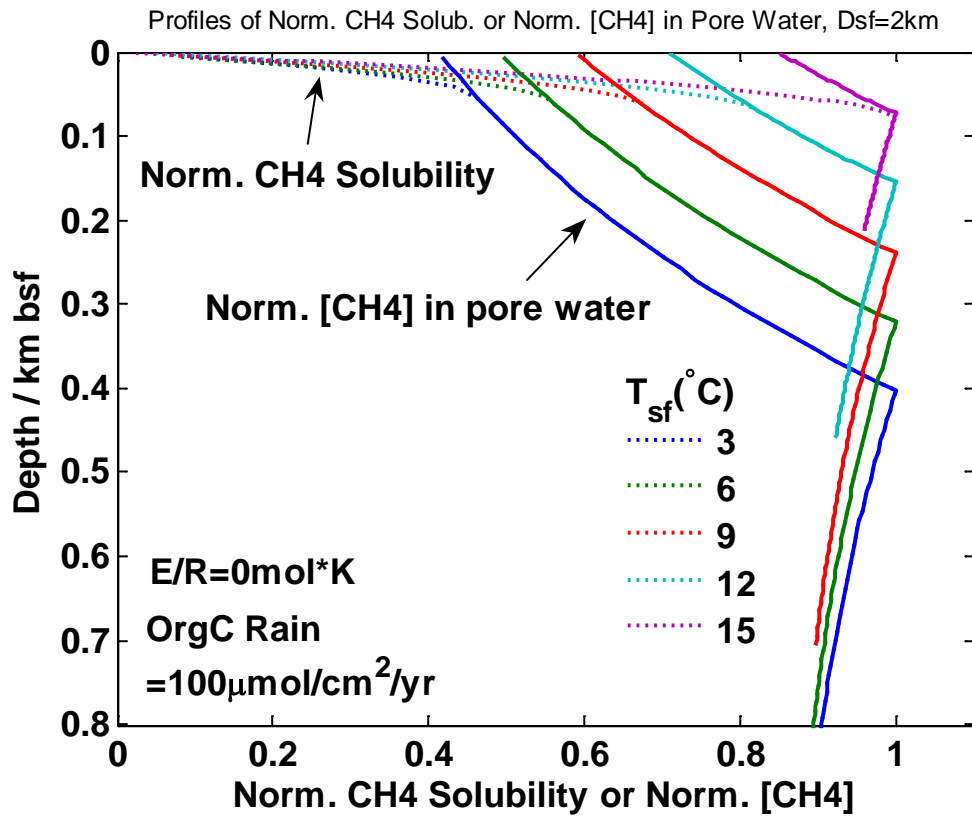


Figure 4.3.1. 8 Normalized Methane Concentration in Pore Water Profile, and Normalized Methane Solubility Profile.

$E/R=0$, and α_0 Remains Constant. The parameters are listed for each curve.

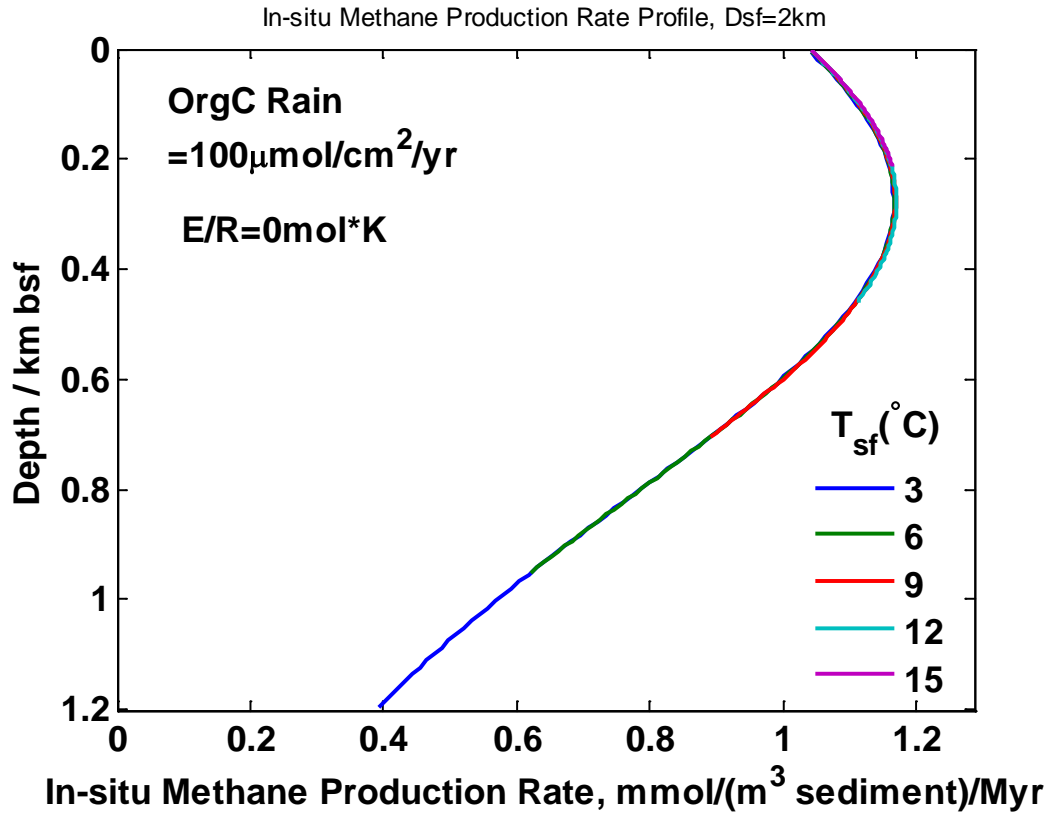


Figure 4.3.1. 9 In-situ Methane Production Rate Profile.

E/R=0, and α_0 Remains Constant. The parameters are listed for each curve. The unit of In-situ Methane Production Rate is mmol/(m³ sediment)/Myr, here sediment includes matrix and pore space. 1Myr= 1 million year. All curves are overlapping with each other.

4.3.2. Activation Energy E/R = 13400 mol*K, Seafloor Organic Rain = 10 \square mol/cm²/yr (Case I)

The change of seafloor organic concentration refers to Figure 4.2.6. The change of Reaction Rate Constant is as the following figure, following Arrhenius Law:

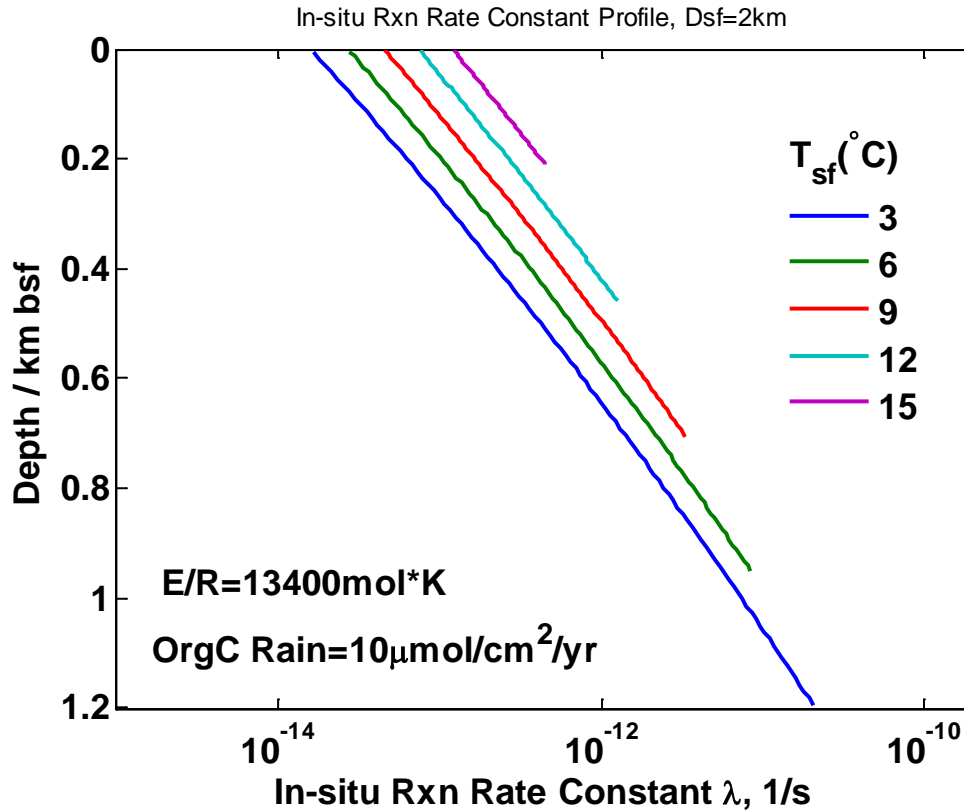


Figure 4.3.2. 1 In-situ Reaction Rate Constant Profile.

E/R=13400 mol*K. Assuming that Average Da is 10 when T_{sf} =3degC. Rate constant changes with increase of T_{sf} following Arrhenius Law.

It can be found out that the reaction rate constant varies in 3 order of magnitude from 0 – 1.2 km bsf, because of the temperature distribution in the sediment.

In Figure 4.3.2-2, the Hydrate Volume Fraction profiles for different seafloor temperatures are shown. Different from the *Base case0* in section 4.3.1, the hydrate volume fraction increases when T_{sf} increases from 3 deg C to 9 deg C. The Total Hydrate Amount increases from 0.63 to 0.96 m³/m², increased by around 52%.

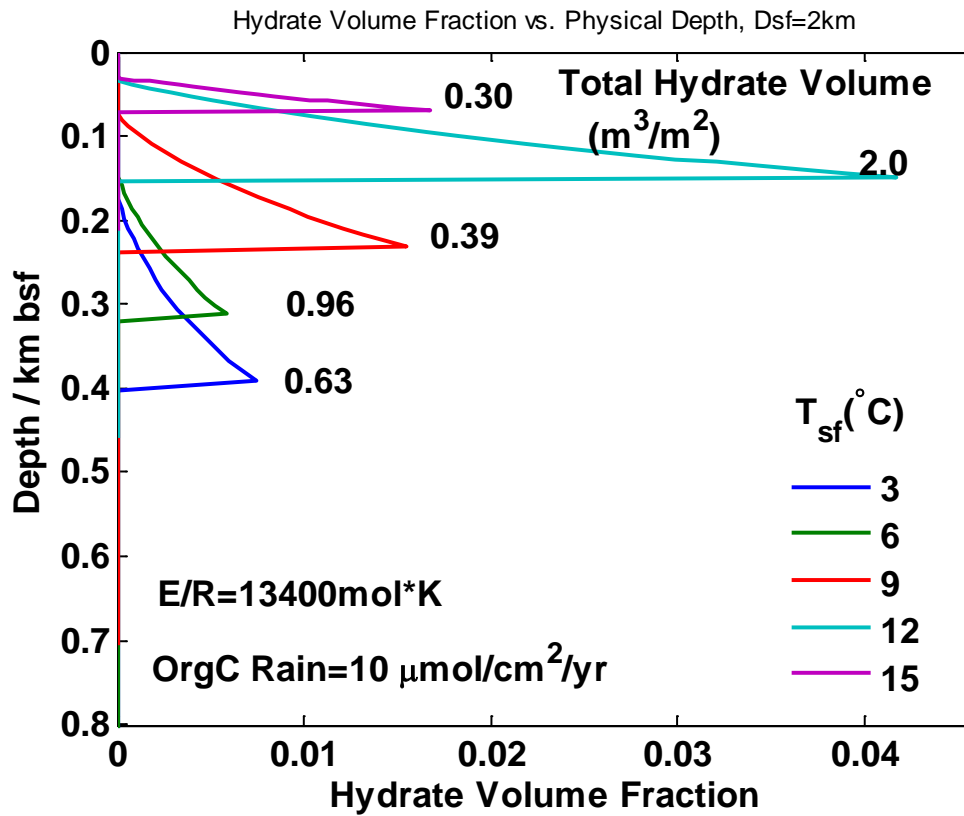


Figure 4.3.2. 2 Hydrate Volume Fraction Profile.

E/R=13400 mol*K, and α_0 changes according to case Organic Rain = 10 $\mu\text{mol}/\text{cm}^2/\text{yr}$. The Total Hydrate Amount (per unit seafloor area) are marked for each curve.

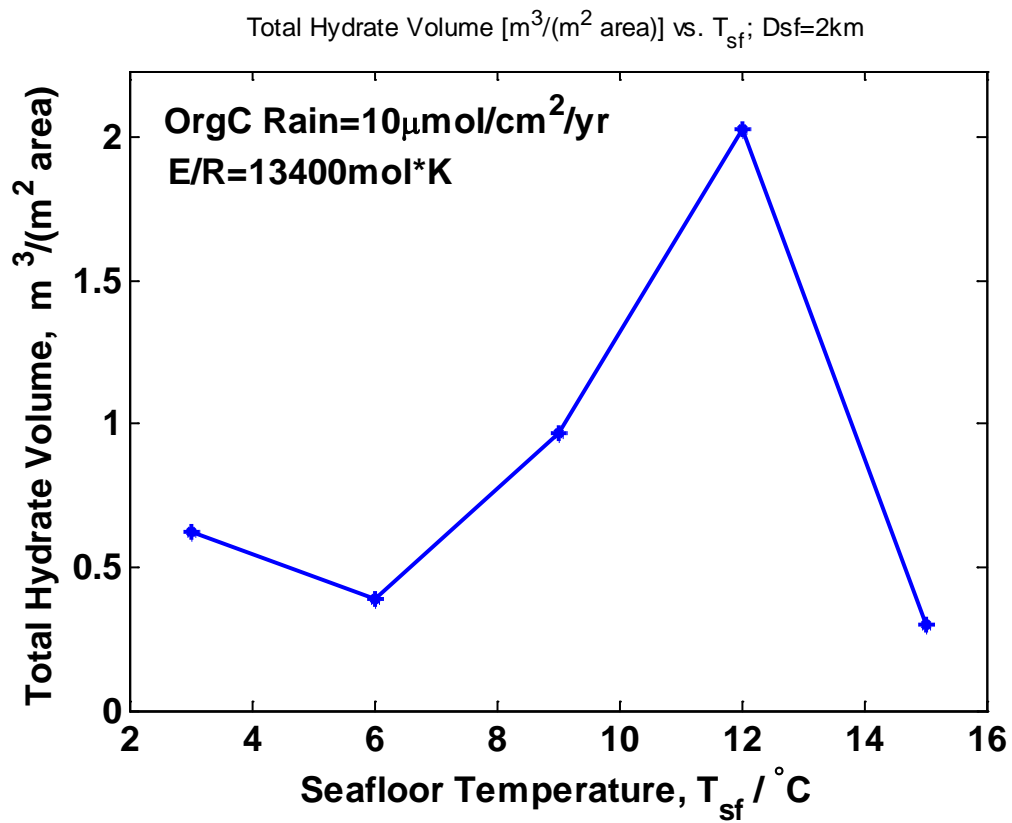


Figure 4.3.2. 3. Total Hydrate Amount (per unit seafloor area) vs Seafloor Temperature.

$E/R=13400 \text{ mol}\cdot\text{K}$, and α_0 changes according to case Organic Rain = $10 \mu\text{mol}/\text{cm}^2/\text{yr}$. The parameters are listed for every seafloor temperature points calculated.

Average Hydrate Saturation, or Average Volume Fraction, vs. T_{sf} ; $D_{sf}=2\text{km}$

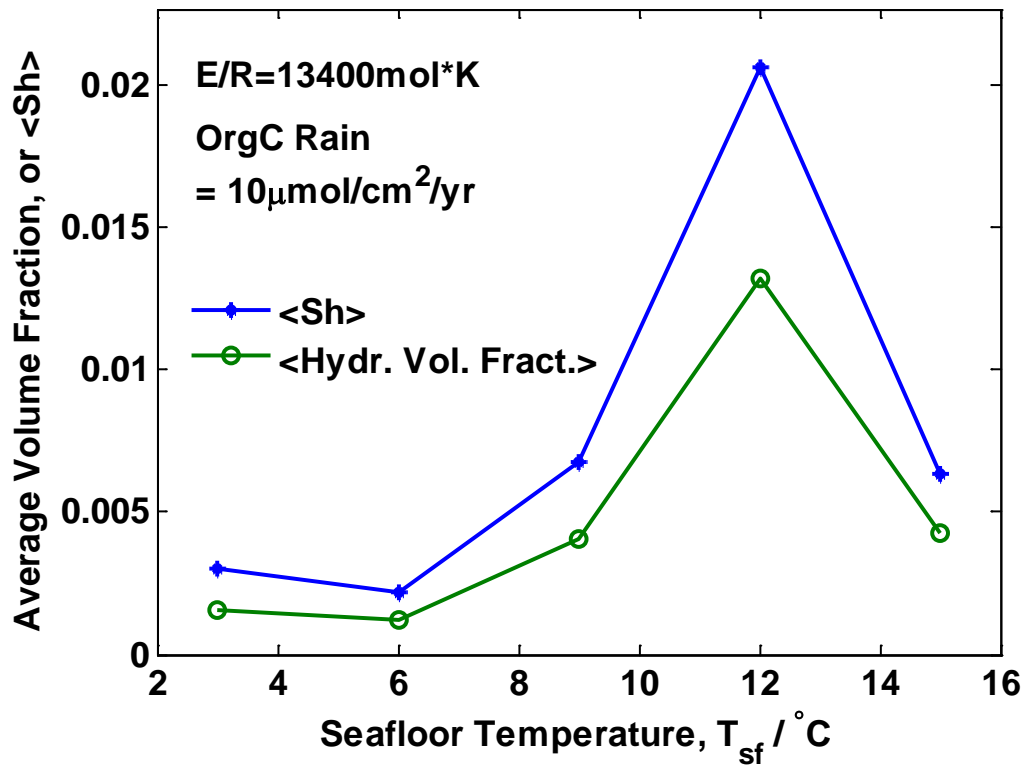


Figure 4.3.2. 4 Average S_h and Average Volume Fraction vs Seafloor Temperature.

$E/R=13400\text{ mol}\cdot\text{K}$, and α_0 changes according to case Organic Rain = $10\mu\text{mol}/\text{cm}^2/\text{yr}$. The parameters are listed for every seafloor temperature points calculated.

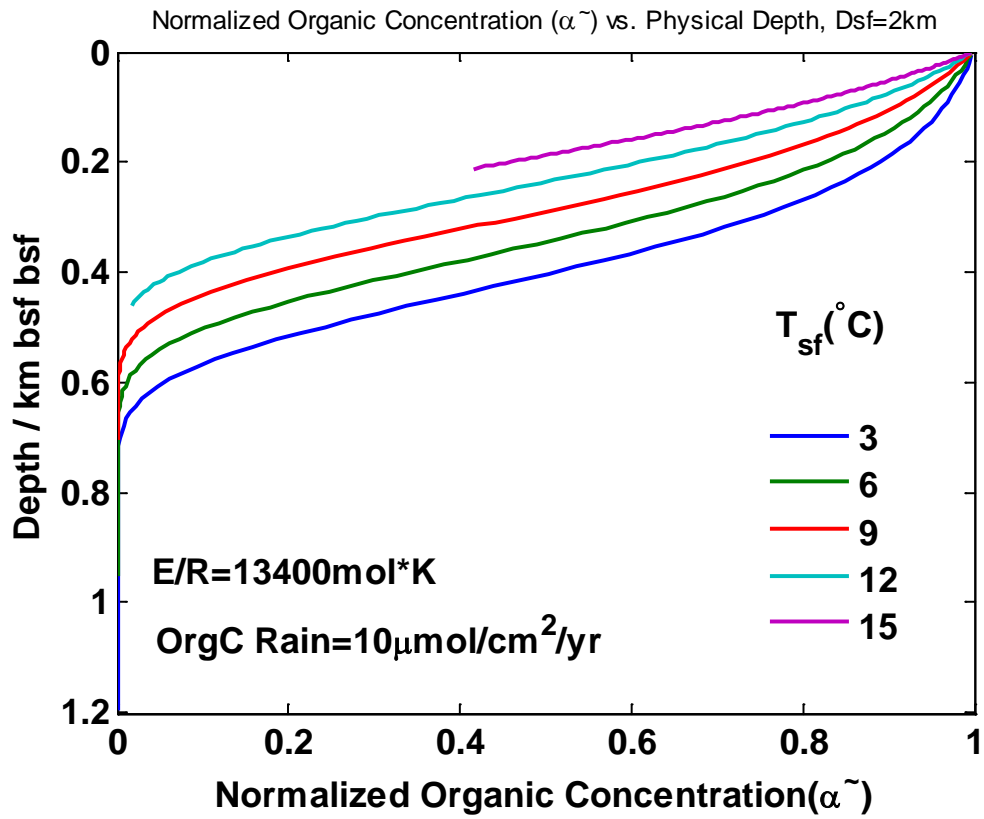
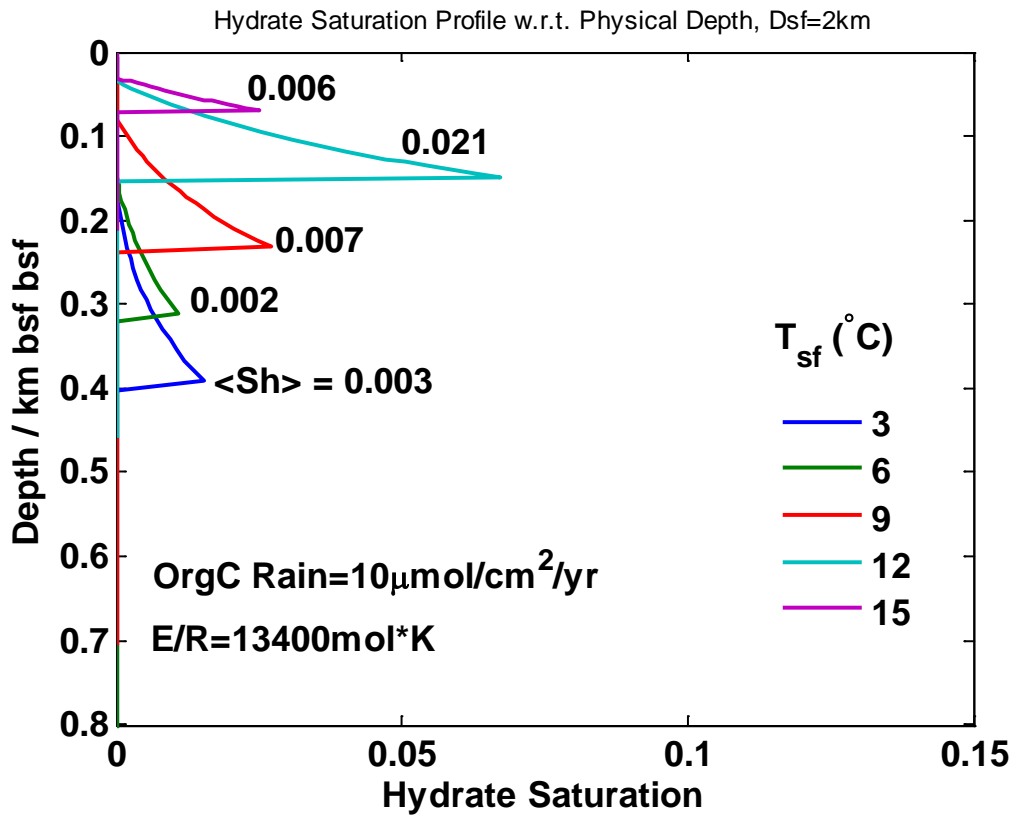


Figure 4.3.2. 5 Normalized Organic Concentration Profile.

$E/R=13400 \text{ mol} \cdot K$, and α_0 changes according to case Organic Rain = $10 \mu\text{mol}/\text{cm}^2/\text{yr}$.



$E/R=13400 \text{ mol}^*K$, and α_0 changes according to case Organic Rain = $10 \mu\text{mol}/\text{cm}^2/\text{yr}$. The Average Hydrate Saturations (in the GHSZ) are marked for each curve.

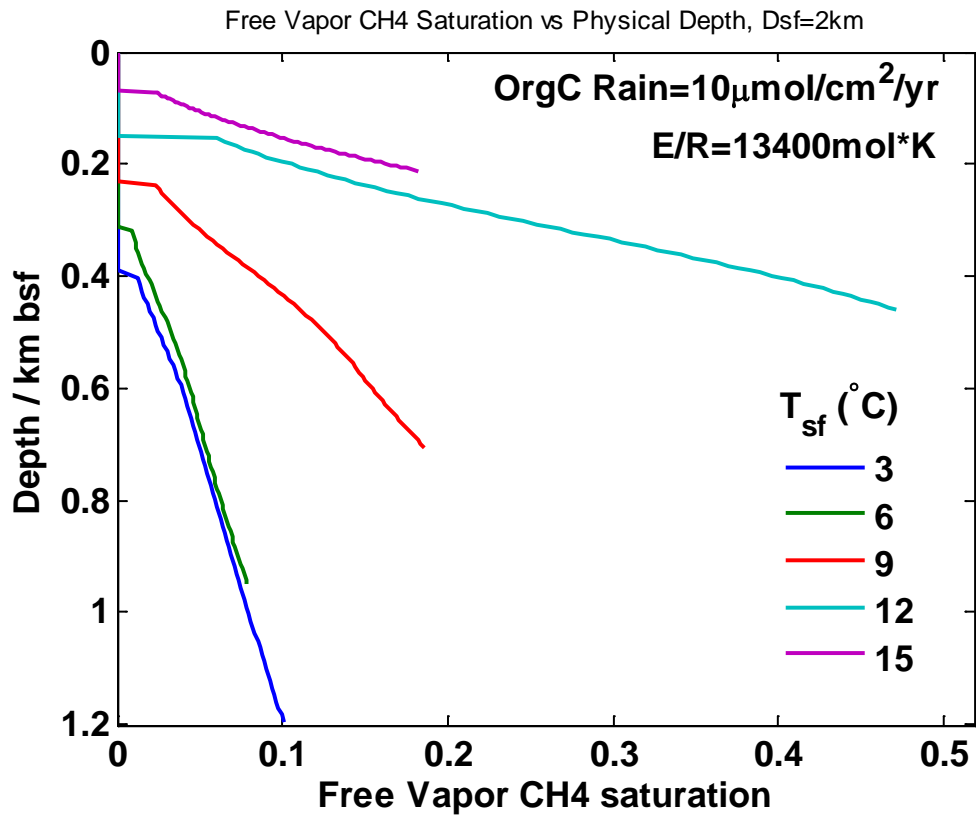


Figure 4.3.2. 7 Gas Phase Saturation Profile.

E/R=13400 mol*K, and α_0 changes according to case Organic Rain = 10 μmol/cm²/yr.

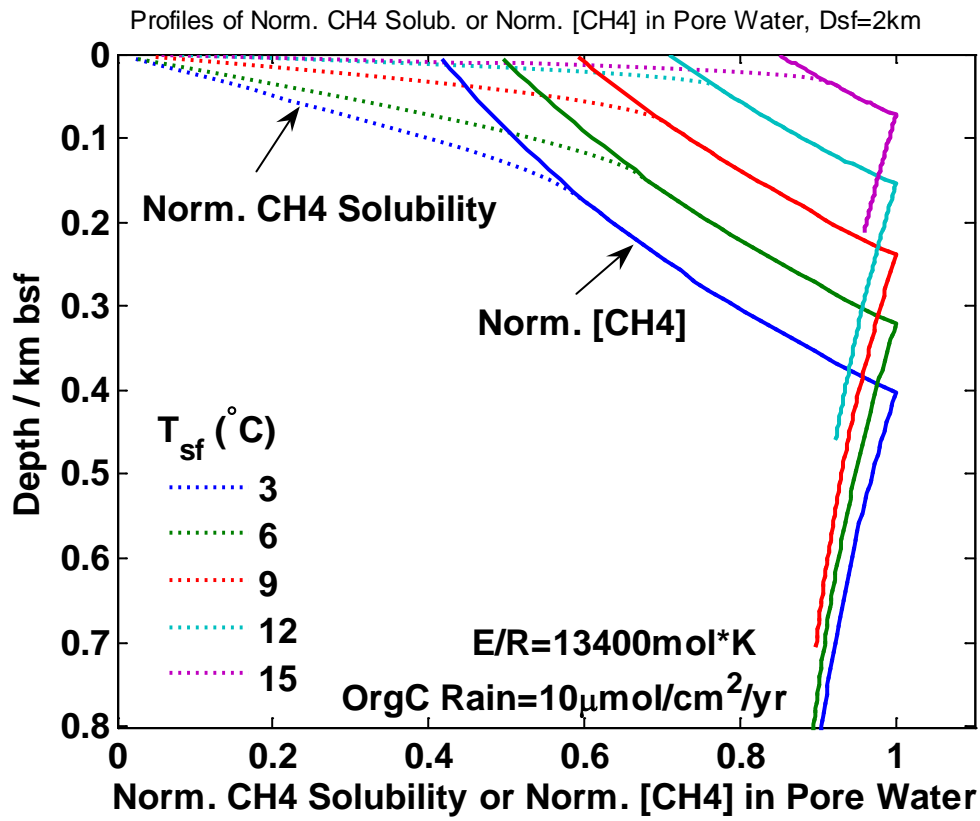


Figure 4.3.2. 8 Normalized Methane Concentration in Pore Water Profile, and Normalized Methane Solubility Profile.

$E/R=13400\text{ mol}\cdot\text{K}$, and α_0 changes according to case Organic Rain = $10\mu\text{mol}/\text{cm}^2/\text{yr}$. The parameters are listed for each curve.

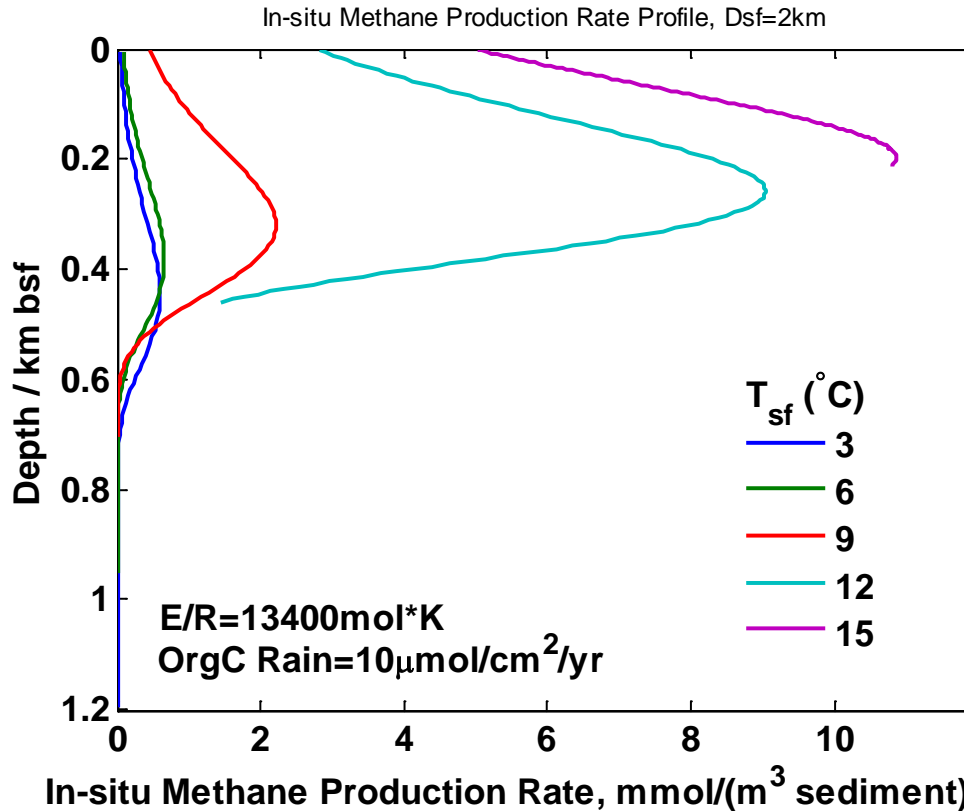


Figure 4.3.2. 9 In-situ Methane Production Rate Profile.

E/R=13400 mol*K, and α_0 changes according to case Organic Rain = 10 $\mu\text{mol}/\text{cm}^2/\text{yr}$. The parameters are listed for each curve. The unit of In-situ Methane Production Rate is $\text{mmol}/(\text{m}^3 \text{ sediment})/\text{Myr}$, here sediment includes matrix and pore space.

The In-situ Methane Production Rate increases when T_{sf} increases from 3 deg C to 9 deg C, this can partly explain why Total Hydrate Amount increases when T_{sf} increases.

4.3.3. Activation Energy E/R = 13400 mol*K, Seafloor Organic Rain = 30 $\mu\text{mol}/\text{cm}^2/\text{yr}$ (Case II)

Rate constant profile has been depicted in the beginning of § 4.3.2. The Hydrate Volume Fraction profiles presented in the following figure, shows that Total Hydrate Amount increases from 2.51 to 3.25 m^3/m^2 , when T_{sf} increases

from 3 deg C to 9 deg C, or increases by around 29.5%.

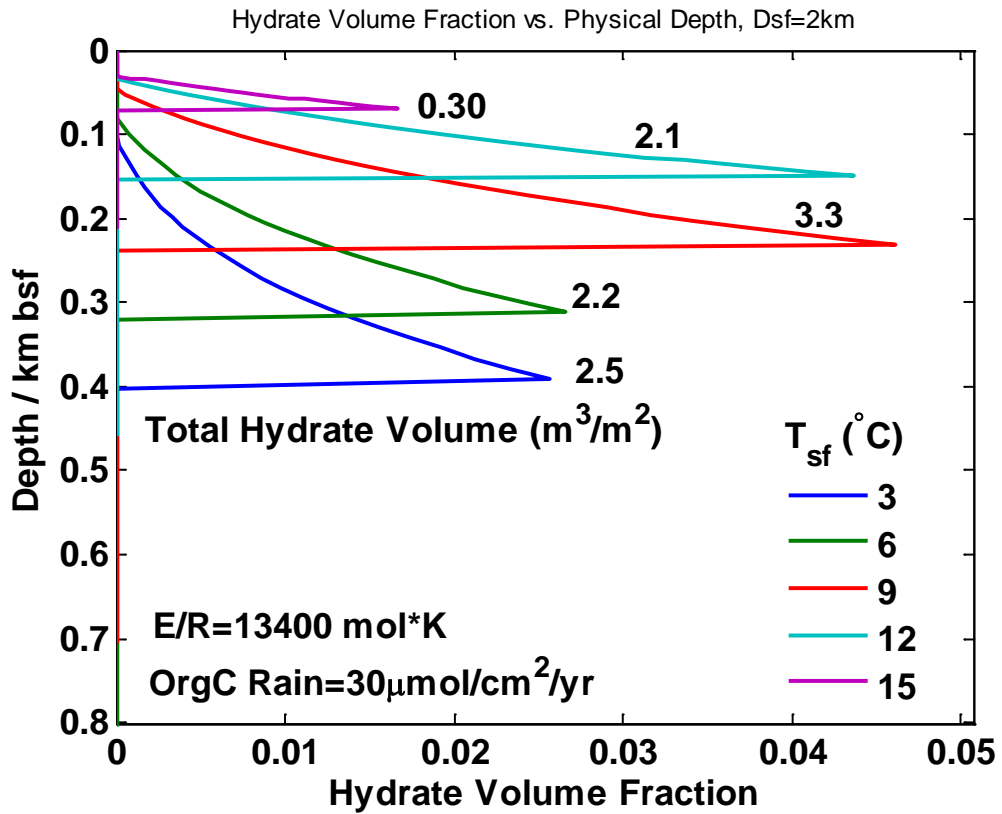


Figure 4.3.3. 1 Hydrate Volume Fraction Profile.

$E/R=13400 \text{ mol}^*K$, and α_0 changes according to case Organic Rain = $30 \mu\text{mol}/\text{cm}^2/\text{yr}$. The Total Hydrate Amount (per unit seafloor area) are marked for each curve.

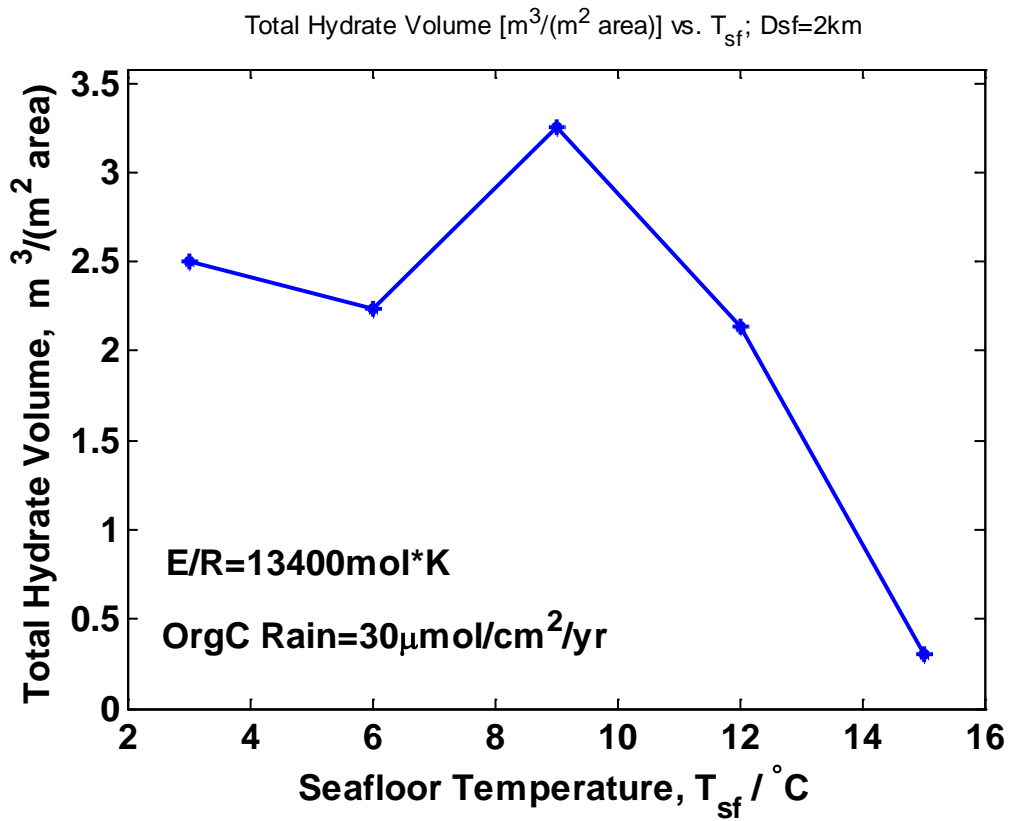


Figure 4.3.3. 2 Total Hydrate Amount (per unit seafloor area) vs Seafloor Temperature.

$E/R=13400 \text{ mol}\cdot\text{K}$, and α_0 changes according to case Organic Rain = $30 \mu\text{mol}/\text{cm}^2/\text{yr}$. The parameters are listed for every seafloor temperature points calculated.

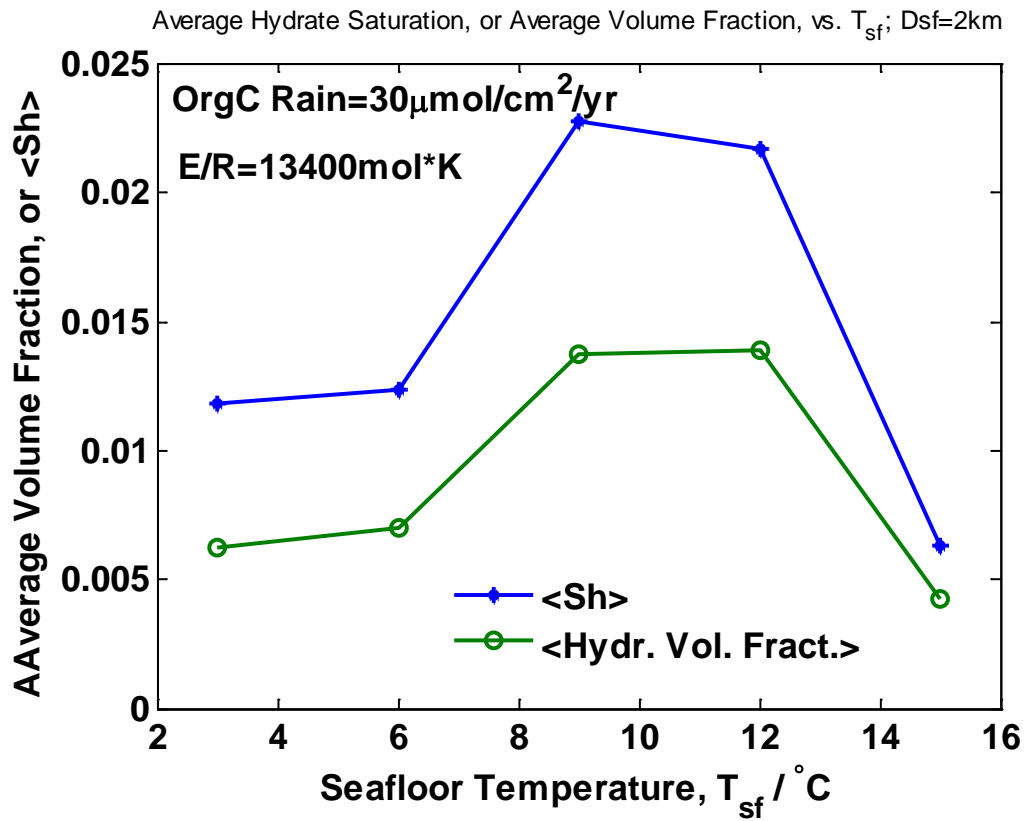


Figure 4.3.3. 3 Average Sh and Average Volume Fraction vs Seafloor Temperature.

$E/R=13400 \text{ mol}\cdot\text{K}$, and α_0 changes according to case Organic Rain = $30 \mu\text{mol}/\text{cm}^2/\text{yr}$. The parameters are listed for every seafloor temperature points calculated.

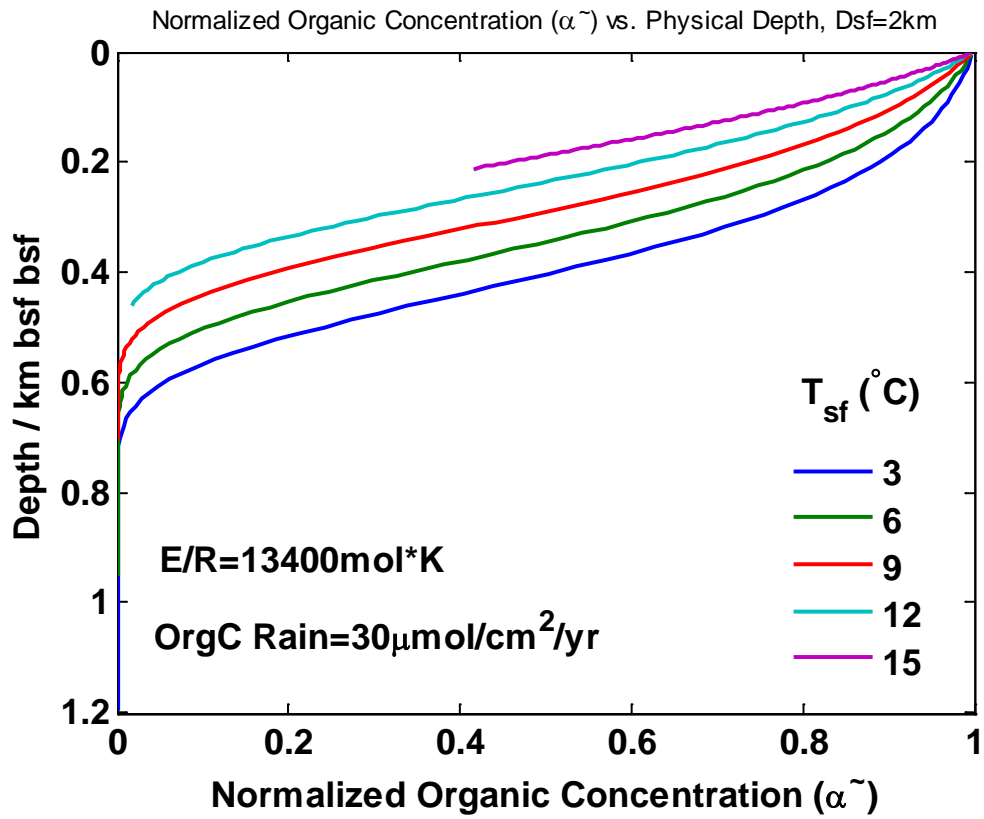


Figure 4.3.3. 4 Normalized Organic Concentration Profile.

$E/R=13400\text{ mol}\cdot\text{K}$, and α_0 changes according to case Organic Rain = $30\mu\text{mol}/\text{cm}^2/\text{yr}$.

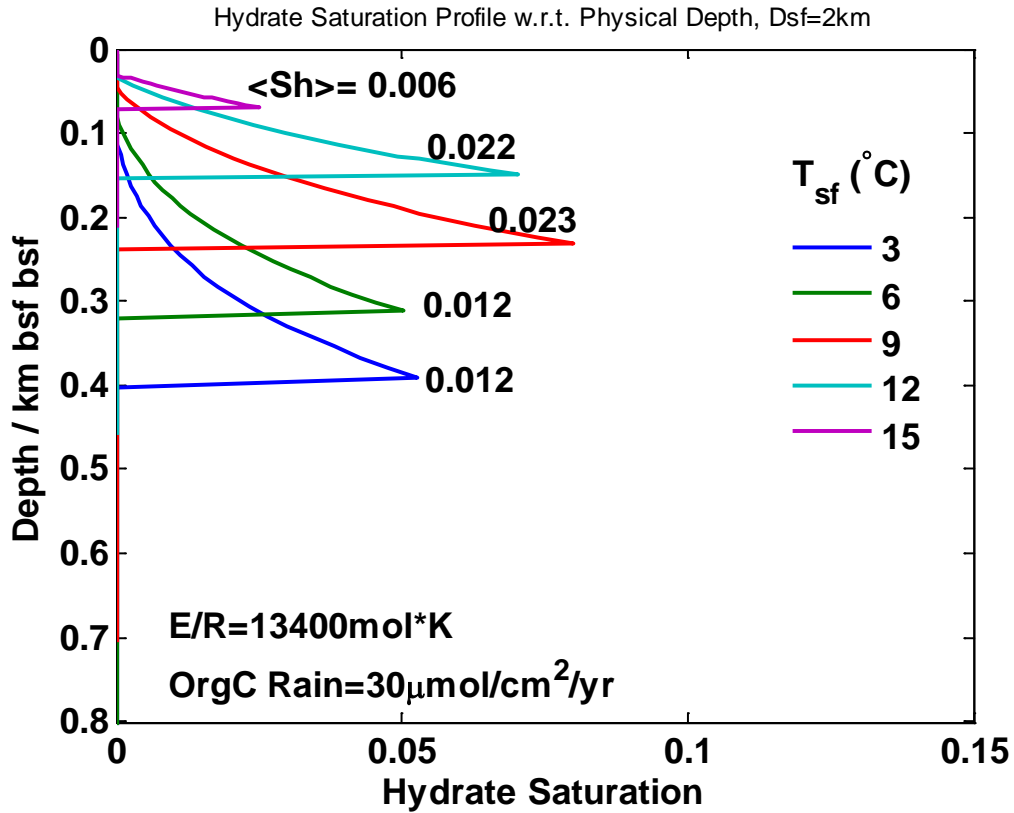


Figure 4.3.3. 5 Hydrate Saturation Profile.
E/R=13400 mol*K, and α_0 changes according to case Organic Rain = 30 μmol/cm²/yr. The Average Hydrate Saturations (in the GHSZ) are marked for each curve.

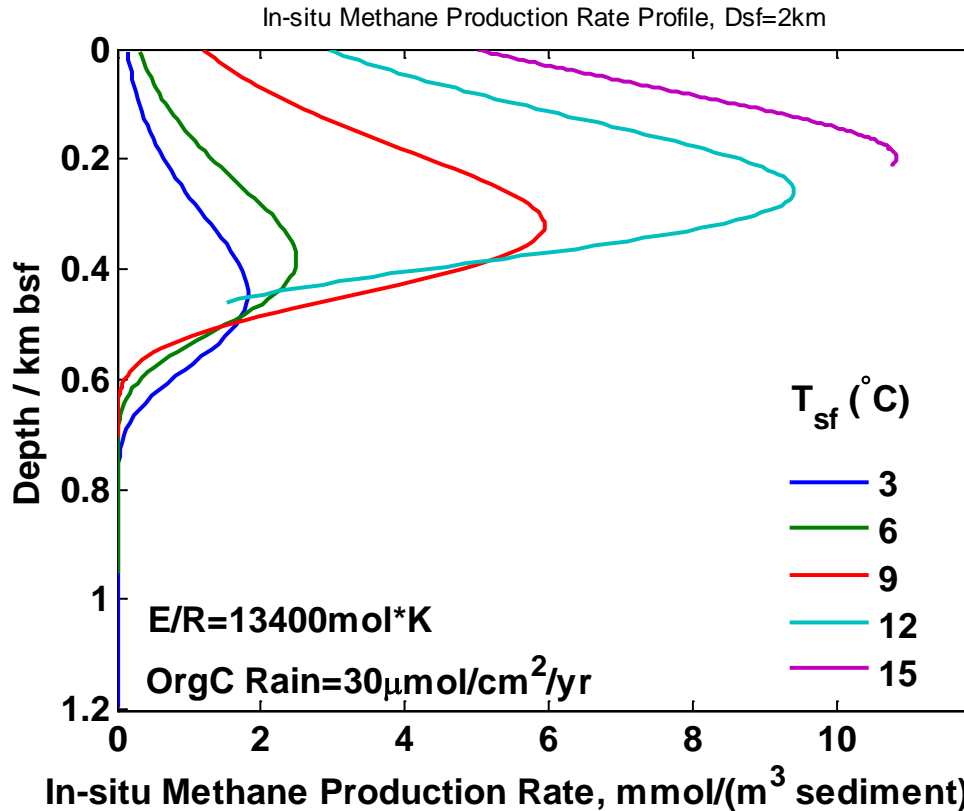


Figure 4.3.3. 6 In-situ Methane Production Rate Profile.

$E/R=13400 \text{ mol}\cdot\text{K}$, and α_0 changes according to case Organic Rain = $30 \mu\text{mol}/\text{cm}^2/\text{yr}$. The parameters are listed for each curve. The unit of In-situ Methane Production Rate is $\text{mmol}/(\text{m}^3 \text{ sediment})/\text{Myr}$, here sediment includes matrix and pore space.

4.4. Contour Plots for Remaining Ratio of Total Hydrate Amount k

The contour plots for the Remaining Ratio of Total Hydrate Amount when T_{sf} rises from 3 deg C to 9 deg C $k = V_{h,9C} / V_{h,3C}$ are presented in the following.

Figure 4.4.1 is the *Base scenery I*, with $E=0$, and constant α_0 . Figure 4.4.2 is *Base scenery II*, with $E/R=13400 \text{ mol}\cdot\text{K}$, while α_0 still remains constant. From Figure 4.4.1, we know that the Total Hydrate Amount decreases much, and in most cases, $V_{h,9C}$ is 0~35% of $V_{h,3C}$. For example, at *Base case0* shown in the figure, i.e., $Pe_{1,3C}=1.0$ and $Da_{3C} = 10$, the result is $k=0.21$ (or 21%). From

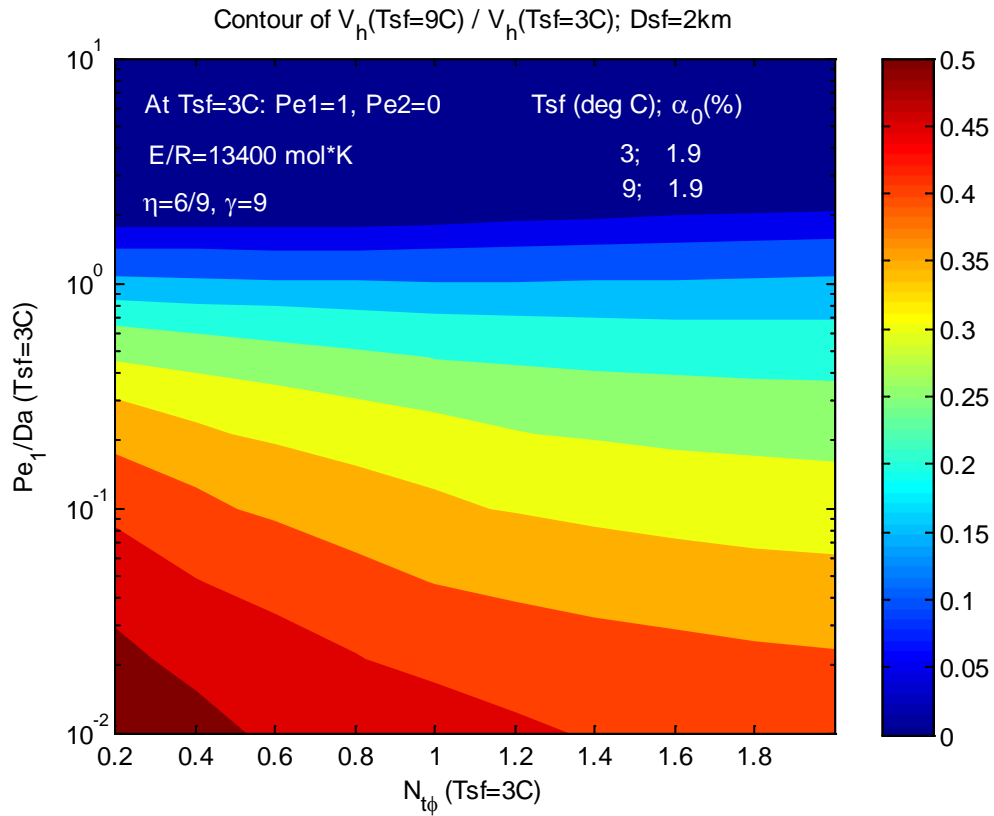
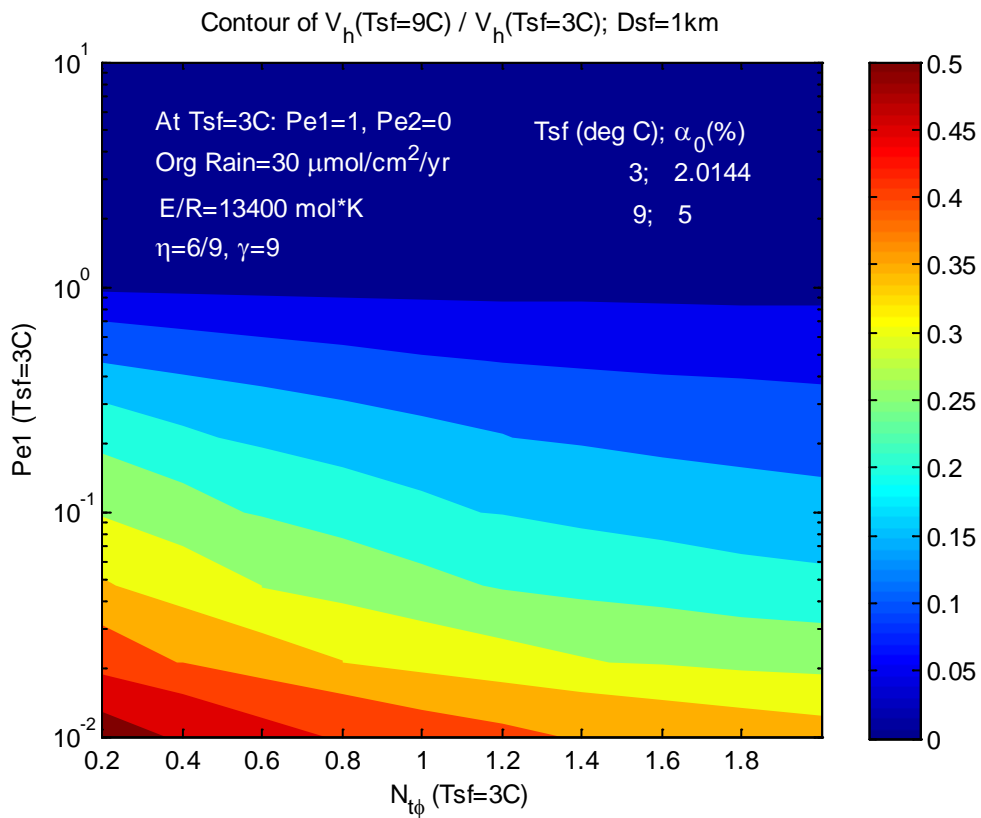
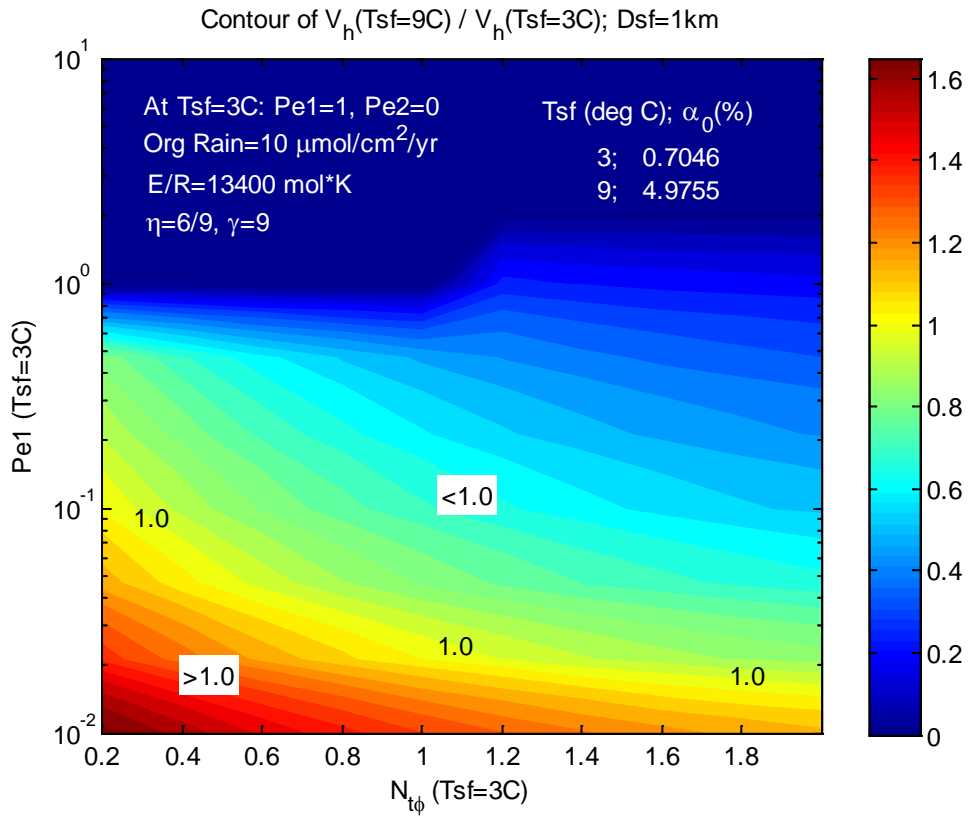


Figure 4.4. 2 Contour Plot for $k = V_{h,9C} / V_{h,3C}$.

$E/R=13400 \text{ mol}\cdot\text{K}$, while α_0 Remains Constant (*Base scenery II*). The parameters are listed for every seafloor temperature points calculated.

What's more, as discussed before, the seafloor organic concentration α_0 may increase due to the decreased oxygen concentration. By applying the changing α_0 models, the remaining Total Hydrate Amount ratios are obtained, and results are presented below.



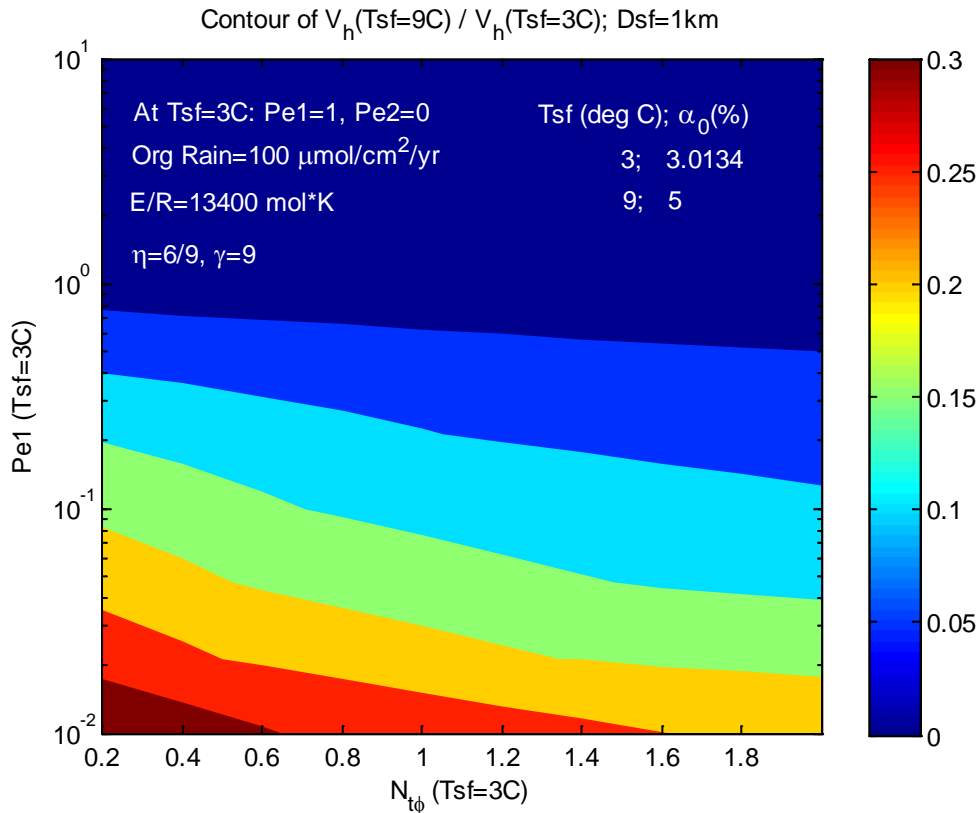
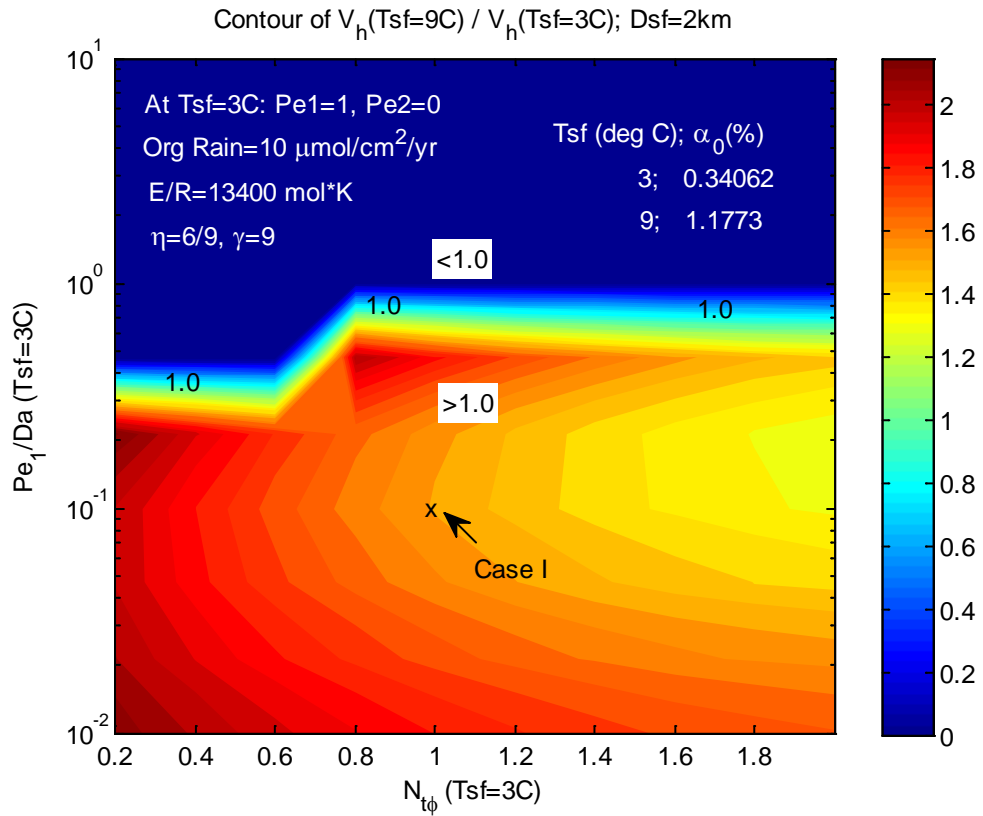
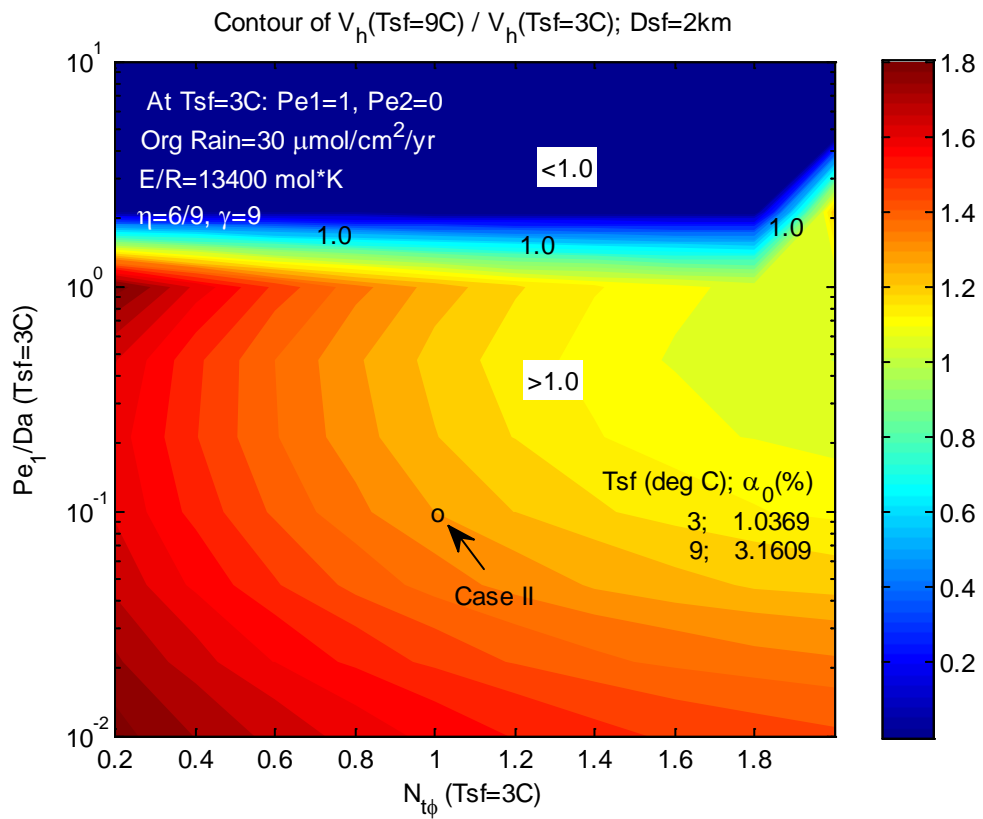


Figure 4.4. 3 Contour Plot for $k = V_{h,9C} / V_{h,3C} \cdot D_{sf} = 1.0 \text{ km}$.

$E/R=13400 \text{ mol}\cdot\text{K}$, and α_0 changes according to case (a) Organic Rain = $10 \mu\text{mol}/\text{cm}^2/\text{yr}$; (b) Organic Rain = $30 \mu\text{mol}/\text{cm}^2/\text{yr}$; (c) Organic Rain = $100 \mu\text{mol}/\text{cm}^2/\text{yr}$. The parameters are listed for every seafloor temperature points calculated. $k > 1.0$ means Total Hydrate Amount V_h increases when T_{sf} increases from 3 deg C to 9 deg C. The boundary of $k = 1.0$ is labeled, and zones for $k > 1.0$ and that for $k < 1.0$ are indicated in the contour plot. The condition for $k > 1.0$ is (approximately) $N_{t\phi 0} Pe_{10} / \bar{D} a_0 < 0.03$, where subscript 0 means that the parameters are for $T_{sf} = T_{sf0} = 3 \text{ deg C}$.



(a) Organic Rain = $10 \mu\text{mol}/\text{cm}^2/\text{yr}$.



(b) Organic Rain = $30 \mu\text{mol}/\text{cm}^2/\text{yr}$.

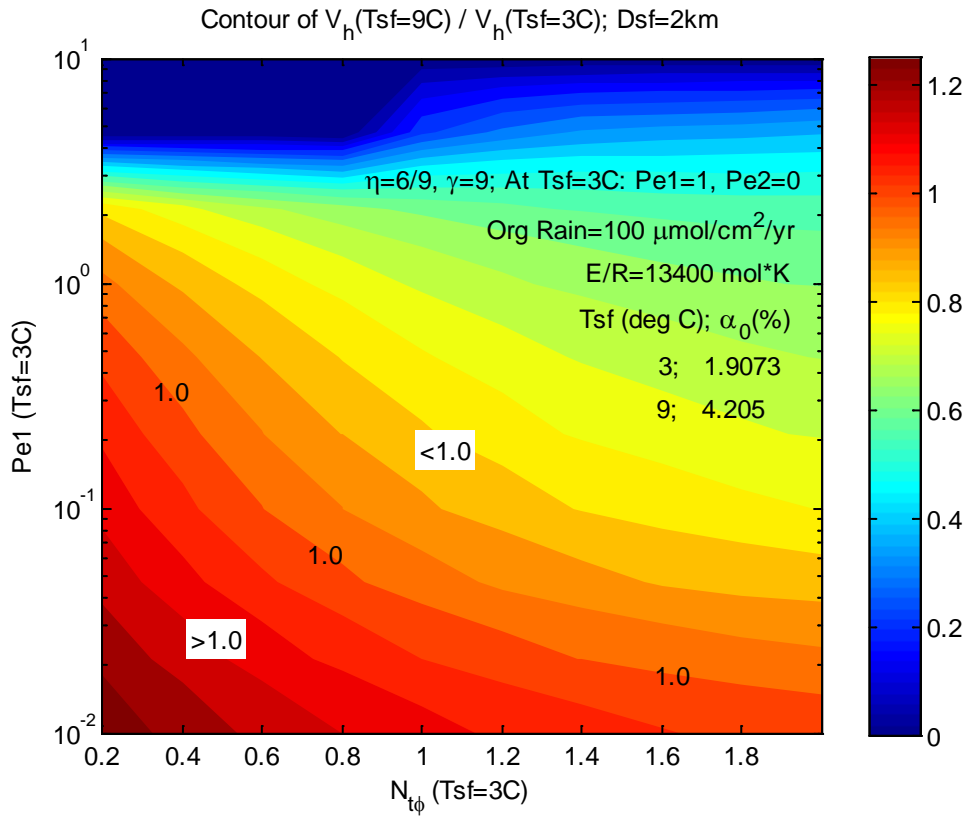
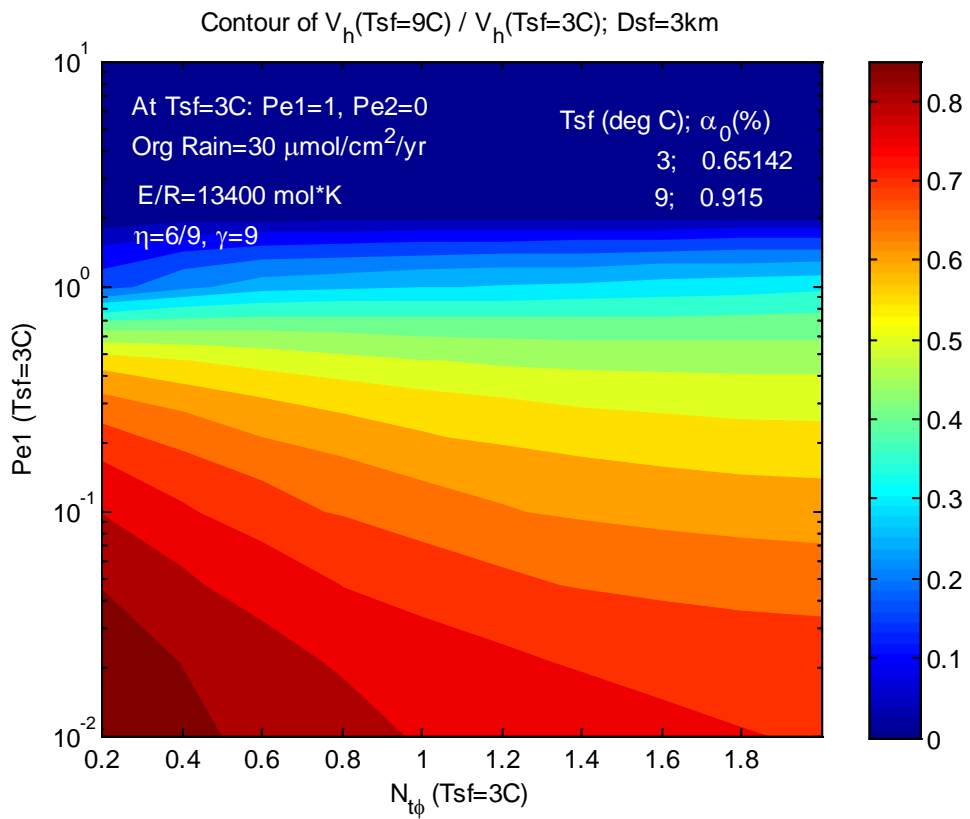
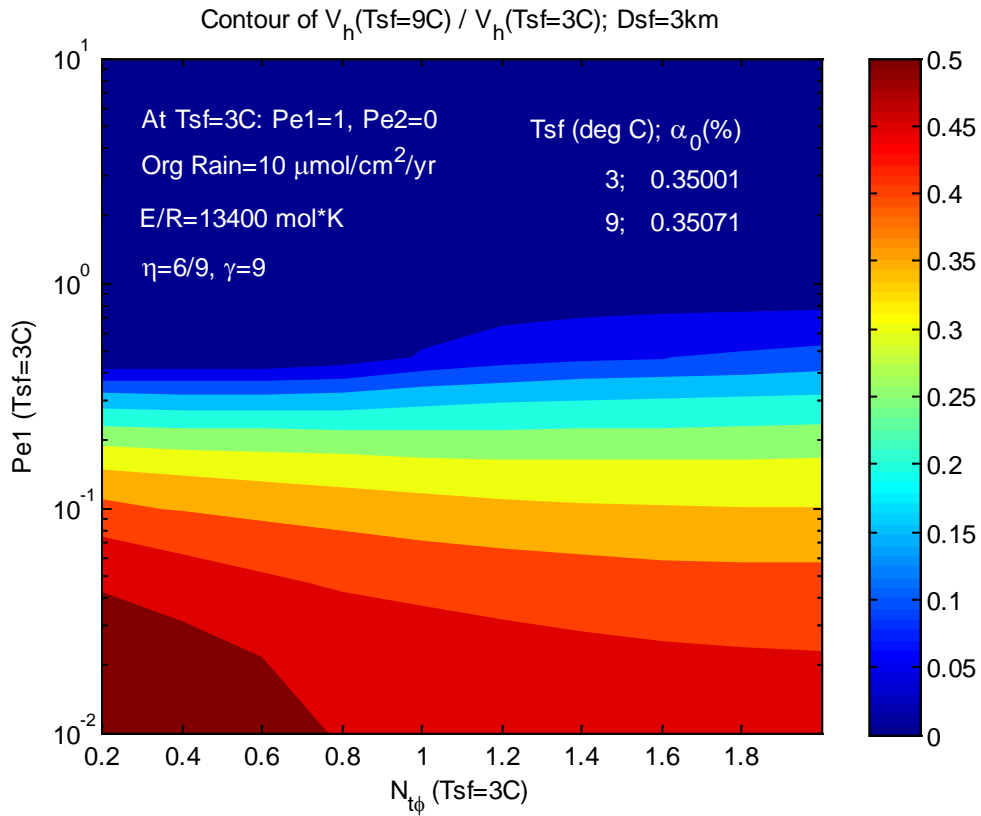


Figure 4.4. 4 Contour Plot for $k = V_{h,9\text{C}} / V_{h,3\text{C}} \cdot D_{\text{sf}} = 2.0 \text{ km}$.

(a) Organic Rain = 10 $\mu\text{mol}/\text{cm}^2/\text{yr}$; (b) Organic Rain = 30 $\mu\text{mol}/\text{cm}^2/\text{yr}$; (c) Organic Rain = 100 $\mu\text{mol}/\text{cm}^2/\text{yr}$. E/R=13400 mol*K, and α_0 changes according to case a, b, c. The parameters are listed for every seafloor temperature points calculated. The condition for $k > 1.0$ is (approximately)

$$N_{t\phi} Pe_{10} / \bar{Da}_0 < 0.04.$$



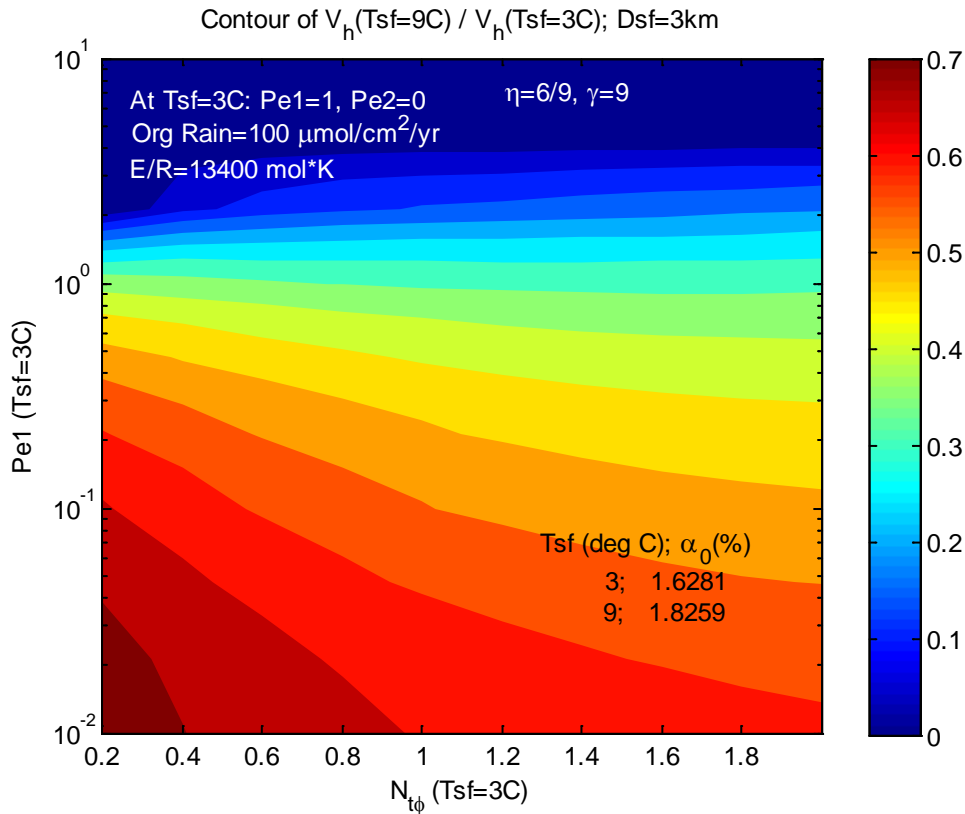


Figure 4.4. 5 Contour Plot for $k = V_{h,9C} / V_{h,3C} \cdot D_{sf} = 3.0 \text{ km}$.

(a) Organic Rain = 10 $\mu\text{mol}/\text{cm}^2/\text{yr}$; (b) Organic Rain = 30 $\mu\text{mol}/\text{cm}^2/\text{yr}$; (c) Organic Rain = 100 $\mu\text{mol}/\text{cm}^2/\text{yr}$. $E/R=13400 \text{ mol}\cdot\text{K}$, and α_0 changes according to case a,b,c. The parameters are listed for every seafloor temperature points calculated.

It is shown that:

(1) Very obviously, for the same seafloor depth, the higher the ratio of seafloor organic concentration increase is, the larger k will be.

(2) For the same sceneries (with same seafloor depth, organic rain, none-0-activation energy, and so on), at the same $N_{t\phi 0}$, the lower $Pe_{10}/\bar{D}a_0$ is, the larger k will be. (Note: subscript 0 means parameter are defined at $T_{sf}=3 \text{ deg C}$). It's because that $Pe_{10}/\bar{D}a_0$ is an indicator of (convection flux/reaction rate) in the system. Lower $Pe_{10}/\bar{D}a_0$ indicates that the system is dominated

more by reaction than done by convection, and when the seafloor temperature rises, reaction rate increases, so it's more possible to get a larger k .

The results are listed in Table 4.4-1. We can find out that the Remaining Ratio of Total Hydrate Amount, k , is different in different sceneries. Definitely, there are many cases for $k > 1.0$; or in some other cases, k may be much higher than 0.5, e.g., for $D_{sf} = 3.0$ km, and $R_{ain} = 30$, $0 < k < 0.85$, which is pretty high to remain enough amount of hydrate.

Table 4.4.1. Results of Different Sceneries

E/R (mol*K)	D_{sf} (km)	Seafloor OrgRain ($\mu\text{mol}/\text{cm}^2/\text{yr}$)	Org Conc change $\alpha_{0,9C} / \alpha_{0,3C}$	Remaining Hydrate Ratio* (k)	Approx. Conditions for $k > 1.0 \pm 0.1$
0	2	Not considered (constant α_0)	1	$0 < k < 0.35$	
13400	2		1	$0 < k < 0.45$	
13400	1	10	7.1	<u>$0 < k < 1.6$</u>	$N_{i\phi} P e_{10} / \bar{D} a_0 < 0.03$
13400		30	2.48	$0 < k < 0.5$	
13400		100	1.66	$0 < k < 0.3$	
13400	2	10	3.45	<u>$0 < k < 2.1$</u>	$P e_{10} / \bar{D} a_0 < 0.25$
13400		30	3.05	<u>$0 < k < 1.8$</u>	$P e_{10} / \bar{D} a_0 < 1$
13400		100	2.2	<u>$0 < k < 1.2$</u>	$N_{i\phi} P e_{10} / \bar{D} a_0 < 0.04$
13400	3	10	1	$0 < k < 0.5$	
13400		30	1.405	<u>$0 < k < 0.85$</u>	
13400		100	1.122	<u>$0 < k < 0.7$</u>	

* Remaining Ratio of Total Hydrate Amount (k), from $T_{sf} = 3$ deg C to 9 deg C

4.5. Conclusions

It has been demonstrated that, in many sceneries, Total Hydrate Amount in the sediment, may increase when T_{sf} rises from 3 deg C to 9 deg C. Especially for seafloor depth = 2.0 km, in many sceneries, the Remaining Total Hydrate Amount can be higher than 100%, if parameters are in appropriate region. For seafloor depth = 1.0 km, when Seafloor Organic Rain = $10 \mu\text{mol}/\text{cm}^2/\text{yr}$, the Remaining Total Hydrate Amount can be higher than 100%. For seafloor depth = 3.0 km, though the Total Hydrate Amount doesn't increase, but the Remaining Ratio of Hydrate Amount may be as high as 85%, which means a large portion of hydrate is still reserved when T_{sf} rises to 9 deg C.

The steady state profiles of some cases are shown. When seafloor temperature increases, hydrate near bottom of GHSZ will dissociate, and diffusion loss increases because Pe_1 is decreased due to the decrease of Lt . This is why hydrate amount will decrease, if the reaction rate constant is constant and the seafloor organic concentration is constant, too.

However, it can be found out that the when the rate constant increases with the increase of seafloor temperature, the methane production rate is also increased in most positions beneath seafloor; what's more, when the seafloor

organic concentration is increased due to the decrease of oxygen concentration, there is more organic material than that in lower seafloor temperature case.

The overall effect of all these factors, is that, the Total Hydrate Amount may increase, or remain a large part of the present hydrate amount. Though it's quite difficult to consider all sceneries, and more work to consider many other sceneries will be helpful, our work indicates that the role hydrate played in the PETM event may be more important than was considered.

Chapter 5: Ocean sulfate as a factor affecting organic carbon and its interaction with methane and hydrate

5. 1. Introduction

The distribution of gas hydrate / free gas and abundance of hydrate, are dependent on location settings and parameters (Dickens et al., 1997; Xu and Ruppel, 1999; Davie and Buffett, 2001; Bhatnagar et al., 2007; Gu et al., 2011; Chatterjee, 2011). In most marine settings, CH₄ is from biogenic sources, and gas hydrate precipitates when CH₄ concentrations exceed solubility curve. Considering systems without external flux (i.e., biogenic gas sources), the gas hydrate abundance is dominated by several factors, mainly the organic carbon input for methanogenesis, ratio of flux of sedimentation to methanogenesis rate, etc. (Figure 5.1).

However, sulfate always exists in oceans everywhere around the world. It interacts with methane via anaerobic oxidation of methane (AOM reaction), and with particulate organic carbon (POC) via organoclastic reaction (denoted as POC reaction simply). Before the organic carbon is available for methanogenesis, it must pass through two zones in the shallow sediment, in which sulfate is consuming a portion of organic carbon. In the upper part of the GHSZ, three biogeochemical zones occur. The three zones are, POC reaction zone; AOM reaction zone (i.e., SMT zone); and Methanogenesis

zone. Sulfate interacts with POC via organoclastic reaction, and with methane via AOM reaction. The POC reaction zone, happens from near the seafloor to the SMT, dissolved $[SO_4^{2-}]$ decreases from seawater concentration (28 mM) at the seafloor to 0 at the bottom of SMT zone.

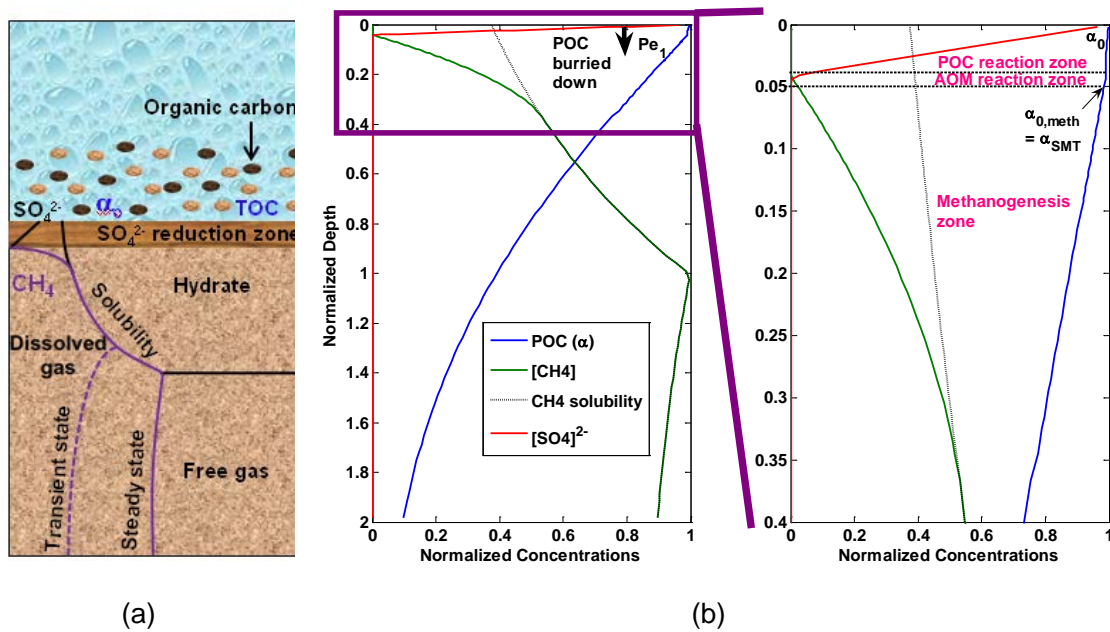


Figure 5. 1 (a). Schematic figure of sulfate and methane hydrate system (b). Schematic profiles of sulfate, POC, and methane concentrations in methane hydrate system. Left: normalized depth $0 < \tilde{z} < 2$; Right: zoomed in. Normalized depth $\tilde{z} = z/L_t$, $L_t = 450$ mbsf for Blake Ridge. Blue curve: POC (α); Red curve: $[SO_4]^{2-}$; Green curve: $[CH_4]$; dotted black curve: CH_4 solubility. $\alpha_{0,meth}$ --- the organic carbon content available for methanogenesis; α_{SMT} --- the organic carbon content at bottom of SMT. At low Da_{POC} , $\alpha_{0,meth} \approx 1$.

Ocean sulfate concentration is not a constant value in the past (Figure 5.2). In lakes, the sulfate concentration would be also quite low. From the past 100

Ma, the ocean sulfate concentration was keeping increasing from a low value of around 10 mM to 28 mM at present day. During PETM (55 Ma), it was about 10 ~ 15 mM. This could have affected the POC consumption and gas hydrate inventory via the organoclastic reactions.

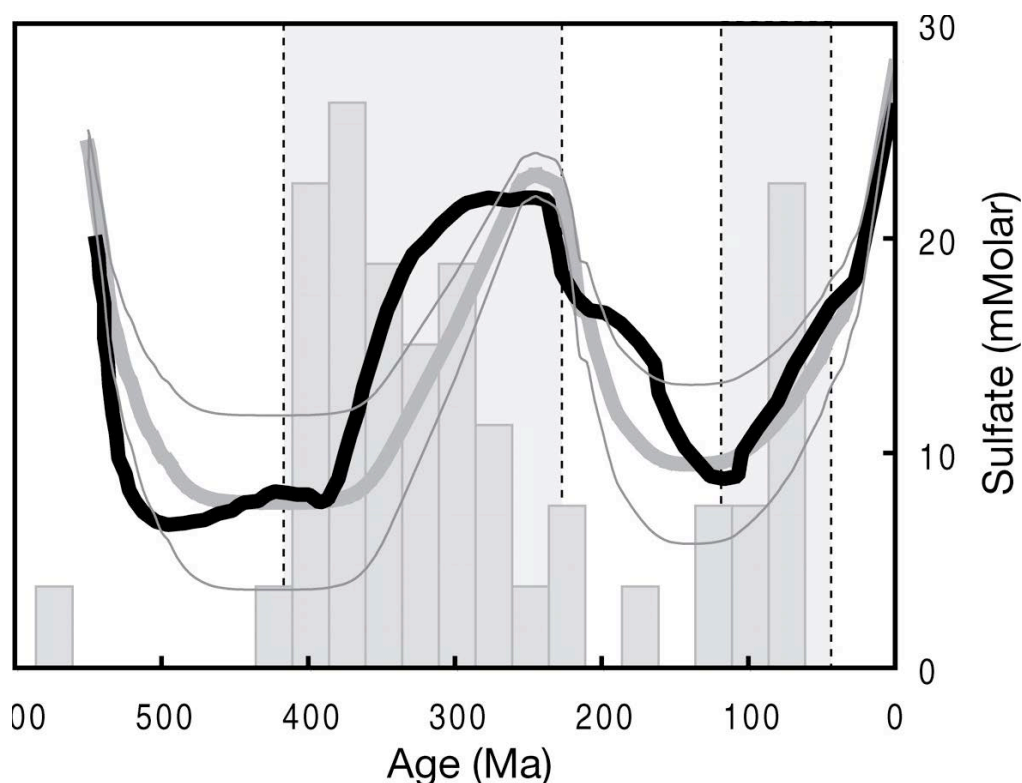


Figure 5.2 Record of Ocean Sulfate Concentration

(Lowenstein et al., Science, 2002.)

Here we revised and applied the model developed by Bhatnagar (2008) and Chatterjee (2012), especially on the following aspects.

- (1) Consider a non-zero critical value of sulfate concentration, $C_{s,crit}$, only above which starts the methane production from organic carbon [Winfrey,

1977]. It was suspected that when sulfate exists, methanogenesis won't start due to inhibition of methanogenesis by sulfate [Bhatnagar, 2008; Chatterjee, 2012]. However, this may result in a conceptual problem in numerical simulation: if sulfate is reacting with organic carbon, then sulfate concentration may never become zero within GHSZ because it's an exponentially decrease profile, therefore methane production never starts. In another word, SMT depth may be infinitely thick, but this is not realistic. Experimental data shows that methane production can begin with presence of a certain concentration of sulfate. The existence of a certain amount of sulfate affects the methane production rate, or delay the reaction to some extent, but did not inhibit it. We may generalize this phenomena in simulation that, when sulfate concentration, C_s , is greater than some critical value, $C_{s,crit}$, methane production won't begin; when it is lower, methane production begins.

(2) Focused on the case where biogenic methane dominates. To investigate the system with changing ocean sulfate on gas hydrate systems, it's better to assume 1-D without external flux. Therefore, we assume no external flux, such as at Blake Ridge. We focused on: (i) the transient process about the interaction among sulfate, POC and methane; (ii) the effects of several parameters on the steady state profiles; (iii) the effect of Da_{POC} on POC consumption and the POC available for methanogenesis, $\alpha_{0, meth}$, (Figure 5.3);

(iv) the effect of different ocean $[\text{SO}_4^{2-}]_0$ values on $\alpha_{0,meth}$ and hydrate abundance.

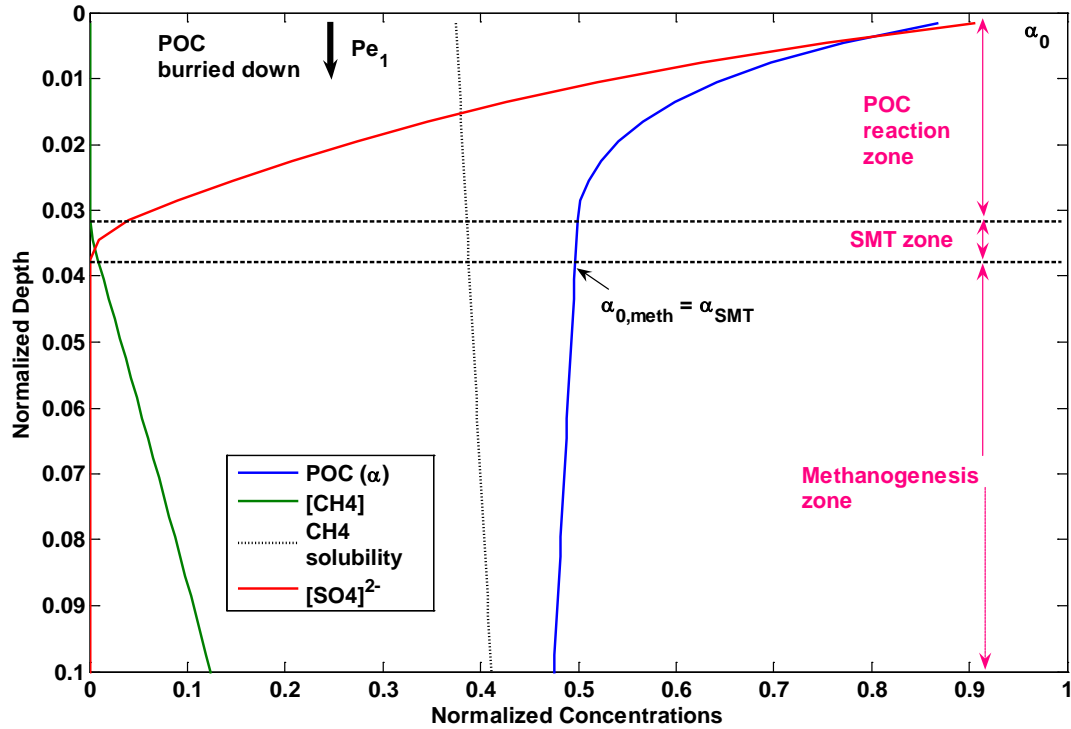
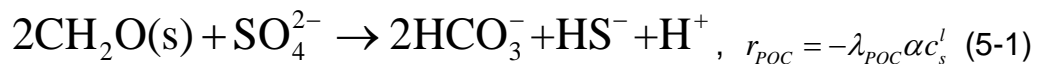


Figure 5.3 Interaction of sulfate with POC and methane at high Da_{POC} . Blue curve: POC (α); Red curve: $[\text{SO}_4^{2-}]$; Green curve: $[\text{CH}_4]$; dotted black curve: CH_4 solubility. $\alpha_{0,meth}$ --- the organic carbon content available for methanogenesis; α_{SMT} --- the organic carbon content at bottom of SMT. At high Da_{POC} , $\alpha_{0,meth} \approx 1$ won't be valid any more.

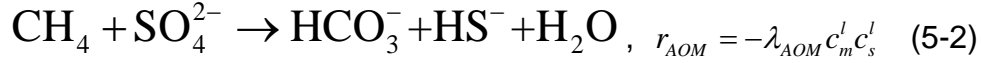
5.2. Generic reactions and model

There are several important reactions in the sulfate – methane hydrate system [Chatterjee, 2012]. Here we focus on the following three ones:

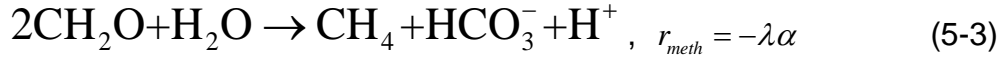
(1) *Organoclastic sulfate consumption (POC) reaction (from seafloor to SMT)*



(2) *Anaerobic oxidation of methane (AOM) reaction (at SMT)*



(3) *Methanogenesis reactions (generally below SMT)*



where

r : reaction rate

λ : methanogenesis reaction rate constant

λ_{POC} : POC reaction rate constant

λ_{AOM} : AOM reaction rate constant

α : organic carbon content in sediment

c : component mass fraction

subscript m, s : refer to methane (CH_4), sulfate (SO_4^{2-}), respectively

phase l, s : liquid and solid phases, respectively.

Importantly, it is very important that there is a critical value of sulfate concentration, only below which can methanogenesis reaction happen.

5.3. Mathematic model: component mass balances

Organic carbon (POC) balance

$$\begin{aligned} & \frac{\partial}{\partial t} [(1-\phi)\rho_{sed}\alpha] + \frac{\partial}{\partial z} [(1-\phi)\rho_{sed}v_s\alpha] \\ & = -\rho_{sed}(1-\phi)\lambda\alpha - \frac{\phi(1-\phi)}{M_{SO_4}} \lambda_{POC}(\rho_{sed}\alpha)(\rho_w c_s^l) \end{aligned} \quad (5-4)$$

where

ϕ : porosity

ρ_{sed} : sediment density

ρ_w : pore water density

α : organic carbon content in sediment

c : component mass fraction

subscript m, s : refer to methane (CH₄), sulfate (SO₄²⁻), respectively

phase l, s : liquid and solid phases, respectively

Methane balance

$$\begin{aligned} \frac{\partial}{\partial t} [\phi \rho_w c_m^l] + \frac{\partial}{\partial z} [U_f \rho_w c_m^l] &= \frac{\partial}{\partial z} \left[\phi \rho_w D_m \frac{\partial c_m^l}{\partial z} \right] \\ + p_m \frac{M_{CH_4}}{2M_{SO_4}} \rho_{sed} (1 - \phi) \lambda \alpha - \frac{\phi \lambda_{AOM}}{M_{SO_4}} (\rho_w c_m^l) (\rho_w c_s^l) & \end{aligned} \quad (5-5)$$

where

c : component mass fraction

D_m : methane diffusivity in pore water

U_f : net fluid flux

$p_m = \begin{cases} 0, & \text{if } C_s > C_{s,crit} \\ 1, & \text{if } C_s \leq C_{s,crit} \end{cases}$: the boolean indicator reflecting beginning of methane

production depending on sulfate concentration.

Sulfate balance

$$\frac{\partial}{\partial t} [\phi \rho_w c_s^l] + \frac{\partial}{\partial z} [U_f \rho_w c_s^l] = \frac{\partial}{\partial z} \left[\phi \rho_w D_s \frac{\partial c_s^l}{\partial z} \right] - \frac{\phi \lambda_{AOM}}{M_{CH_4}} (\rho_w c_m^l) (\rho_w c_s^l) - \frac{\phi(1-\phi)}{2M_{POC}} \lambda_{POC} (\rho_{sed} \alpha) (\rho_w c_s^l) \quad (5-6)$$

Similar with those defined in chapter 3-4, define dimensionless groups:

Damkohler numbers:

$$\text{For methanogenesis: } Da = \frac{\lambda L_t^2}{D_m} \quad (5-7)$$

$$\text{For AOM reaction: } Da_{AOM} = \frac{\rho_w c_{m,eqb}}{M_{CH_4}} \frac{\lambda_{AOM} L_t^2}{D_m} \quad (5-8)$$

$$\text{For POC reaction: } Da_{POC} = \frac{\rho_w c_{m,eqb}}{M_{POC}} \frac{\lambda_{POC} L_t^2}{D_s} \quad (5-9)$$

$$\text{Peclet number: } Pe_1 = \frac{U_{f, sed} L_t}{D_m} \quad (5-10)$$

$$Pe_2 = \frac{U_{f, ext} L_t}{D_m} \quad (5-11)$$

Define dimensionless variables, similar to those defined in chapter 3-4:

$$\text{Dimensionless depth and time, respectively: } \tilde{z} = \frac{z}{L_t}, \quad \tilde{t} = \frac{t}{L_t^2 / D_m} \quad (5-12)$$

$$\text{Dimensionless organic carbon: } \tilde{\alpha} = \alpha / \alpha_0 \quad (5-13)$$

$$\text{Organic carbon at seafloor normalized to } c_{m,eqb}: \beta = \frac{\alpha_0}{c_{m,eqb}} \quad (5-14)$$

Dimensionless concentrations of methane and sulfate, respectively:

$$\tilde{c}_m^l = \frac{c_m^l}{c_{m,eqb}}, \quad \tilde{c}_s^l = \frac{c_s^l}{c_{s,o}} \quad (5-15)$$

$$\tilde{\phi} = \frac{\phi - \phi_\infty}{1 - \phi_\infty}, \quad \eta = \frac{\phi_o - \phi_\infty}{1 - \phi_\infty}, \quad \gamma = \frac{1 - \phi_\infty}{\phi_\infty} \quad (5-16)$$

Net downward component fluid flux due to sedimentation:

$$U_{f, sed} = \frac{1 - \phi_o}{1 - \phi_\infty} \dot{S} \phi_\infty \quad (5-17)$$

At steady state, the sediment flux is a constant:

$$U_{sed} = v_s (1 - \phi) = v_{s,0} (1 - \phi_0) = \dot{S} (1 - \phi_0) = v_{s,\infty} (1 - \phi_\infty) \quad (5-18)$$

here \dot{S} is sedimentation rate (at seafloor).

Dimensionless sedimentation rate:

$$\tilde{U}_{sed} = U_{sed} / U_{f, sed} = \frac{1 - \phi_\infty}{\phi_\infty} = \gamma \quad (5-19)$$

Porosity profile (*Bhatnagar et al.*, 2007):

$$\tilde{\phi} = \frac{\eta}{\eta + (1 - \eta) \exp(N_{t\phi} \tilde{z})} \quad (5-20)$$

$$\text{where } N_{t\phi} = L_t / L_\phi \quad (5-21)$$

$$\text{characteristic length of compaction: } L_\phi = \frac{\sigma_\phi}{(1 - \phi_\infty)(\rho_{sed} - \rho_w)g} \quad (5-22)$$

Dimensionless mass balance equations

By nomarlization, the equations become:

Organic carbon (POC) balance:

$$\begin{aligned} \frac{\partial}{\partial \tilde{t}} \left[(1 - \tilde{\phi}) \tilde{\alpha} \right] + Pe_1 \left(\frac{1 + \gamma}{\gamma} \right) \tilde{U}_{sed} \frac{\partial \tilde{\alpha}}{\partial \tilde{z}} = -Da(1 - \tilde{\phi}) \tilde{\alpha} \\ - \frac{(1 - \tilde{\phi})(1 + \gamma \tilde{\phi})}{1 + \gamma} \frac{D_s M_{POC} c_{s,o}}{D_m M_{SO_4} c_{m,eqb}} Da_{POC} \tilde{\alpha} \tilde{c}_s^l \end{aligned} \quad (5-23)$$

Methane balance:

$$\begin{aligned} \frac{\partial}{\partial \tilde{t}} \left[\left(\frac{1+\gamma\tilde{\phi}}{\gamma} \right) \tilde{c}_m^l \right] + \left(\frac{1+\gamma}{\gamma} \right) (Pe_1 + Pe_2) \frac{\partial \tilde{c}_m^l}{\partial \tilde{z}} = \frac{\partial}{\partial \tilde{z}} \left[\left(\frac{1+\gamma\tilde{\phi}}{\gamma} \right) \frac{\partial \tilde{c}_m^l}{\partial \tilde{z}} \right] \\ + p_m \frac{M_{CH_4}}{2M_{POC}} \tilde{\rho}_{sed} Da(1-\tilde{\phi})\tilde{\alpha}\tilde{\beta} - \left(\frac{1+\gamma\tilde{\phi}}{\gamma} \right) \frac{M_{CH_4}c_{s,o}}{M_{SO_4}c_{m,eqb}} Da_{AOM} \tilde{c}_m^l \tilde{c}_s^l \end{aligned} \quad (5-24)$$

Sulfate balance:

$$\begin{aligned} \frac{\partial}{\partial \tilde{t}} \left[\left(\frac{1+\gamma\tilde{\phi}}{\gamma} \right) \tilde{c}_s^l \right] + \left(\frac{1+\gamma}{\gamma} \right) (Pe_1 + Pe_2) \frac{\partial \tilde{c}_s^l}{\partial \tilde{z}} = \frac{D_s}{D_m} \frac{\partial}{\partial \tilde{z}} \left[\left(\frac{1+\gamma\tilde{\phi}}{\gamma} \right) \frac{\partial \tilde{c}_s^l}{\partial \tilde{z}} \right] \\ - \left(\frac{1+\gamma\tilde{\phi}}{\gamma} \right) Da_{AOM} \tilde{c}_m^l \tilde{c}_s^l - \frac{(1-\tilde{\phi})(1+\gamma\tilde{\phi})}{1+\gamma} \frac{D_s}{2D_m} \tilde{\rho}_{sed} Da_{POC} \tilde{\alpha}\tilde{\beta}\tilde{c}_s^l \end{aligned} \quad (5-25)$$

Initial conditions (I.C.): (5-26)

$$\tilde{\alpha}(\tilde{z}) = 0, \text{ at } \tilde{t} = 0$$

$$\tilde{c}_m^l(\tilde{z}) = 0, \text{ at } \tilde{t} = 0$$

$$\tilde{c}_s^l(\tilde{z}) = 1, \text{ at } \tilde{t} = 0$$

Boundary conditions 1 (B.C. 1, at $\tilde{z} = 0$): (5-27)

$$\tilde{\alpha} = 1, \text{ at } \tilde{z} = 0$$

$$\tilde{c}_m^l = 0, \text{ at } \tilde{z} = 0$$

$$\tilde{c}_s^l = 1, \text{ at } \tilde{z} = 0$$

Boundary conditions 2 (B.C. 2, at $\tilde{z} = 2$): (5-28)

$$\frac{\partial \tilde{c}_m^l}{\partial \tilde{z}} = 0, \text{ if } |Pe_2| < |Pe_1|, \text{ at } \tilde{z} = 2$$

$$\text{or } \tilde{c}_m^l = \tilde{c}_{m,ext}, \text{ if } |Pe_2| > |Pe_1|, \text{ at } \tilde{z} = 2$$

$$\frac{\partial \tilde{c}_s^l}{\partial \tilde{z}} = 0, \text{ if } |Pe_2| < |Pe_1|, \text{ at } \tilde{z} = 2$$

$$\text{or } \tilde{c}_s^l = 0, \text{ if } |Pe_2| > |Pe_1|, \text{ at } \tilde{z} = 2.$$

5.4. Base case: Blake Ridge

Blake Ridge site 997, a typical site of gas hydrate, with SMT depth at ~ 21 mbsf, is simulated with good fit. The sulfate profile is well simulated in Figures 5.4 and 5.5. The simulated average hydrate saturation, $\langle S_h \rangle = 1.6\%$, is also fitted well to simulations and site data [Bhatnagar, 2008].

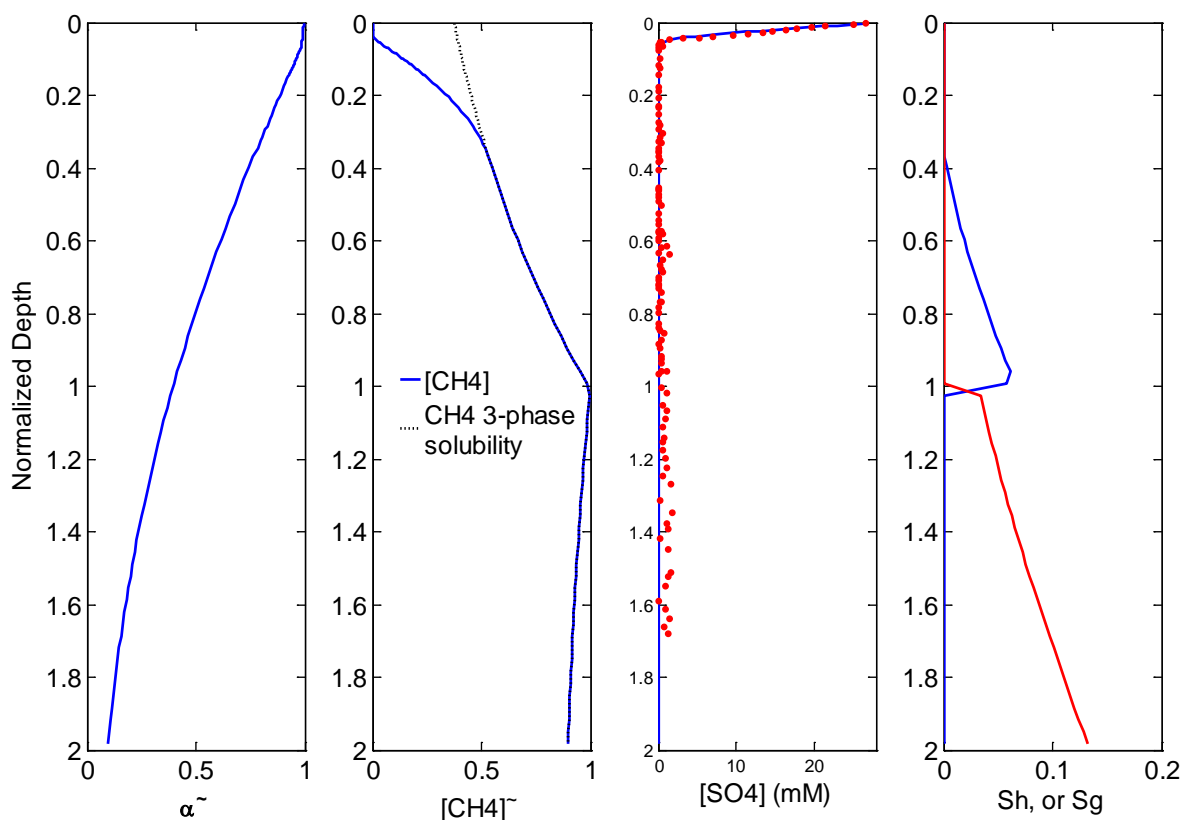


Figure 5. 4 Base case: Blake Ridge, site 997.

The sulfate – methane transition is well matched. Simulated $\langle S_h \rangle = 1.6\%$, similar with 1.5% in site data. Parameter set: $Pe_1 = 0.1$, $Pe_2 = 0$, $T_{sf} = 3 \text{ degC}$, $D_{sf} = 2.7 \text{ km}$, $Da_{meth} = 2.1$, $Da_{POC} = 30$, $Da_{AOM} = 5E5$.

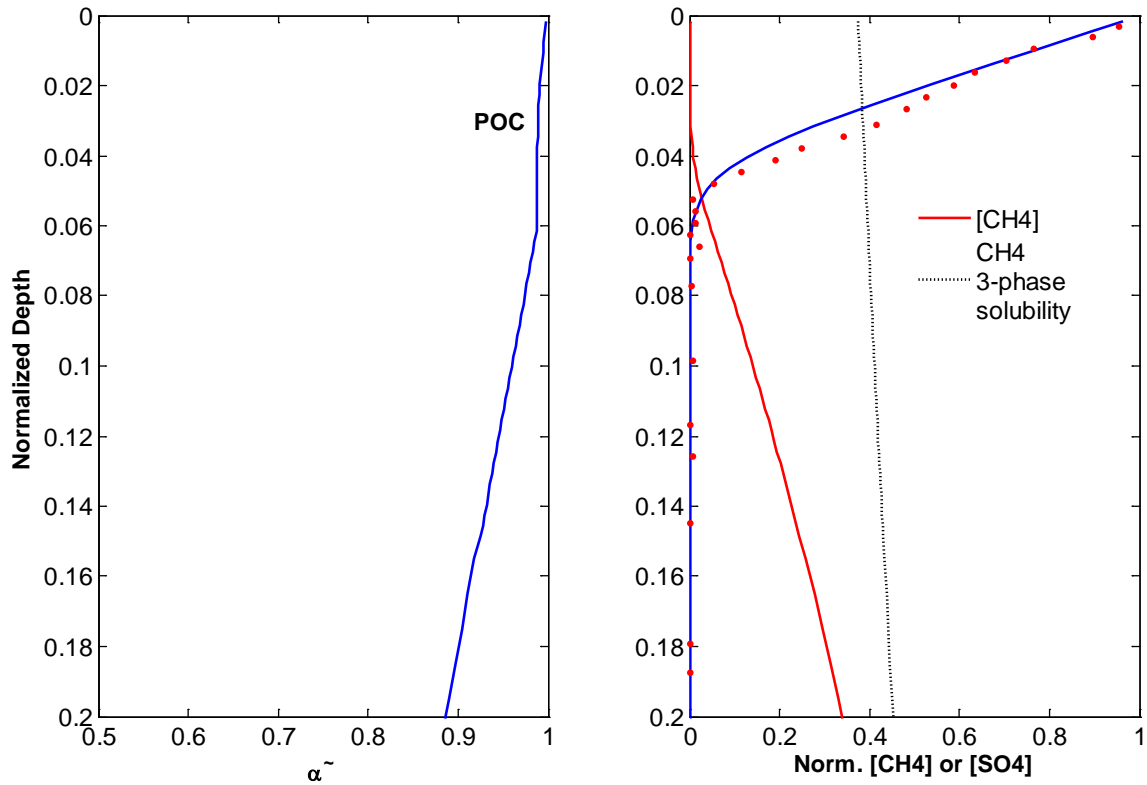


Figure 5.5 Base case: Blake Ridge, site 997 (zoomed in).

“POC” means the region for POC reaction.

In the following simulations, we use this as the base case for further evaluations of parameter sensitivity study.

5.5. Transient Processes

The initial dissolved sulfate is consumed by POC, until it reaches a critical value ($C_{s,crit}$), below which methanogenesis starts. After methane is produced, it will rapidly react with sulfate, and makes the dissolved sulfate concentration decreases quickly. Figures 5.6 - 5.7 show the transient processes. It clearly show that the initial sulfate concentration is 28 mM, and is reduced by POC

reaction gradually. Once sulfate concentration decreases to below $C_{s,crit}$ ($=0.1$ mM in Figure 5.6 – 5.7), then methanogenesis starts, methane rapidly reacts with sulfate so that sulfate concentration becomes 0 very quickly, because AOM reaction is much faster than organoclastic reaction. Due to increased region of methane production and methane diffusion, the zone with zero C_s increases rapidly.

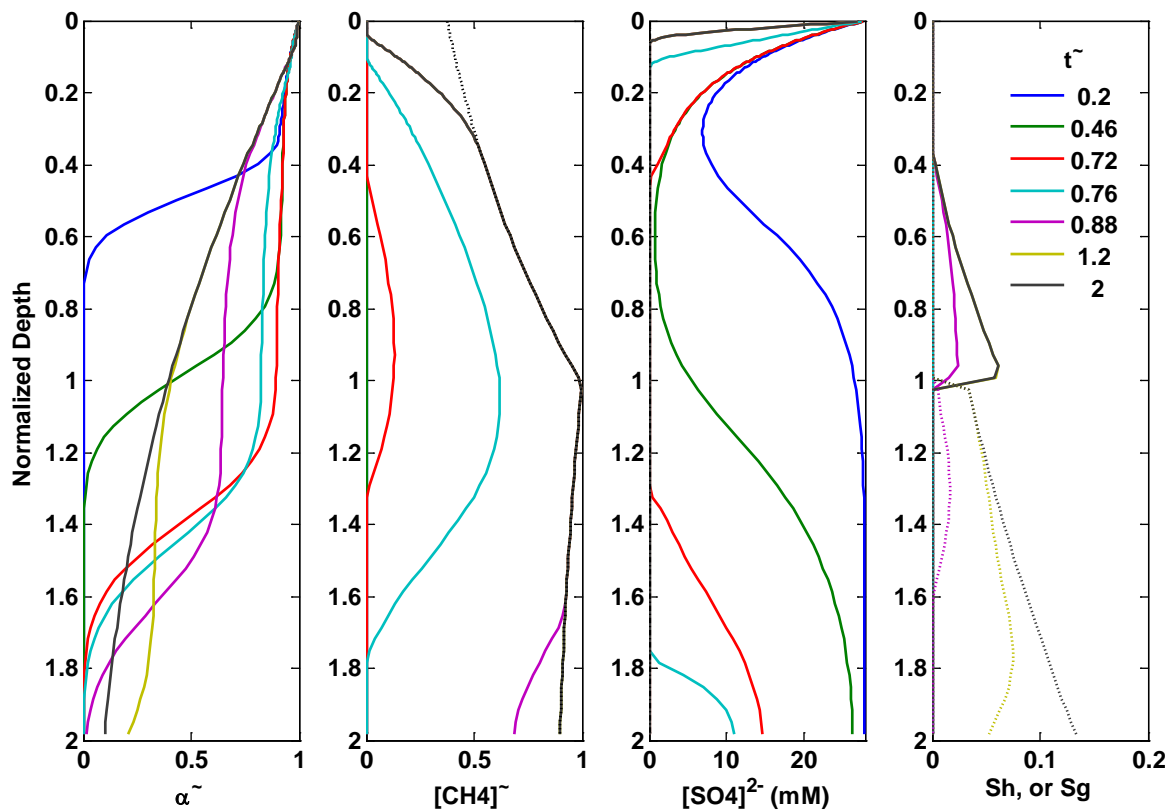


Figure 5. 6. Transient Processes, $Da_{POC} = 30$, $C_{s,crit} = 0.1$ mM is shown as a black dash line in $[SO_4]^{2-}$ profile. (from $\tilde{t} = 0.2$ to steady state).

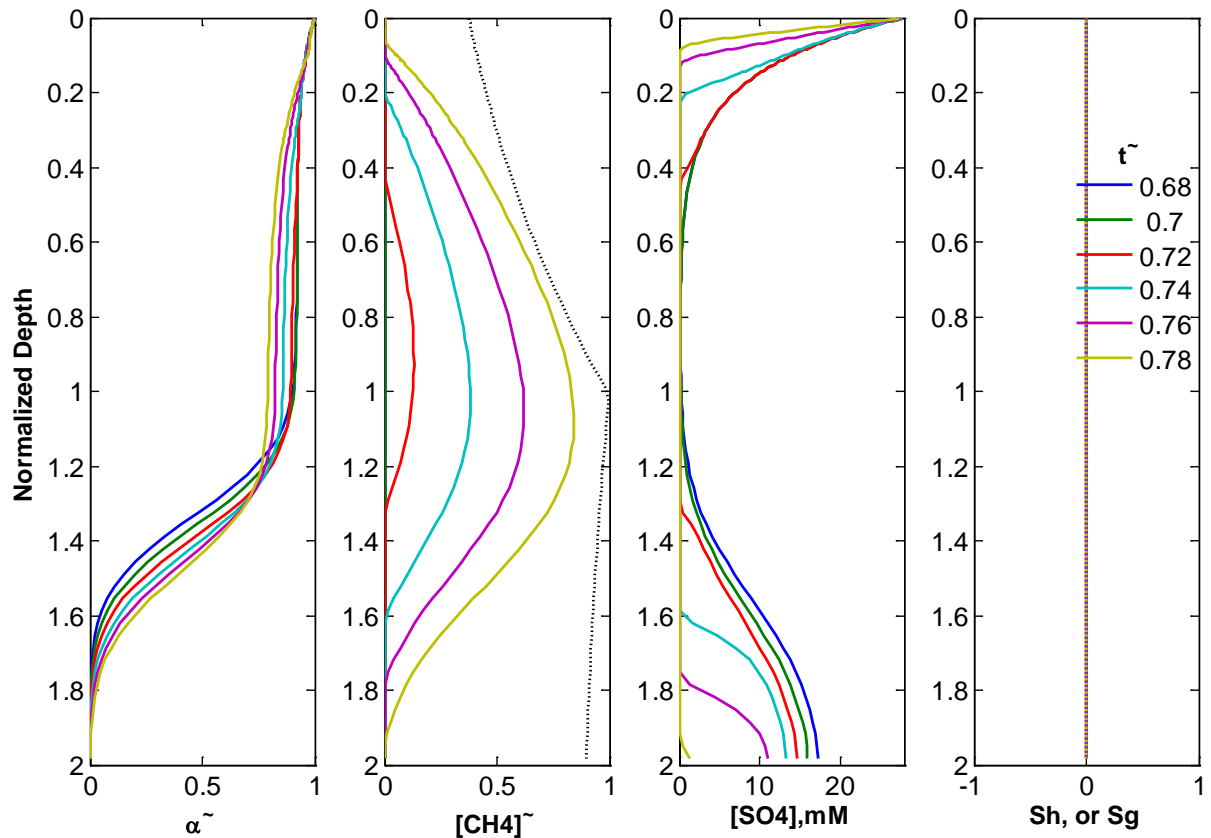


Figure 5. 7 Details of the rapid process of sulfate elimination below SMT. $Da_{POC} = 30$, $C_{s,crit} = 0.1$ mM , is shown as a black dash line in $[SO_4]^{2-}$ profile. (from $\tilde{t} = 0.68$ to 0.78).

Figure 5.7 shows the details of the rapid process of sulfate elimination for normalized time \tilde{t} from 0.68 ~ 0.78. It costs a long time (\tilde{t} from 0 to 0.68) for sulfate concentration to decrease from 28 mM to 0.1 mM at $\tilde{z} \sim 0.8$, and until now, there is no methane produced. However, once sulfate concentration reaches 0.1 mM, the critical concentration, $C_{s,crit}$, methane production from POC starts, and methane reacts with sulfate at a much higher rate to eliminate sulfate quickly. Therefore zero sulfate zone will expand quickly, and so does methane production zone. As a result, methane

production zone increases from 0 thickness (at $\tilde{t} = 0.68$) to almost the whole domain (at $\tilde{t} = 0.78$). This is due to the quick reaction between methane and sulfate, and also due to the diffusion of methane.

5.6. Steady State Results depending on several important parameters

The steady state results are very important to reveal the effects of different parameters. Here we demonstrate the simulation results on changing different parameters and concentrations. In the following simulations, we use the Blake Ridge site 997 as the base case. The simulation domain is from $\tilde{z} = 0$ to 2.

5.6.1. Factor 1: Da_{POC}

One of the most important factors affecting the organic carbon consumption

by POC reaction is Da_{POC} , which is defined as:
$$Da_{POC} = \frac{\rho_w c_{m,eqb} \lambda_{POC} L_t^2}{M_{POC} D_s}.$$

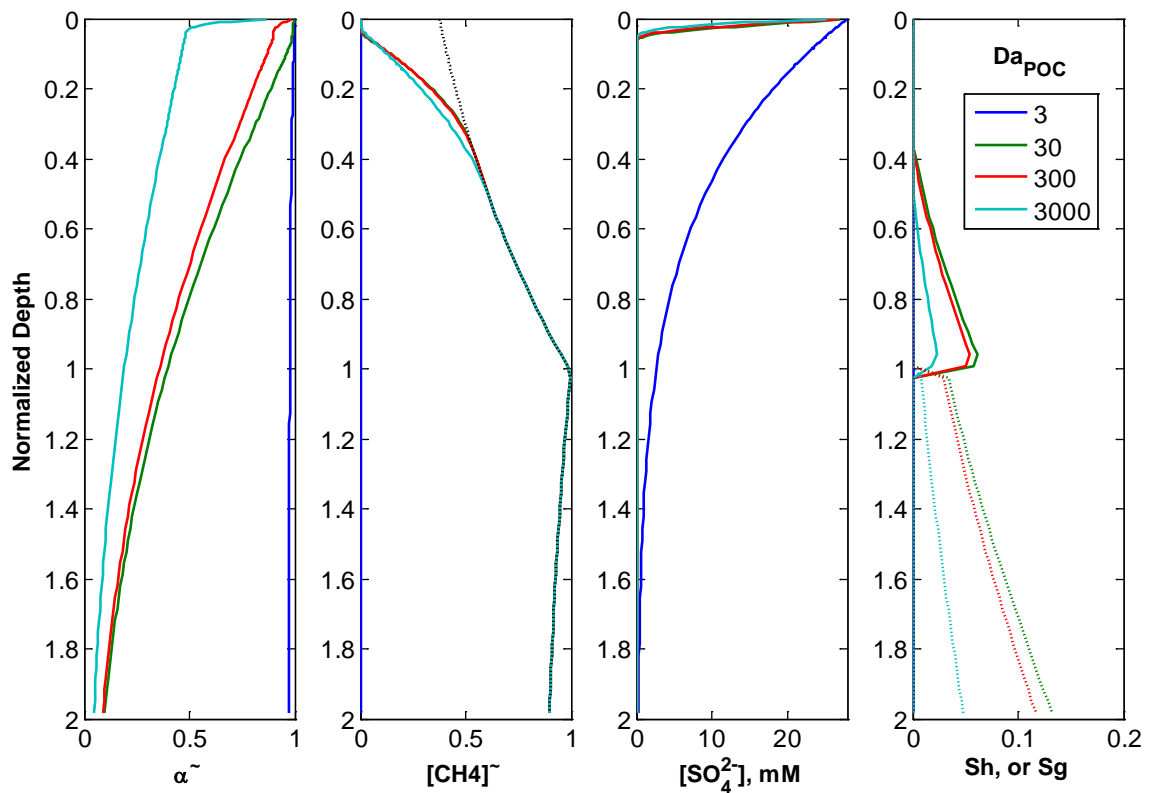


Figure 5. 8. Effect of Da_{POC} , at steady state. $C_{s,crit} = 0.1$ mM.

Figure 5.8 shows the effect of Da_{POC} on hydrate system at steady state. If $Da_{POC} \leq 3$, the reaction between sulfate and POC is too slow, so that sulfate cannot decrease to $C_{s,crit} = 0.1$ mM. Therefore, methane production cannot start, and no methane accumulates in the simulation domain. If $Da_{POC} \geq 30$, then sulfate concentration can be reduced by the reaction with POC to be lower than $C_{s,crit} = 0.1$ mM, and methane production will begin. As a result, methane will accumulate throughout almost the whole domain except for the sulfate reduction zone. So when $Da_{POC} \geq 30$, the gate for methane and hydrate accumulation opens.

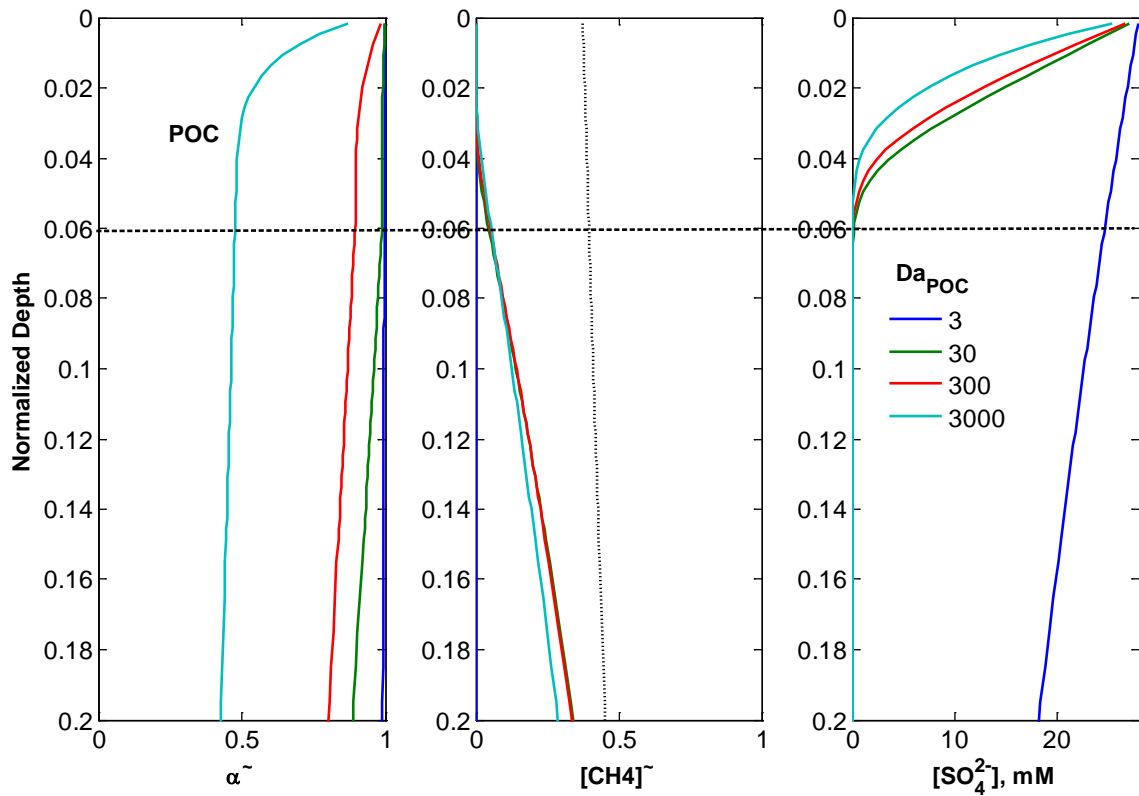


Figure 5.7. Effect of Da_{POC} (zoomed in). “POC” means the region for POC reaction. The black horizontal dash line is refers to the bottom of SMT zone.

However, this doesn't mean that the higher the Da_{POC} , the higher the $\langle S_h \rangle$ will be. On the contrary, $\langle S_h \rangle$ is dependent on how much amount of POC is remained for methane production below SMT. The higher Da_{POC} , the faster the reaction rate between POC and sulfate will be, and the higher ratio of POC will be consumed by sulfate within SMT; consequently, the lower ratio of POC will be remained at SMT for methane production (Figure 5.9) in the methanogenesis zone below SMT, and $\langle S_h \rangle$ would be lower, too. Another phenomena is, when Da_{POC} is high enough (e.g., 3000 or higher), the consumption of POC by POC reaction with sulfate will significantly decrease the ratio of POC remained at SMT compared to that at seafloor (which is

normalized to 1), otherwise, if Da_{POC} is low (e.g., 30 or lower), the effect is trivial.

5.6.2. Factor 2: Da_{meth} (or Da , methanogenesis Damkohler number)

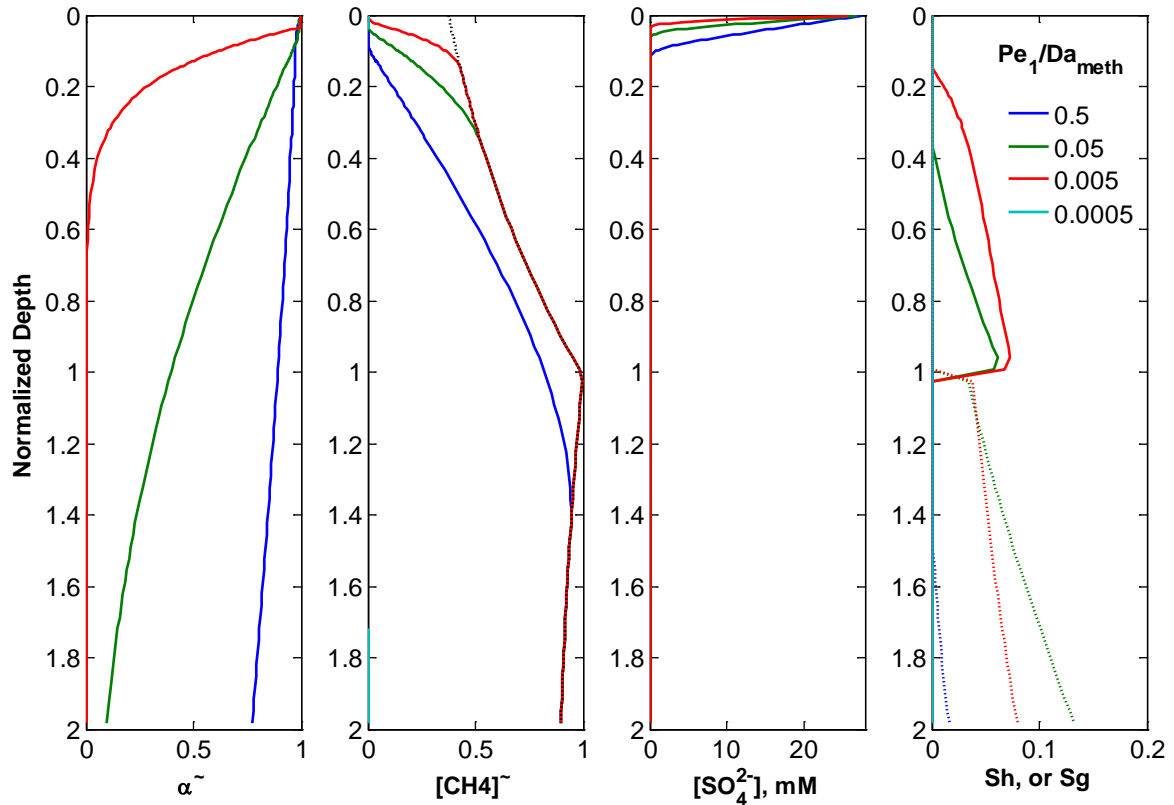


Figure 5.80. Effect of Pe_1/Da (ratio of sedimentation flux / methane production rate)

Figure 5.10 shows the effect of Pe_1/Da on hydrate system at steady state. When the system is dominated by methanogenesis reaction rather than sedimentation, i.e., Da is high and Pe_1/Da is low, more methane will be produced, and saturations $\langle S_h \rangle$ or $\langle S_g \rangle$ would be higher. Ofcourse, sometime the distribution of methane in hydrate or gas phase may be dependent on the Pe_1/Da .

5.6.3. Factor 3: Da_{AOM}

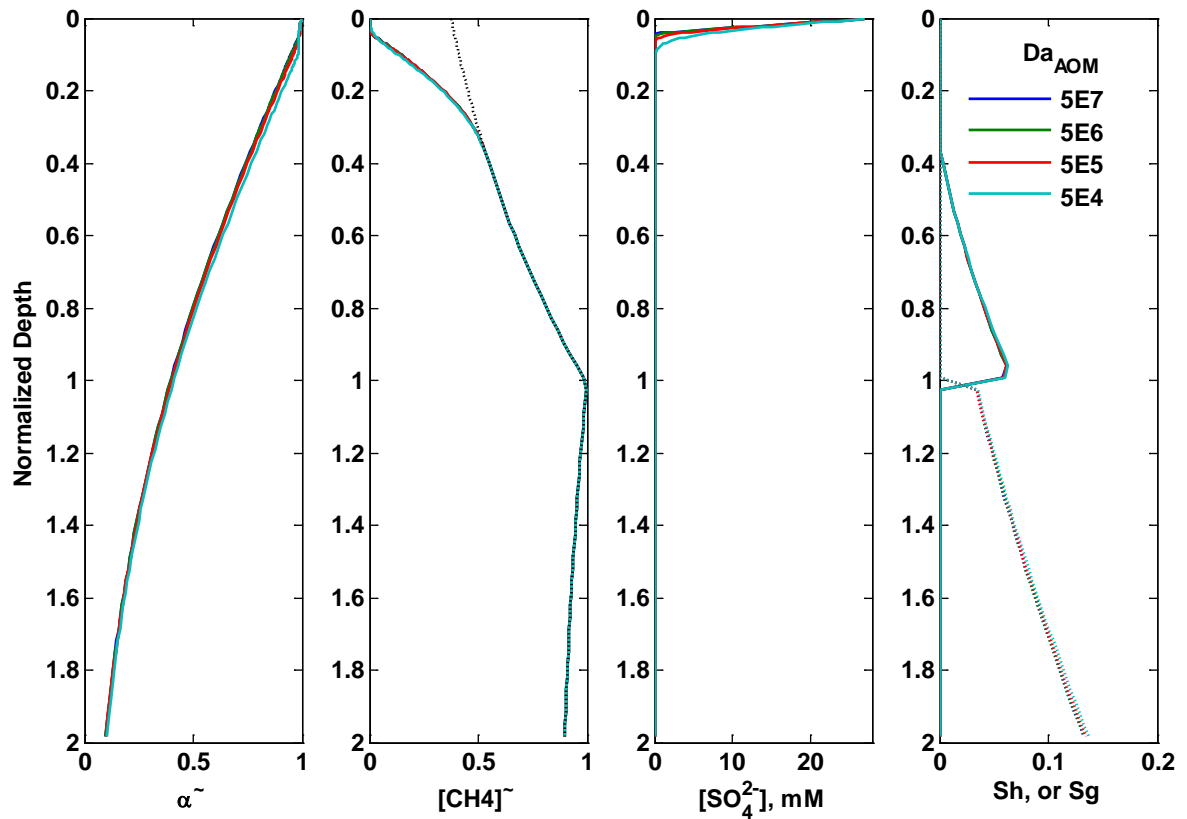


Figure 5. 9. Effect of Da_{AOM} (indicator of reaction rate between sulfate and methane)

Figure 5.11 shows the effect of Da_{AOM} on hydrate system at steady state. Throughout the simulation domain, the methane production and hydrate accumulation are not greatly affected by Da_{AOM} . This is reasonable, because the reaction between sulfate and methane only occurs at a thin layer near the bottom of SMT.

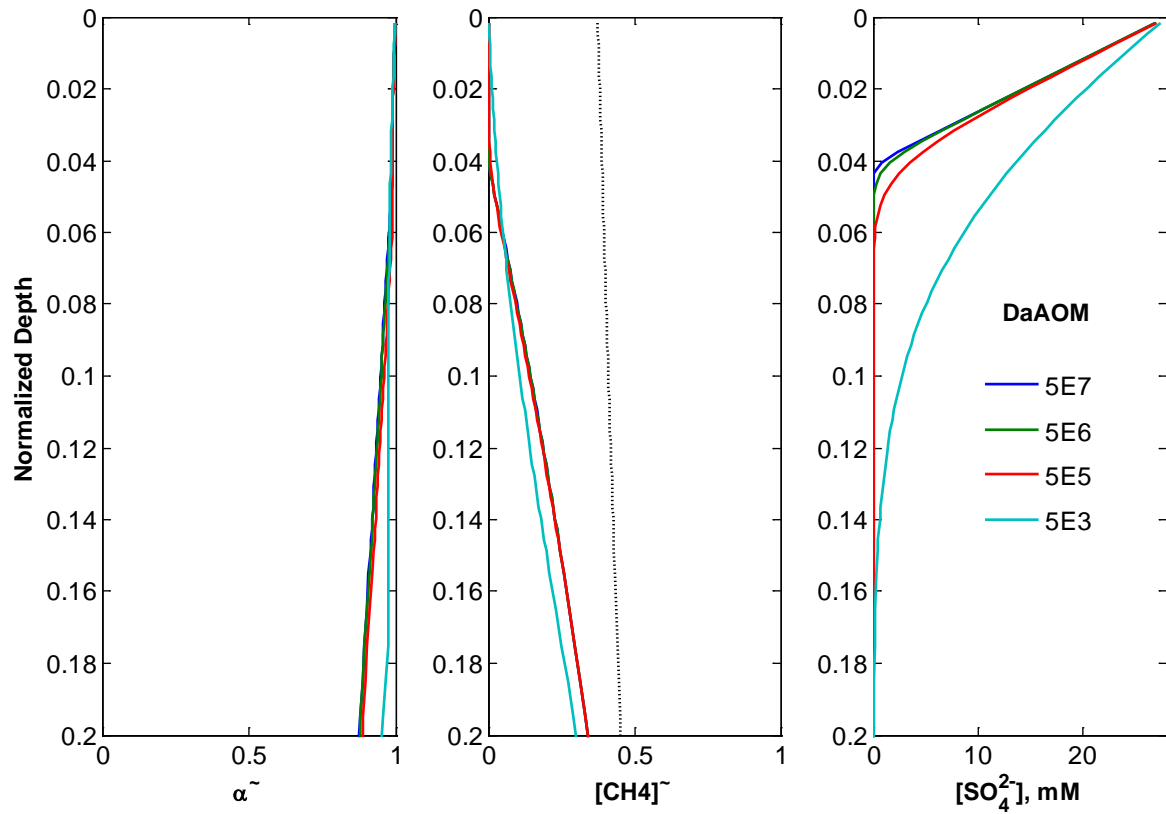


Figure 5. 10. Effect of Da_{AOM} (zoomed in)

However, Da_{AOM} does affect the thickness of sulfate reduction zone (Figure 5.12). If $Da_{AOM} \geq 5 \cdot 10^5$, 10000 higher than Da_{POC} ($= 30$), the reaction rate between sulfate and methane can be considered as ultra-fast than that between sulfate and POC, therefore, the sulfate profile is almost straight (see the lines with color of blue, green and red in Figure 5.12). So in the case $Da_{AOM} \geq 5 \cdot 10^5$, the sulfate concentration becomes zero at at a certain depth (i.e., the bottom of SMT) which is mainly controlled by the diffusion of sulfate from seafloor.

On the other hand, if $Da_{AOM} \leq 5 \cdot 10^3$, the reaction rate between sulfate and

methane can not be considered as ultra-fast than that between sulfate and POC, therefore, the sulfate profile is not straight (see the light blue curve in Figure 5.12). In the case $Da_{AOM} \leq 5 \cdot 10^3$, the sulfate concentration becomes zero at a deeper depth which is controlled jointly by the diffusion of sulfate from seafloor, and the reaction among POC, methane, and sulfate.

More simply, higher Da_{AOM} makes the AOM reaction faster, so that the SMT zone thinner, and sulfate profile more linear.

5.6.4. Factor 4: β

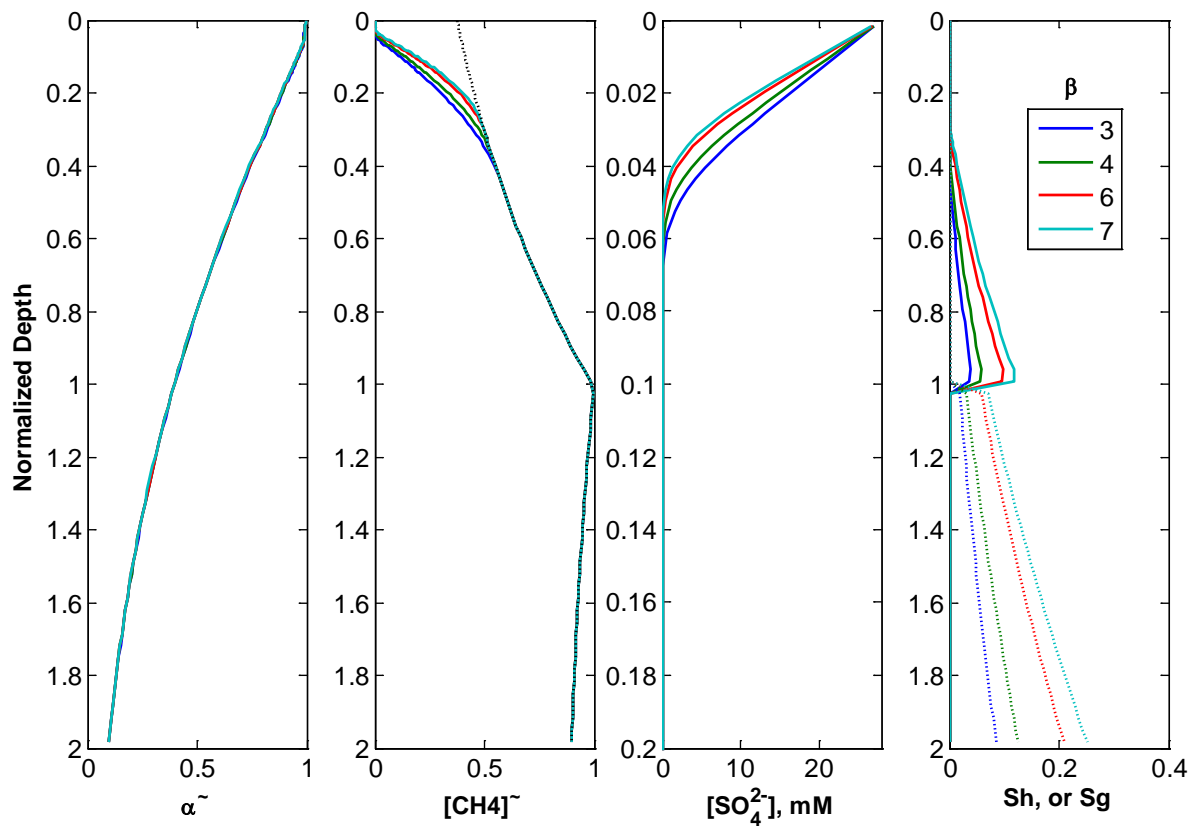


Figure 5. 11. Effect of Organic Carbon Content at Seafloor (β)

Figure 5.13 shows the effect of Organic Carbon Content at Seafloor (β) on hydrate system at steady state. Throughout the simulation domain, the methane production and hydrate accumulation are increasing with the increase of organic carbon content. Higher organic carbon input makes more methane produced, and induces higher hydrate abundance. This confirms the simulation by Bhatnagar (2008) and Chatterjee (2012).

5.6.5. Other factors: D_{sf} , T_{sf} , etc.

Other factors such as seafloor depth, and temperature, will cause different phase boundaries of hydrate system, and will induce different hydrate stability zone, as discussed in Chapter 3 and 4.

5.7. Effect of ocean sulfate concentration (C_{so})

Since ocean sulfate concentration (C_{so}) is not as high as present-day value in the past, it's valuable to show what happens if C_{so} is lower than present-day value. The results below will show the profiles in accordance to $C_{so} = 28\text{mM}$, 14 mM, 7 mM, and 0.1 mM. The other most important factor affecting the system is Da_{POC} , as categorized below.

5.7.1. Using standard Da_{POC} value ($Da_{POC} = 30$)

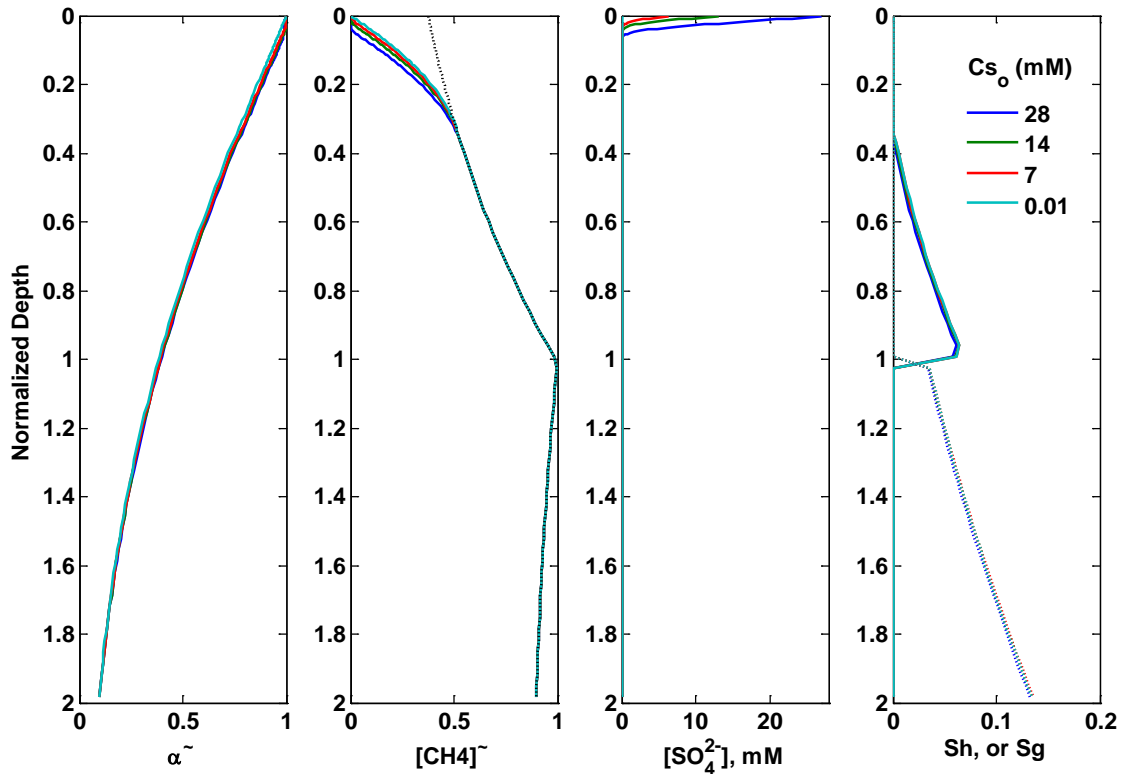


Figure 5.12. Effect of Ocean Sulfate Concentration (C_{so}), at steady state, with $Da_{POC} = 30$ (standard value)

Figure 5.14 shows the effect of Ocean Sulfate Concentration (C_{so}) with standard $Da_{POC} = 30$, on hydrate system at steady state. Values of C_{so} are set to be 28, 14, 7, and 0.01 mM. Throughout the simulation domain, the methane production and hydrate accumulation are not significantly affected by change of C_{so} . It is because Da_{POC} is low (e.g., 30 or lower), though it opens the gate to produce methane, the reaction rate between POC and sulfate is low, therefore, not much ratio of POC was consumed by sulfate in sulfate reduction zone. It also means that the majority of POC (> 98%) was remained at bottom of SMT for further methanogenesis reaction. The majority of sulfate below SMT, is consumed by methane produced near the bottom of

SMT, not by POC reaction. In this case, because $Da_{POC} = 30$ is quite low, the change of Ocean Sulfate Concentration, C_{SO} , doesn't affect the methane and hydrate accumulation. Of course, the SMT depth is somewhat affected by change of C_{SO} (Figure 5.15).

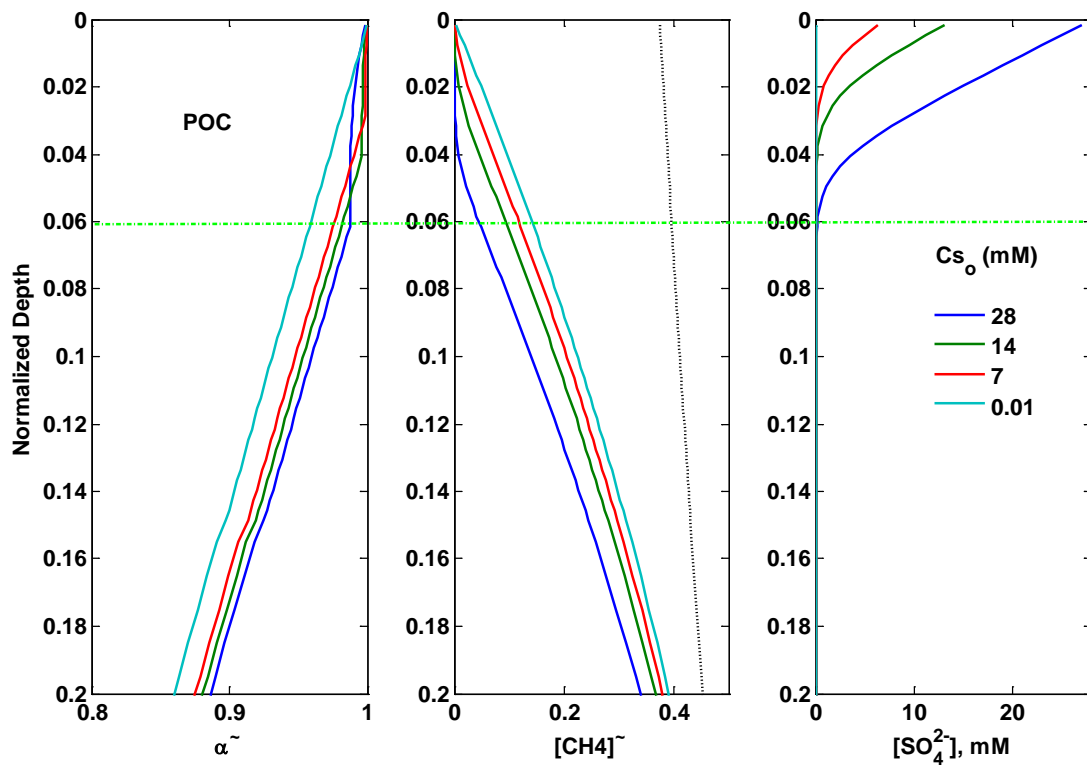


Figure 5. 13. Effect of Ocean Sulfate Concentration (C_{SO}), at steady state, with $Da_{POC} = 30$ (standard value). zoomed in. "POC" means the region for POC reaction.

5.7.2. High Da_{POC} ($Da_{POC} = 3000$)

Using $Da_{POC} = 3000$, the consumption of POC by POC reaction would be quite significant.

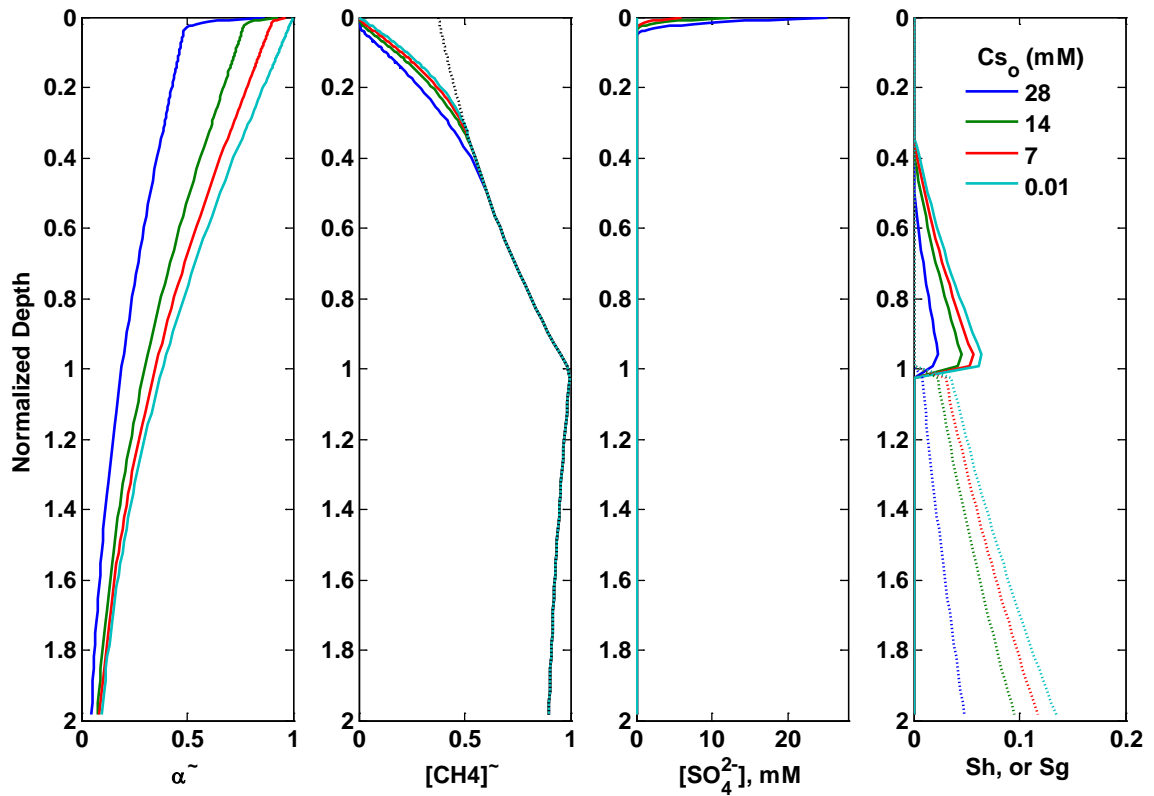


Figure 5.146. Effect of Ocean Sulfate Concentration (C_{so}), with $Da_{POC} = 3000$ (high value).

Figure 5.16 shows the effect of Ocean Sulfate Concentration (C_{so}) with high value $Da_{POC} = 3000$, on hydrate system at steady state. Values of C_{so} are set to be 28, 14, 7, and 0.01 mM. Throughout the simulation domain, the methane production and hydrate accumulation are significantly affected by change of C_{so} , with a positive relationship. It is because Da_{POC} is high (e.g., 3000 or higher), it not only opens the gate to produce methane, but the reaction rate between POC and sulfate is high. Therefore, much ratio of POC was consumed by sulfate in sulfate reduction zone. It means that only a portion of POC (50% ~ 90% depends on C_{so}) was remained at bottom of SMT for further methanogenesis reaction. Sulfate can be regarded as an reactant

consuming large portion of POC before POC entered methane production zone. In this case, because $Da_{POC} = 3000$ is quite high, the change of Ocean Sulfate Concentration, C_{SO} , affects the methane and hydrate accumulation significantly. Of course, the SMT depth is also affected by change of C_{SO} (Figure 5.17).

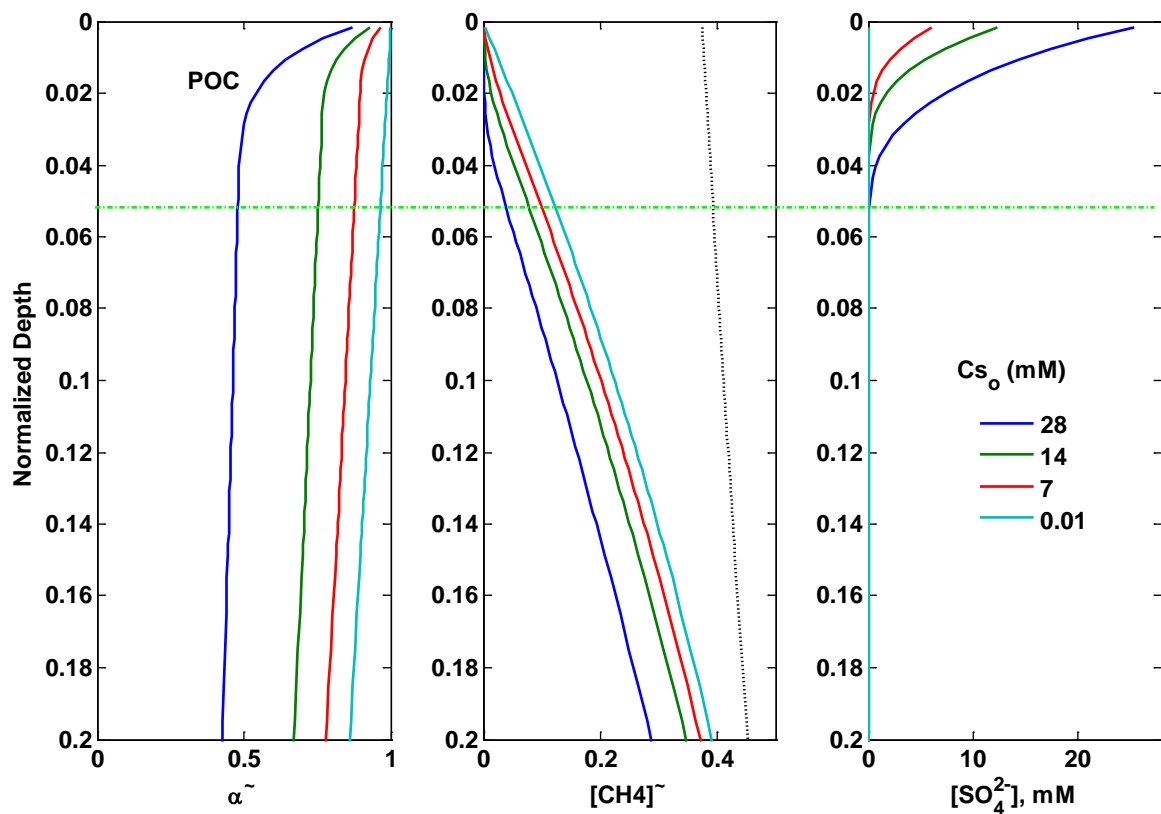


Figure 5.17. Effect of Ocean Sulfate Concentration (C_{SO}), with $Da_{POC} = 3000$ (high value). zoomed in. “POC” means the region for POC reaction.

5.7.3. Low Da_{POC} ($Da_{POC} = 0.3$)

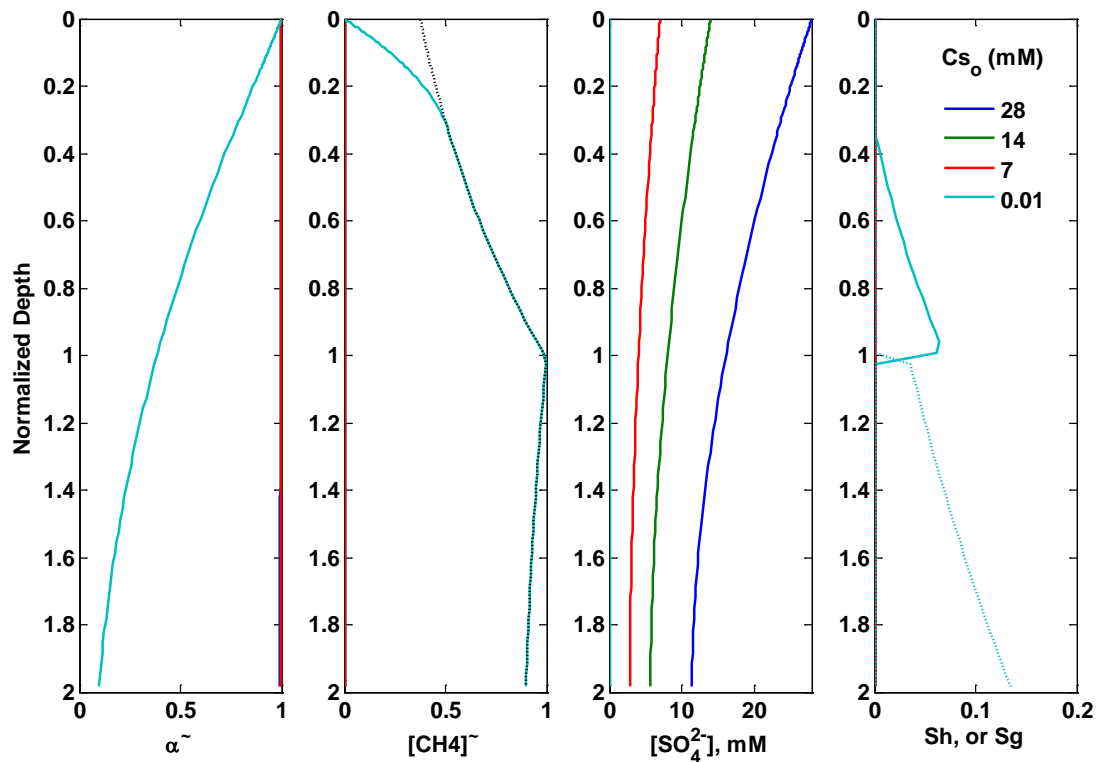


Figure 5. 18. Effect of Ocean Sulfate Concentration (C_{SO}), with $Da_{POC} = 0.3$ (low value).

Figure 5.18 shows the effect of Ocean Sulfate Concentration (C_{SO}) with very low value $Da_{POC} = 0.3$, on hydrate system at steady state. Values of C_{SO} are set to be 28, 14, 7, and 0.01 mM. Throughout the simulation domain, the methane production and hydrate accumulation are significantly affected by change of C_{SO} , with an ON-OFF scenario. The simulation results in Figure 5.18 show that only for $C_{SO} = 0.01$ mM, methane and hydrate accumulation is possible. For $C_{SO} = 28, 14, 7$ mM, no methane and hydrate is present in the system. It is because Da_{POC} is too low, it may not open the gate to produce methane if initial C_{SO} is much higher than $C_{S,crit}$. Only if the initial sulfate concentration, is lower than the critical sulfate concentration, $C_{S,crit}$, which set

the limit for the ON-OFF gate for methane production from POC, methane production can be possible. Otherwise, sulfate will dominate the system, and no methane is produced.

In summary, it's shown that when Da_{POC} is high enough, e.g., $Da_{POC} \geq 3000$, POC can be greatly consumed by sulfate within sulfate reduction zone. Therefore, a lower ocean sulfate concentration would consume less POC, and hydrate and free gas saturations would be significantly higher than present day values when $C_{so} = 28$ mM. When Da_{POC} is low, e.g., $Da_{POC} < 30$, the effect of low C_{so} is trivial because the consumption of POC is not significant even at $C_{so} = 28$ mM.

5.8. Effect of Critical sulfate concentration ($C_{s,crit}$)

Low value $C_{s,crit} = 0.1$ mM:

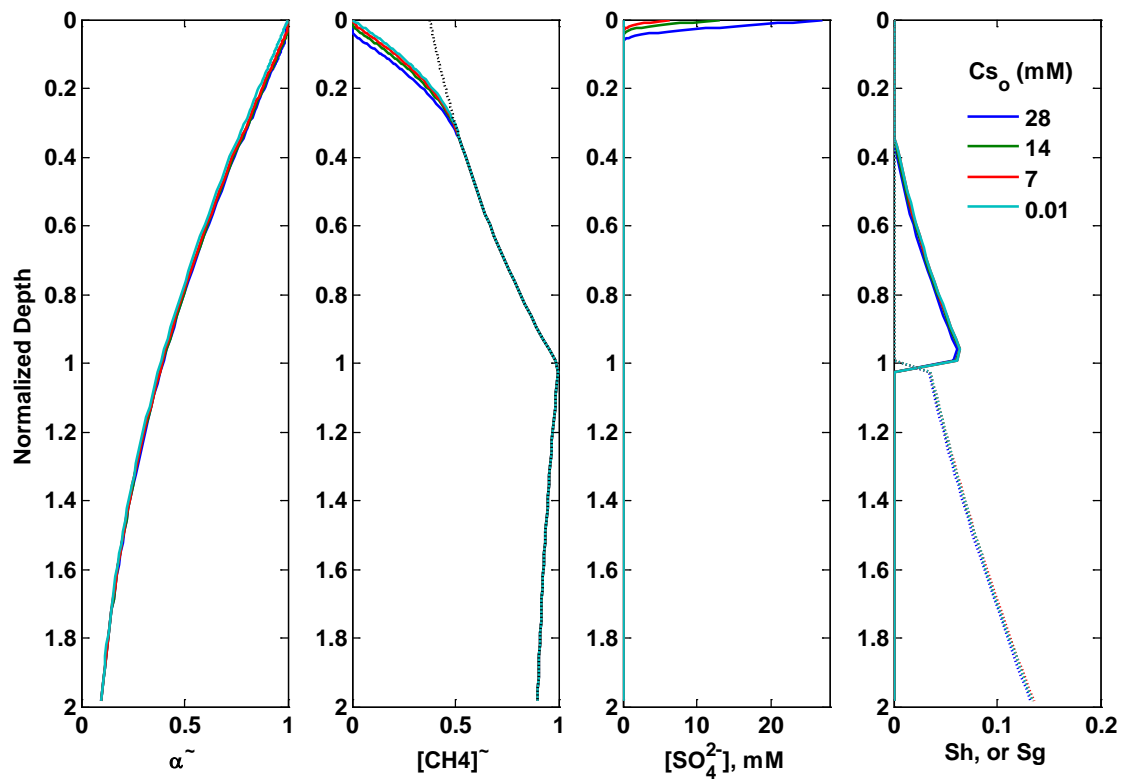


Figure 5. 1915. Effect of Ocean Sulfate Concentration (C_{s_o}), with $Da_{POC} = 30$ (standard value), $C_{s,crit} = 0.1$ mM

Middle value $C_{s,crit} = 1$ mM:

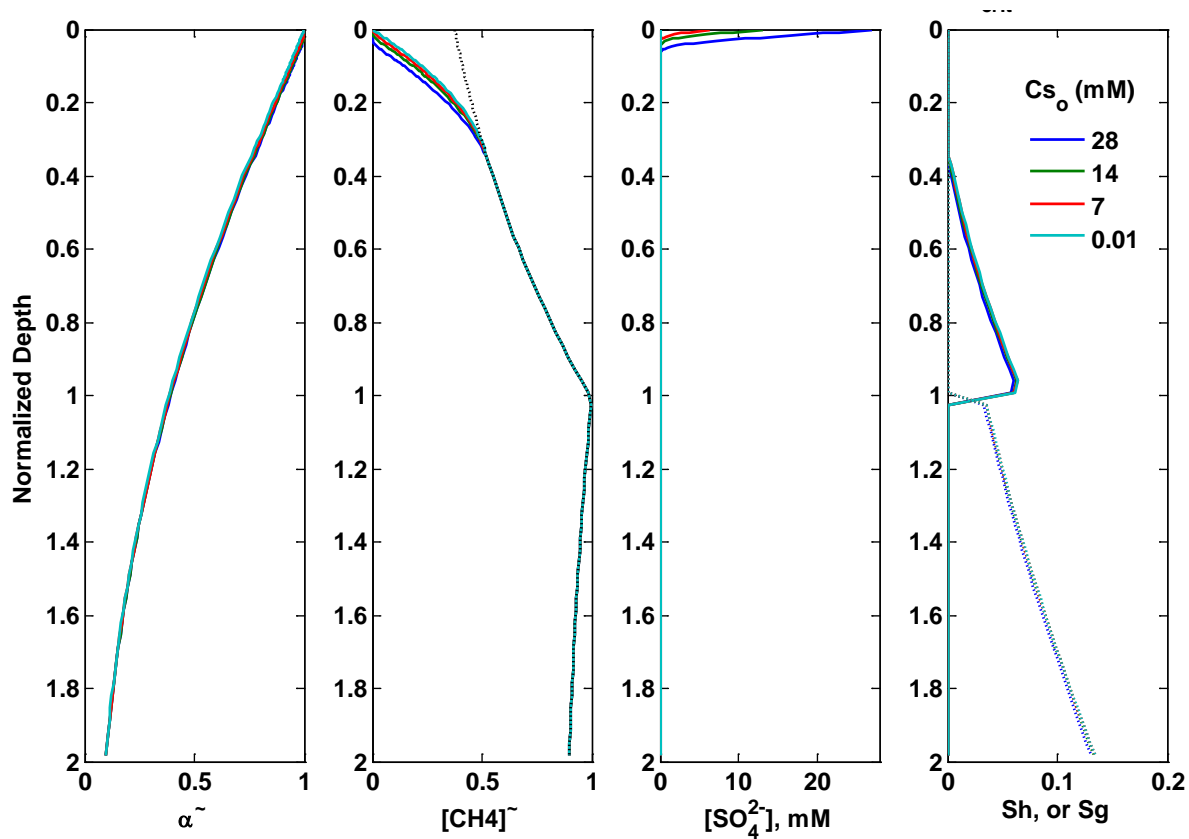


Figure 5. 160. Effect of Ocean Sulfate Concentration (C_{s_o}), with $Da_{POC} = 30$ (standard value), $C_{s,crit}=1$ mM.

High value $C_{s,crit}=10$ mM:

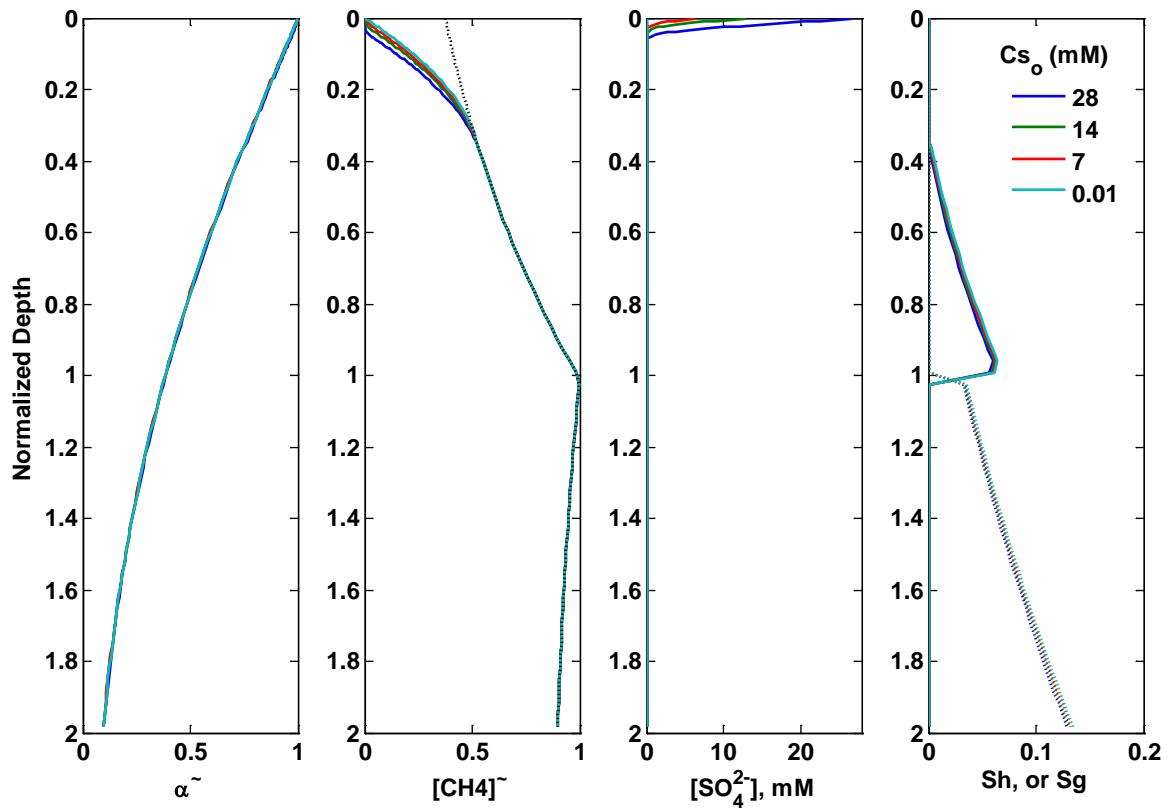


Figure 5.171 Effect of Ocean Sulfate Concentration (C_{s0}), with $Da_{POC} = 30$ (standard value), $C_{s,crit} = 10$ mM.

Figure 5.19 – 5.21 show the effect of Ocean Sulfate Concentration (C_{s0}) with standard value $Da_{POC} = 30$, but with different critical sulfate concentration $C_{s,crit} = 0.1, 1,$ and 10 mM, on hydrate system at steady state. Values of C_{s0} are set to be 28, 14, 7, and 0.01 mM for each figure. Throughout the simulation domain, the methane production and hydrate accumulation are not significantly affected by change of C_{s0} or change of $C_{s,crit}$. Because $C_{s,crit}$ operates as a gate value for the ON-OFF switch of methane production. $Da_{POC} = 30$ is high enough to cause the sulfate concentration to be reduced below 0.1 mM, the minimum $C_{s,crit}$ value we have simulated here, therefore,

methane production is ON for all these simulations at steady state. And because $C_{s,crit}$ doesn't affect POC consumption in sulfate reduction zone once methane production is switched to ON status, therefore, change of $C_{s,crit}$ doesn't affect methane and hydrate accumulation in all these scenarios.

In summary, if the sulfate concentration can be reduced below $C_{s,crit}$, methanogenesis will start and eliminates sulfate quite rapidly, then the steady state result doesn't depend on $C_{s,crit}$. Of course $C_{s,crit}$ can not be 0, otherwise, methanogenesis won't start. However, if Da_{POC} is too low, the sulfate concentration may not be reduced enough. In this case, it's important that $C_{s,crit}$ is high enough so that methanogenesis will start. Of course, $C_{s,crit}$ affects transient process because it controls when and where methane production starts.

5.9. Conclusion

Da_{POC} affects the system greatly. When Da_{POC} is high enough, e.g., $Da_{POC} \geq 3000$, the POC can be greatly consumed by POC reaction before SMT when using present-day ocean sulfate value $C_{s0}=28\text{mM}$, and therefore, a lower ocean sulfate concentration would consume less POC, therefore hydrate and free gas saturations would be significantly higher than present day values. When Da_{POC} is low, e.g., $Da_{POC} < 30$, the effect of low C_{s0} is trivial because the consumption of POC is not significant even $C_{s0} = 28 \text{ mM}$.

If sulfate concentration can be reduced to be lower than $C_{s,crit}$, methanogenesis starts, then the value of $C_{s,crit}$ doesn't affect steady state results. However, if methanogenesis cannot start, the result would be greatly different (because no methane will be produced).

Chapter 6. Gas Hydrate and Free Gas Distribution in Marine Sediment for a Mixed Methane - Propane System and the Associated Weak Seismic Response

6.1. Introduction

Solid gas hydrates form when cages of water molecules encapsulate low molecule weight gas molecules at high pressure, low temperature and high gas concentration. Beyond man-made pipelines, such conditions manifest in sediment pore space along continental margins and in permafrost regions. An extensive literature now exists for naturally occurring gas hydrate (Macdonald, 1994; Buffett, 2000; Xu, 1999) as they may represent a potential energy resource (Boswell & Collett, 2011; Walsh et al, 2009; Collett, 2002), a submarine geohazard (Hadley, et al., 2008; McConnell, et al., 2012) and an important component of the global carbon cycle, especially during times of rapid warming (Kvenvolden, 1988; Dickens, 1999; Gu et al., 2011; Boswell & Collett, 2011; Chatterjee et al., 2011; Reagan, et al, 2011).

The amount and distribution of gas hydrates on continental margins can be typically obtained through ocean drilling, such as at ODP 994, 995, 997 at Blake Ridge (Egeberg & Dickens, 1999), ODP 204 at Hydrate Ridge (Trehu, et al, 2004), ODP 201 at Peru Margin (Fehn et al, 2007), IODP 311 at Cascadia Margin (Torres, 2008), and JIP-II at Gulf of Mexico (Boswell, et al.,

2012). However, such direct assessment requires considerable cost and time; it also gives spatially restricted results. More commonly, areas with gas hydrate are mapped through indirect geophysical techniques, particularly seismic reflection (Wood 1994; Chapman, 2002; Riedel, 2012; Lee, 2012; Shelander, 2012). Gas hydrates and free gas in pore space alter the elastic properties of bulk sediments, especially P-wave velocity and bulk density, which respectively lead to an increase or decrease in acoustic impedance (Wood et al, 1994). The most common indicator of gas hydrate in seismic data is the presence of a bottom simulating reflector (BSR), which marks the base of the gas hydrate stability zone (GHSZ) (Hyndman & Spence, 1992). The BSR originates when seismic impedance changes sufficiently within one wavelength of the dominant seismic frequency (Shelander, 2012). More specifically, it results where, across the base of the GHSZ, sediment pore space contains solid gas hydrate in contact with free gas below (Xu & Ruppel, 1999).

Three basic issues arise when using the BSR as a proxy for defining the distribution of gas hydrate in marine sediment. Firstly, the presence of gas hydrate does not always lead to a BSR. Known examples include several Deep-Sea Drilling Project (DSDP) and Ocean Drilling Program (ODP) Sites, where hydrate is present but BSR is not observed, such as at sites ODP site 889B (Yuan & Edwards, 2000); ODP 164, site 994 (Xu & Ruppel, 1999); 490,

498, 565, and 570 on DSDP Leg 84 (Finley & Krason, 1986). Secondly, in some locations, a BSR may result from changes in sediment composition or property rather than an interface between gas hydrate and free gas. For example, at off the west coast of India, BSR is due to carbonate deposit *etc* (Collett, personal communication in Sloan & Koh, 2007, p.575.). Finally, in many cases though a BSR represents the base of the GHSZ, it does not give the vertical extent of gas hydrate. Typically, the top occurrence of gas hydrate lies at some depth between the base of the GHSZ and the seafloor (Xu & Ruppel, 1999).

For the pure methane-water system, the three phases equilibrium curve, Aqueous phase (Aq) – hydrate (H) – free gas (V), predicts a sharp boundary at the base of the GHSZ: above this interface, only water and gas hydrate can exist; below this interface, only water and free gas can exist (Dickens, 1997). A strong BSR will occur with modest to high free gas saturation right below the base of the GHSZ. However, gas hydrate can also exist in sediment without free gas immediately underneath. This occurs when methane concentrations are close to or less than those for gas solubility at the base of the GHSZ, and likely explains why no BSR exists at Site 994 (Blake Ridge), despite modest amounts of methane hydrate in pore space (> 2% average) spanning at least 200 m of the GHSZ (Xu & Ruppel, 1999).

When marine sediment contains methane and other gases, an intriguing alternative scenario for abundant gas hydrate without a strong BSR arises. At locations where thermogenesis of organic matter prevails, concentrations of ethane (C₂H₆), propane (C₃H₈), or butane (C₄H₁₀), can exceed 10% (Brooks, et al., 1986; Hadley, 2008). Hydrocarbons heavier than CH₄ appear with mixed hydrate present below base of pure methane hydrate (sl hydrate) stability zone (Hadley, 2008). Complex gas components will greatly affect the hydrate phase diagram (Brown et al., 1989; Sloan & Koh, 2007), therefore compositional effects should be seriously evaluated. Here we explore an example CH₄-C₃H₈-H₂O hydrate system in which the hydrate distribution and seismic response are greatly affected by a small fraction of propane, though theoretical, however, it's possible to explain some sites situation if all appropriate gas components are included.

6.2. Phase Diagrams for Systems with Multiple Gas Components

Overview

Abundant experimental data exists for gas hydrate phase boundaries for multiple gas components. Flash calculations have been published to simulate the gas hydrate phase boundaries, including for mixed gases (Ballard & Sloan, 2002, 2004; Sloan & Koh, 2007). Here we use the flash calculation software CSMGem v1.0 (Sloan & Koh, 2007), and focus on a mixed system

of methane, propane and pure water (assuming zero salinity due to certain limitation of convergence of the software).

According to Gibbs' phase rule, the degrees of freedom (F) for an equilibrium multi-phase system are expressed as:

$$F = C - P + 2 , \quad (6-1)$$

where C and P are the number of components and the number of co-existing phases, respectively. For a pure methane-pure water system ($C = 2$), when these phases Aq (aqueous) + sl-H (structure I hydrate) + V (free gas) co-exist, $P = 3$, and thus $F = 1$. This means that a curve of temperature and pressure can describe three-phase equilibrium conditions. A geothermal gradient (or geotherm curve), where temperature increases with depth below the seafloor, also constrains the relationship between temperature and pressure. Combining the three-phase equilibrium condition of gas hydrate together with geotherm curve, the Base of HSZ (BHSZ) will be uniquely determined, and there is no three phase co-existing area in the phase diagram. Collectively, in marine sediment sequences, three phases will co-exist only at a single depth, and there is no expansion of this coexistence in vertical direction. However, with an additional gas component, $C = 3$, and thus $F = 2$, and several important consequences arise. Firstly, both sl and slI hydrate will appear in the phase diagram. Secondly, at a certain temperature, the minimum hydrate formation pressure can be greatly reduced due to the lower pressure required

for all hydrate formation, even when the fraction of heavier gas components is as low as 1%. Finally but most importantly, there will be a wide region in the P-T phase diagram having three phase (Aq + H + V) co-existence. Accordingly, in the sediment sequence, when considering the geotherm curve, a thick zone expanding along the vertical direction is appropriate to host three phases co-existence.

Methane-Propane Example

Taking a CH₄-C₃H₈-H₂O system as the example, the molar fraction of species *i* in the entire system can be expressed as:

$$x_i = \frac{n_i}{n_{CH_4} + n_{C_3H_8} + n_{H_2O}}, \quad (6-2)$$

where n_i is the molar concentration of species *i*, and $i = CH_4, C_3H_8, \text{ or } H_2O$.

In turn, the water free molar fraction of species *i* is denoted as:

$$x_i^{wf} = \frac{n_i}{n_{CH_4} + n_{C_3H_8}} = \frac{x_i}{x_{CH_4} + x_{C_3H_8}}, \quad (6-3)$$

The incipient hydrate formation pressure curve, shows the minimum pressure conditions at which hydrate starts to form in the system assuming pressure is increasing from 0 (Figure 6.1). Both the curves for pure methane and those for mixed methane-propane systems exhibit similar generic *P-T* relationships. With higher temperature, a greater pressure (and depth) is necessary to form hydrate.

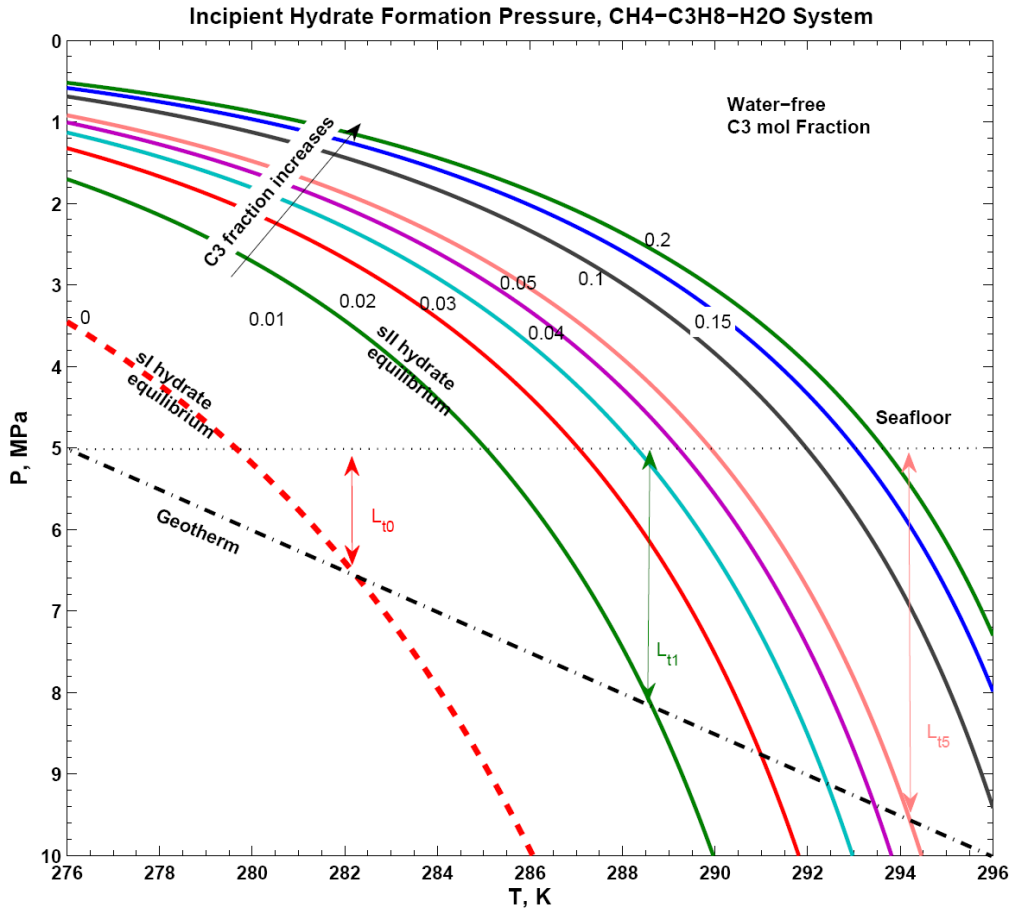


Figure 6. 1. The Incipient Hydrate Formation Pressure of a $\text{CH}_4\text{-C}_3\text{H}_8\text{-H}_2\text{O}$ System. Data were obtained using CSM Gem v1.0, showing the equilibrium conditions at which hydrate starts to form. C_3 fraction: water-free molar fraction of C_3H_8 , $x_{\text{C}_3\text{H}_8}^{\text{wf}}$. Black dot curve: seafloor. Black dash-dot curve: geotherm. Red dash curve: sl hydrate equilibrium condition; Solid curves: sll hydrate equilibrium conditions at different values of $x_{\text{C}_3\text{H}_8}^{\text{wf}}$. L_{t0} , L_{t1} , L_{t5} : thicknesses of GHSZ at $x_{\text{C}_3\text{H}_8}^{\text{wf}} = 0, 0.01, 0.05$, respectively. Seafloor temperature $T_{\text{sf}} = 276.15$ K, seafloor pressure $P_{\text{sf}} = 5.0$ MPa, and geothermal gradient $G = 0.04$ K/m.

Pressures and temperatures along three-phase equilibrium curves depend markedly on gas composition. A small fraction of propane causes a large

change in the incipient formation pressure for gas hydrate. For example, at 276.15K, the incipient hydrate formation pressure in pure methane hydrate system is 3.49 MPa (sl hydrate), while that for a system with 1% propane is only 1.71 MPa (sll hydrate). Higher fractions of propane lead to lower incipient formation pressures. In summary, for the same pressure (depth), increasing amounts of propane make gas hydrate more stable at higher temperature.

Taking an example CH₄-C₃H₈-H₂O system with fixed propane fraction $x_{C_3H_8}^{wf} = 0.05$, the P-T space can be divided into three regions (Figure 6.2). In Region A, both sl and sll hydrates are stable; while in Region B and C, only sll is, and neither is in Region C. Obviously, in Region B, 3 phases can co-exist: Aq, H, and V.

Considering an example geothermal curve as M₁M₄ in Figure 6.2, three different zones exist in the sediment along the geothermal curve, due to the 3 different phase regions described above. Zone B is a special one: 3 phases, Aq + H (sll) + V, co-exist. It's obvious that Zone B (Line segment M₂M₃) is a phase-transition-zone from hydrate-only zone (zone A) to gas-only zone (zone C). The length of Zone B is around 300 m in thickness which is longer than the thickness of sl hydrate stability zone, i.e., zone A, which is around 150 m in thickness as seen in Figure 6.3.

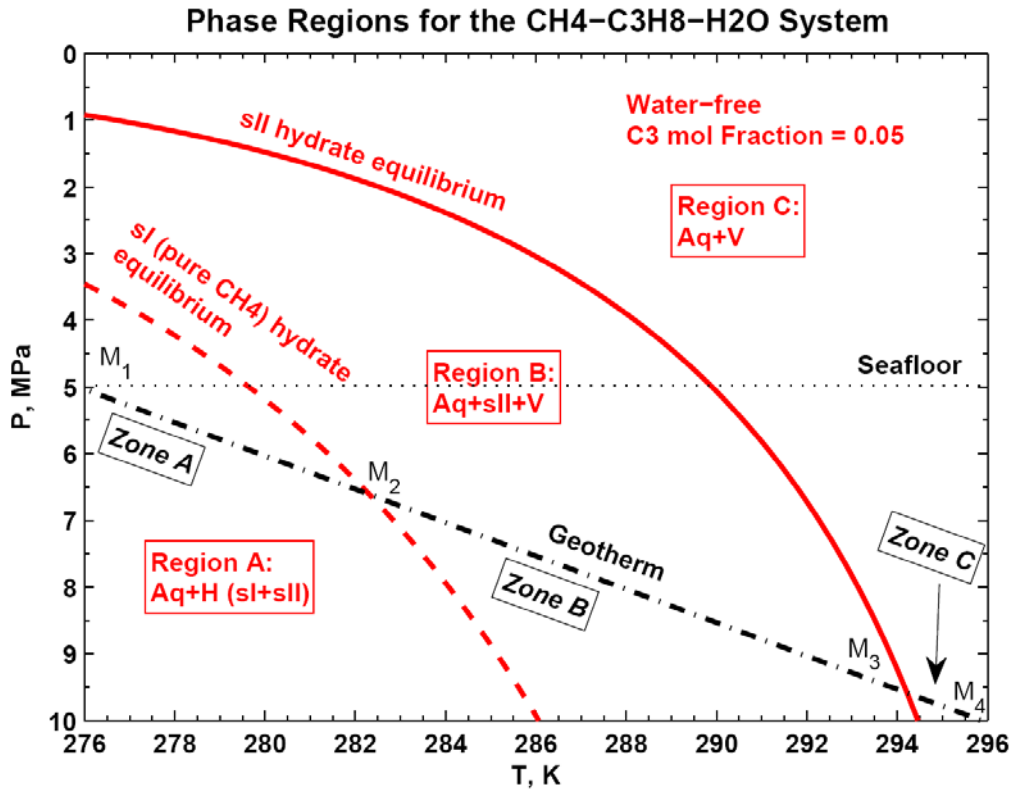


Figure 6. 2. Phase Diagram and Sediment Zones in a $\text{CH}_4\text{-C}_3\text{H}_8\text{-H}_2\text{O}$ System, assuming $x_{\text{C}_3\text{H}_8}^{\text{wf}} = 0.05$ everywhere. Black dot curve: seafloor. Black dash-dot curve: geotherm. Red dash curve: sI hydrate equilibrium condition; Red solid curve: sII hydrate equilibrium condition at $x_{\text{C}_3\text{H}_8}^{\text{wf}} = 0.05$. Region A, B, C: phase regions. Zone A, B, C: zones in sediment according to corresponding phase regions. M_1 , M_2 , M_3 , M_4 : point of interest for different zones in sediment. T_{sf} , P_{sf} , and G are same with Figure 6.1.

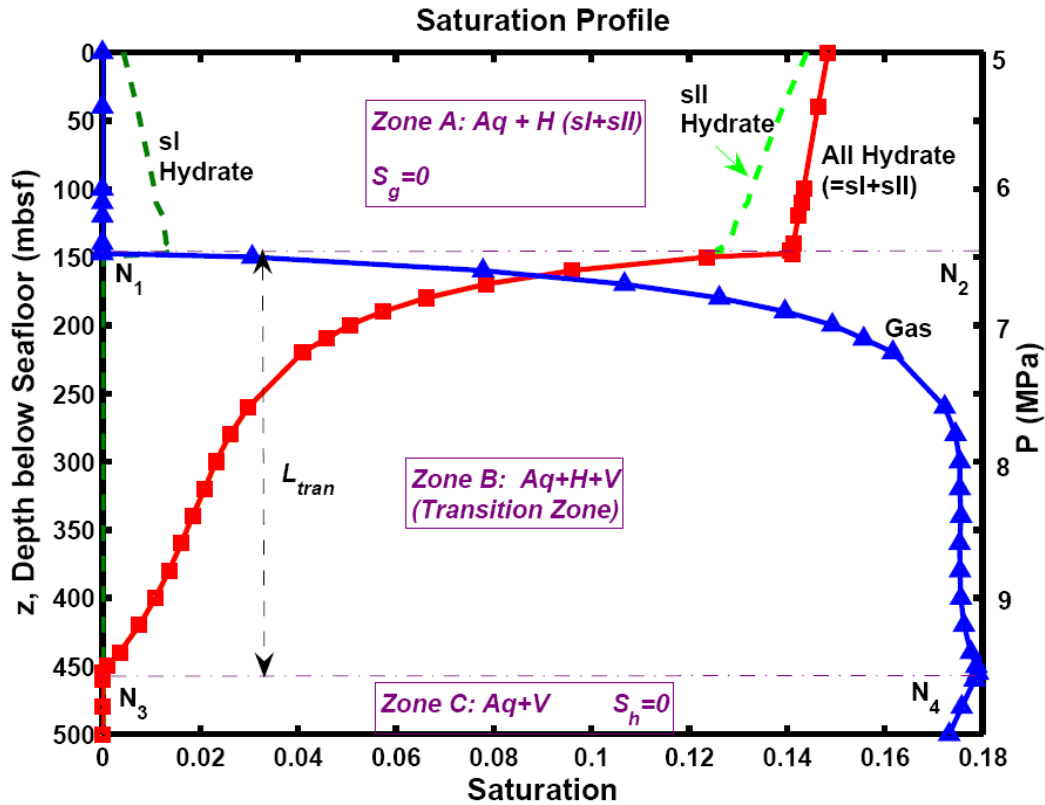


Figure 6. 3. Saturation Profiles of an example of the CH₄-C₃H₈-H₂O System.

Conditions: water-free propane molar fraction is 0.05 and overall composition is the same everywhere: $x_{CH_4}=0.019$, $x_{C_3H_8}=0.001$, $x_{H_2O}=0.98$; T_{sf} , P_{sf} , and G are same with Figure 6.1.

Assume: The overall composition is the same in the spatial domain. There are 3 zones of sediments in the domain. Zone A: $Aq + Hydrate (= sl + sll)$; Zone B: $Aq + sll + V$; Zone C: $Aq + V$. Dash-dot line N_1N_2 and N_3N_4 , are boundaries for $S_g=0$ and $S_h=0$ in the sediment, respectively. Red solid curve and blue solid curve are saturation profiles for All Hydrate (=sl + sll), and for Vapor, respectively. Pressure is marked on the right side.

To demonstrate how this will affect the hydrate/free gas distribution, hydrate / free gas saturation profiles have been calculated at typical conditions. The following conditions and assumptions were applied: (1) Water-free propane

molar fraction is 0.05. (2) Overall composition is $x_{\text{CH}_4} = 0.019$, $x_{\text{C}_3\text{H}_8} = 0.001$, $x_{\text{H}_2\text{O}} = 0.98$ everywhere. Overall composition is constant in the spatial domain. (3) Seafloor temperature $T_{\text{sf}} = 276.15$ K, and geothermal gradient $G = 0.04$ K/m. (4) Seafloor Pressure $P_{\text{sf}} = 5.0$ MPa. The results were obtained by using CSMGem v1.0 (Figure 6.3).

Synthetic seismic responses were generated as below, where weak BSR was observed as a result of gradual change of saturations within a long spatial distance and gradual change of sediment acoustic properties.

6.3. Acoustic Properties and Synthetic Seismic Response

In the previous section, the saturation profiles were calculated for a typical example system. Its acoustic property profiles containing hydrate/free gas are evaluated (Figure 6.4). The normalized density varies slightly from seafloor (at 150 mbsf) to deeper sediment till 500 mbsf, therefore it's not the major factor for acoustic impedance change. However, the normalized compressive velocity varies much, and thus the normalized acoustic impedance varies much too, due to this variation. The variation of acoustic impedance can be divided into two parts. One part, named as the significant transition zone (STZ), defined by the thickness in which 99% of impedance variation has been achieved, whose thickness is denoted as $L_{\text{stz}} \sim 130$ m, is the part inducing a more obvious seismic reflection than the other part; the second

part is the rest of the transition zone, which is not as significant as the significant transition zone, and the seismic reflection due to this part is almost negligible for a typical range of seismic frequencies.

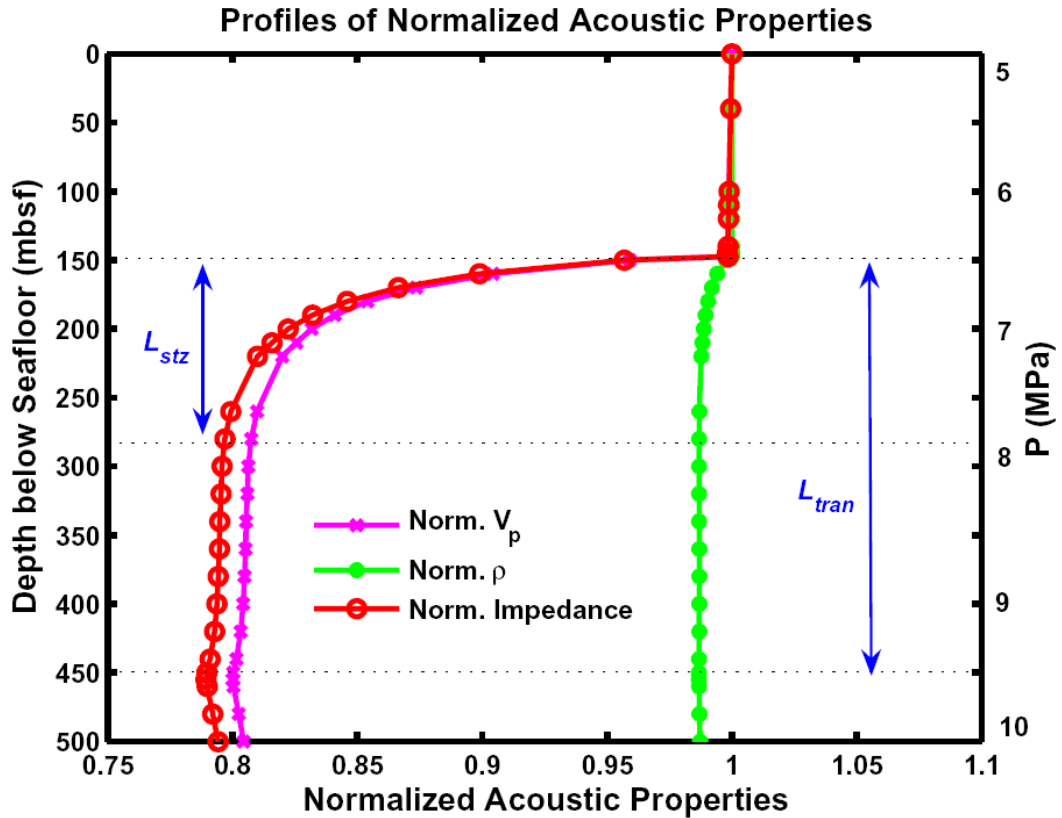


Figure 6. 4. Profiles of normalized acoustic properties in an example $\text{CH}_4\text{-C}_3\text{H}_8\text{-H}_2\text{O}$ System. Conditions are the same as Figure 6.3. Impedance $Z = \rho V_p$. Data are normalized so that those at seafloor are 1. L_{tran} : the thickness of the whole transition zone in which hydrate and gas phase coexist. L_{STZ} : the thickness of the significant transition zone in which 99% of impedance variation from top of the transition zone has been achieved.

Average acoustic velocities were calculated via Time-average Equation

(Pearson et al., 1983):

$$\frac{1}{V_p} = \frac{\phi(1 - S_h - S_g)}{V_{Aq}} + \frac{\phi S_h}{V_h} + \frac{(1 - \phi)}{V_m} + \frac{\phi S_g}{V_g}, \quad (6-4)$$

where

V_p --- average compressive velocity of the sediment;

V_h --- compressive velocity of the pure hydrate;

V_{Aq} --- compressive velocity of the pore water (aqueous phase);

V_m --- compressive velocity of the mineral;

V_g --- compressive velocity of the gas phase;

S_h --- hydrate saturation;

S_g --- vapor (gas) saturation;

ϕ --- porosity;

and average densities via equation:

$$\bar{\rho} = (1 - \phi)\rho_m + \phi \sum_i S_i \rho_i, \quad \text{phase } i = Aq, h, g \quad (6-5).$$

The parameters are in Table 6.1.

For comparison purpose, two different types of V_p profiles from seafloor to deeper sediment are estimated (Figure 6.5 ~ 6.6). The V_p profile and its impulse response for a pure methane hydrate system are shown in Figure 6.5, while those for a methane-propane hydrate system are shown in Figure 6.6. For a pure methane hydrate system, there is an abrupt decrease of V_p at

Base of GHSZ, therefore, its impulse response at Base of GHSZ (BGHSZ) is in the similar order of magnitude of that at seafloor (Figure 6.5), which is also called a strong BSR. However, for a methane-propane hydrate system, the change of Vp at Base of GHSZ is gradual, therefore the amplitude of reflection at BGHSZ is much weaker than that at seafloor (Figure 6.6).

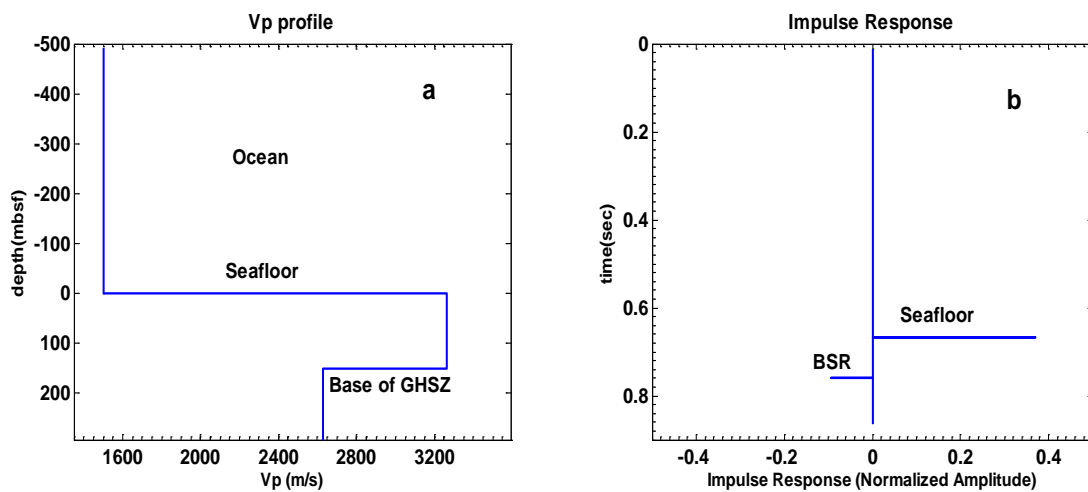


Figure 6. 5. Impulse response of a step change Vp system (BSR)

(a) Vp profile; (b) Impulse response. Figure (b) is generated by assuming an impulse was generated and reflected due to the Vp profile in (a).

Synthetic seismic responses are generated by using Ricker wavelets, which can be expressed as:

$$g(t) = (1 - 2\pi^2 f_p^2 t^2) \exp(-\pi^2 f_p^2 t^2) \quad , \quad (6-6)$$

where f_p is the peak frequency. A sample is shown in Figure 6.7. This Ricker wavelet has a smooth power spectrum curve, with a peak frequency, $f_p = 30$ Hz (Figure 6.7). They are widely used in seismic simulations. In exploration seismic simulation, the peak frequency is mostly in a range from 10 to 100 Hz, and 30 Hz is a typical frequency (Yilmaz & Doherty, 1987).

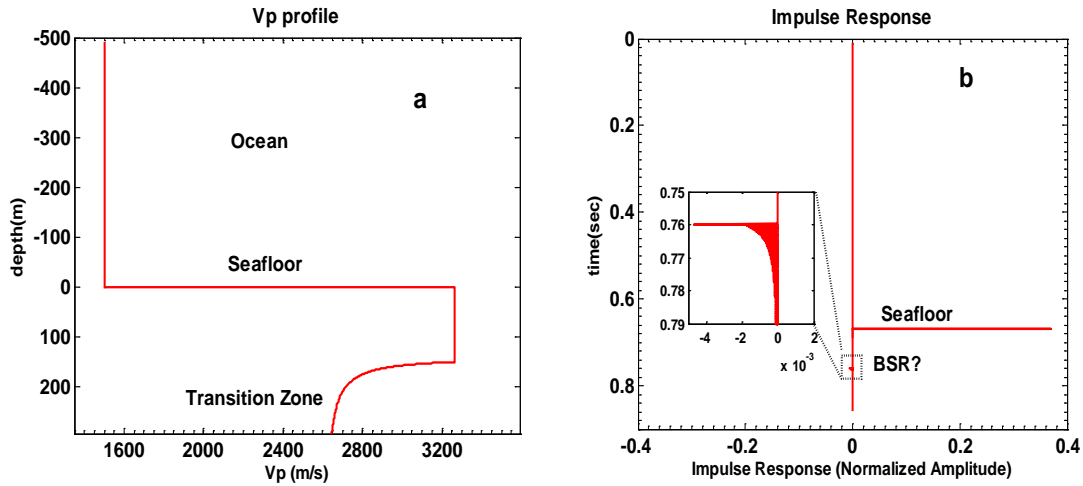


Figure 6. 6. Impulse Response of a system with a transition zone

(a) Vp profile; (b) Impulse Response. The square region in (b) is a magnified figure of the seismic response at transition zone. The Vp and density profile in transition zone are discretized into tiny segments in space to approximate the seismic response with the space step <math>< 0.05</math> of the minimum wavelength.

The synthetic seismic response is generated by convolving the source wavelet (here is Ricker wavelet) and the system impulse response.

$$f_r(t) = I_r(t) * g(t) , \quad (6-7)$$

where $I_r(t)$ --- the Impulse Response of the hydrate system;

$f_r(t)$ --- the reflection of the hydrate system due to an input signal

(e.g., a Ricker wavelet).

By using Ricker wavelets, with frequency from 10 to 100 Hz, we obtained the synthetic seismogram (Figure 6.8), both for that from a step change Vp profile (i.e., for pure methane hydrate system), and for that from a gradual transition zone. For the same thickness of the significant transition zone L_{stz} , different

peak frequencies are used; for each wavelet with a certain peak frequency, the characteristic wavelength is denoted as λ . The thickness ratios, L_{stz}/λ , are calculated and shown on the synthetic seismograms (Figure 6.8).

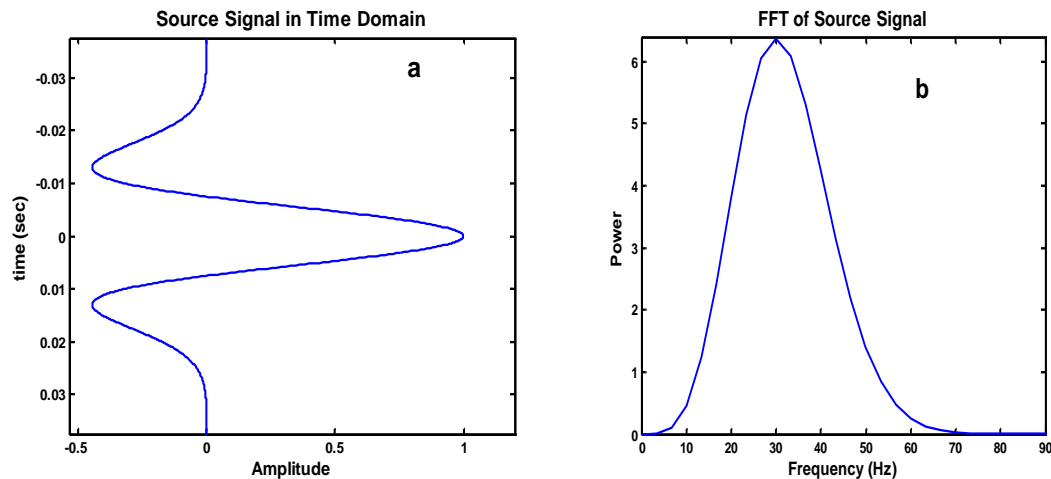


Figure 6. 7. A sample Ricker wavelet, $f_{peak}=30$ Hz

(a) In time domain; (b) Power spectrum in frequency domain

To quantitatively understand the seismic response, the Ratio of Amplitude at Hydrate/Gas Transition to that at Seafloor, A_{tran}/A_{sf} , is defined. If $A_{tran}/A_{sf} \leq 0.1$, the reflection is considered as a “weak reflection” (i.e., weak BSR). From the relationship between A_{tran}/A_{sf} and thickness ratio L_{stz}/λ , we find out both qualitatively (Figure 6.8) and quantitatively (Figure 6.9) that:

If $L_{stz}/\lambda > 1.5$, then $A_{tran}/A_{sf} \leq 0.1$, i.e., a weak reflection will be observed.

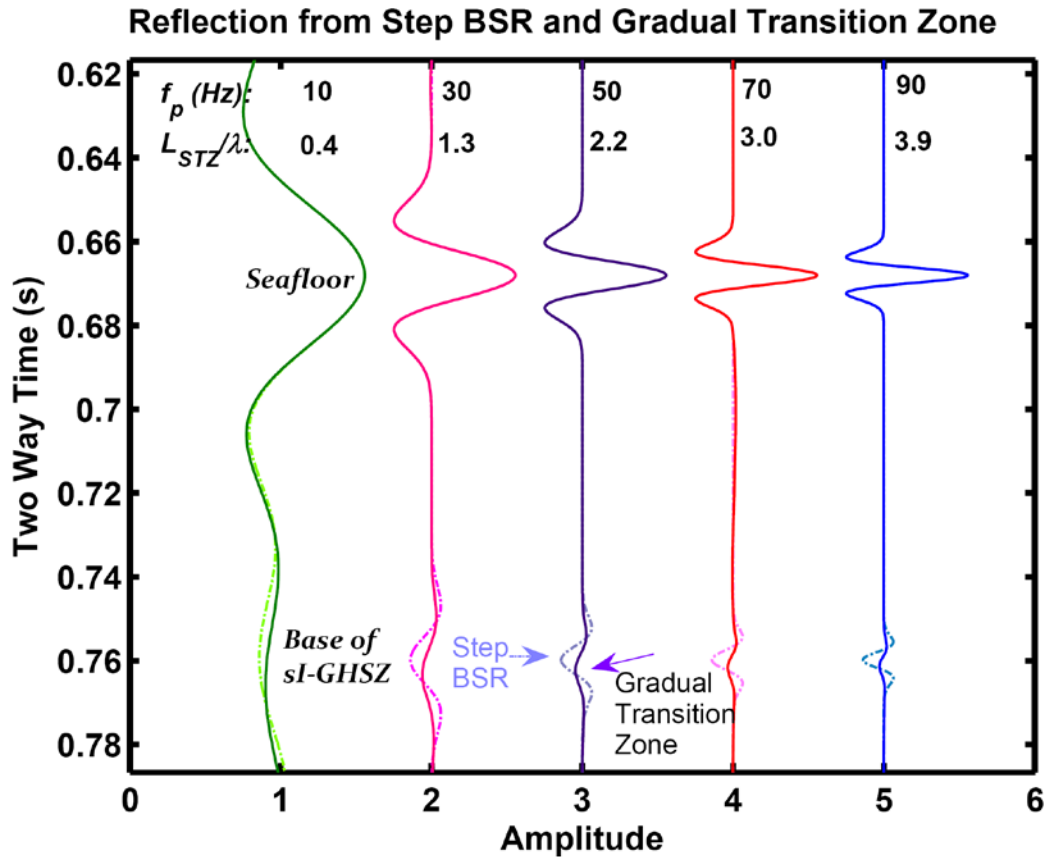


Figure 6. 8. Seismic Response from Step BSR and Gradual Transition Zone.

Dotted lines: for the response from a step change velocity system (i.e., step BSR in a pure methane hydrate system); solid lines: for those from a gradually changed velocity system (i.e., Gradual Transition Zone in a mixed hydrate system).

For peak frequencies at 30 Hz, a typical frequency in seismic survey, A_{tran}/A_{sf} is close to 0.1 (Figure 6.8). Therefore, in a mixed-hydrate system with gradual transition zones, when peak frequencies are equal to or higher than 30 Hz, it's possible to observe a weak BSR at some sites.

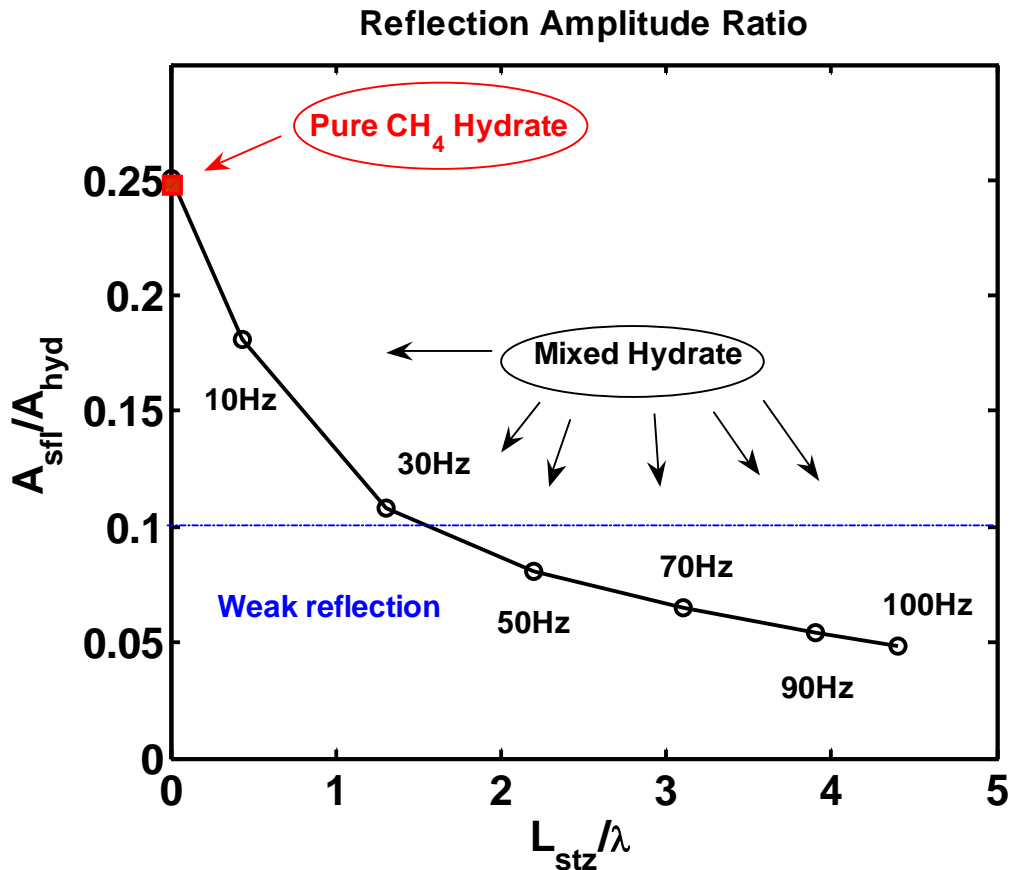


Figure 6. 9. Amplitude Ratio as a Function of L_{stz}/λ .

Amplitude ratio: the ratio of amplitude at Hydrate/Gas transition, to that at Seafloor, A_{tran}/A_{sf} . If $A_{tran}/A_{sf} \leq 0.1$, the reflection is called a “weak reflection”, as shown in the shadowed region. The peak frequency for each point is also labeled.

6.4. Discussion

Not only C_3H_8 , but also other gas hydrocarbons are also often present in hydrate system (Sloan & Koh, 2007; C. Hadley, 2008). Though several other multi-gas systems have not been detailed simulated in this work due to limitation of tools, however, their phase diagrams have indicated some major patterns similar with those in a $CH_4-C_3H_8-H_2O$ system: (1) the co-existence of Aq-H-V three phases and (2) presence of hydrate below sl hydrate depth, (3)

possibility of a weak seismic response. Though different from the example $\text{CH}_4\text{-C}_3\text{H}_8\text{-H}_2\text{O}$ system shown in this work, the phase diagrams of several types of multi-gas hydrate systems also show Aq-H-V co-existence regions, mainly due to the forming of sII-hydrate. For example, in the phase diagram of the $\text{CH}_4\text{-C}_2\text{H}_6\text{-H}_2\text{O}$ system, a Aq-H-V region appears in phase diagram with lower pressure required by the Aq-H hydrate region. These indicate that Aq-H-V can co-exist within a range of P, T zone in the sediment below the base of sI hydrate stability zone (sI -HSZ). As another example, in a $\text{CH}_4\text{-CO}_2\text{-H}_2\text{O}$ hydrate system (Bigalke & Enstad *et al.*, 2010), at some certain pressure conditions, CO_2 hydrate may dissociate while CH_4 hydrate is still stable, this may generate a zone with Aq – H (sI CH_4 hydrate) – V (CO_2) coexistence. Experimental and simulation works on mixed gas hydrate systems have been reported extensively recently (Ballard *et al.*, 2001, 2002, 2004; Sloan & Koh, 2007). Site data about mixed hydrate systems are also reported (C. Hadley, 2008; Sloan & Koh, 2007). In summary, quite different from pure methane hydrate system, in several types of mixed hydrate system, sII hydrate could be present below the equilibrium depth for sI -hydrate, which will be identified as the BHSZ in the pure methane hydrate systems. Though the effects on seismic responses haven't been well explored, this work suggests that the seismic response may be affected significantly by the mixed gas components. For example, in a vertical high permeability conduit, the mixed gas components from thermogenic source may have played an

important role on the hydrate/free gas distribution and seismic response, which may appear as discontinuous BSRs.

Table 6.1. Parameters for Acoustic Properties Estimation*

Component	V_p (m/s)	ρ (kg/m³)
Sea water (w)	1500	1030
Hydrate (H)	3300	900
Sediment	2000	2600
Mineral (m)		
Vapor (V, average)	~ 400	~ 50

Data from: Sloan and Koh (2007). Density of vapor estimated via CSMGem 1.0.

6.5. Conclusion

In a conventional pure methane system, hydrate cannot be present below the GHSZ, and a step transition of impedance often occur at the base of GHSZ due to the sharp transition from hydrate to gas phase, which results a strong BSR. However, in a mixed-gas system, such as shown in this work, hydrate can co-exist with gas phase (and aqueous phase) below the base of sl hydrate within a transition zone. For CH₄-C₃H₈-H₂O hydrate system with 5% C₃H₈, the transition zone could be as thick as 300m because sl hydrate can be stable in such a thick zone. A gradual change of hydrate and free-gas saturation within this zone results in gradual change of acoustic properties. 95% of the change in acoustic properties occurs in roughly the upper 80 m of

the transition zone, marked as the significant transition zone (STZ). A weak BSR may occur depending on thickness ratio of the significant transition zone and the dominant seismic wavelength.

Chapter 7. Future work

As the interest on gas hydrate systems keep growing, several important and interesting topics can be studies following this work.

Salinity effect

Since salinity change is very important in the gas hydrate system [Flemings, 2006], the simulation with consideration of salinity may be able to reveal the effect of salinity on hydrate phase boundary change, 3-phase co-existence, etc. Methane hydrate model with consideration of salinity should be included in the hydrate and free gas accumulation simulation. The simulation with salinity change may be able to explain the fluctuation of base of gas hydrate stability zone, and the possible gas invasion into gas hydrate stability zone.

The hydrate inventory in the past

The hydrate in the past is very important to demonstrate role of hydrate on earth, and also is an indicator of global hydrate amount. For example, in the PETM, the gas hydrate amount should be similar with that at present day even when the temperatures were much warmer than present day. Possible factors affecting gas hydrate inventory, may include sulfate, organic carbon change, etc.

The transient process in hydrate systems

The actual input of organic carbon, or temperature, or pressure was varying in the history and in the future, so it is very important to study the transient effects. It is possible to use numeric models such as Laplace function and transfer functions to explore the effect of varying inputs.

The environmental effect of gas hydrate dissociation

The environmental effect of gas hydrate dissociation is very important, so it'll be very valuable to study cases of gas hydrate response to climate change at present day and in the future.

Bibliography

- Archer, D., *et al.*, *The importance of ocean temperature to global biogeochemistry*. Earth and Planetary Science Letters, 2004. **222**(2): p. 333-348.
- Ballard, A. L., M. D. Jager, *et al.* (2001). "Pseudo-retrograde hydrate phenomena at low pressures." Fluid Phase Equilibria **185**(1-2): 77-87.
- Ballard, A.L., Sloan Jr, E.D., (2002). The next generation of hydrate prediction: I. Hydrate standard states and incorporation of spectroscopy, Fluid Phase Equilibria, 194–197, 371–383.
- Ballard, A.L., Sloan Jr, E.D., (2004). The next generation of hydrate prediction: Part III. Gibbs energy minimization formalism, Fluid Phase Equilibria, 218, 15-31.
- Ballard, L. and E.D. Sloan, *The next generation of hydrate prediction IV - A comparison of available hydrate prediction programs*. Fluid Phase Equilibria, 2004. **216**(2): p. 257-270.
- Barnard, L.A., K.A. Kvenvolden, and D.A. Wiesenburg, *Geochemistry of a Marine Gas Hydrate Associated with a Bottom Simulating Reflector*. Aapg Bulletin-American Association of Petroleum Geologists, 1981. **65**(5): p. 894-895.
- Buffett, B. A. (2000). "Clathrate hydrates." Annual Review of Earth and Planetary Sciences **28**: 477-507.
- Bhatnagar, G., W. G. Chapman, *et al.* (2007). "Generalization of gas hydrate distribution and saturation in marine sediments by scaling of thermodynamic and transport processes." American Journal of Science **307**(6): 861-900.
- Bhatnagar, G. , W. G. Chapman, G. R. Dickens, B. Dugan, G. J. Hirasaki, Sulfate-methane transition as a proxy for average methane hydrate saturation in marine sediments, Geophys. Resear. Lett., 35, L03611, doi:10.1029/2007GL032500, 2008.
- Bhatnagar, G., PhD Dissertation, *Accumulation of gas hydrates in marine sediments*, in *Dept. Chemical and Biomolecular Engineering*. 2008, Rice University: Houston.
- Bigalke N.K., Enstad L.I., Rehder G., Alendal G., Terminal velocities of pure and hydrate coated CO₂ droplets and CH₄ bubbles rising in a simulated oceanic environment. Deep-Sea Research I, 57 (2010) 1102–1110.
- Boswell, R. and T. S. Collett (2011). "Current perspectives on gas hydrate resources." Energy & Environmental Science **4**(4): 1206-1215.
- Boswell, R., M. Frye, *et al.* (2012). "Architecture of gas-hydrate-bearing sands from Walker Ridge 313, Green Canyon 955, and Alaminos Canyon 21: Northern deepwater Gulf of Mexico." Marine and Petroleum Geology **34**(1): 134-149.

- Brooks, J. M., A. W. A. Jeffrey, et al. (1985). "Geochemistry of Hydrate Gas and Water from Site-570, Deep-Sea Drilling Project Leg-84." Initial Reports of the Deep Sea Drilling Project **84**(May): 699-703.
- Brooks, J. M., H. B. Cox, et al. (1986). "Association of Gas Hydrates and Oil Seepage in the Gulf-of-Mexico." Organic Geochemistry **10**(1-3): 221-234.
- Brown, T. S., A. J. Kidnay, et al. (1988). "Vapor Liquid Equilibria in the Carbon Dioxide-Ethane System." Fluid Phase Equilibria **40**(1-2): 169-184.
- Brown, T. S., E. D. Sloan, et al. (1989). "Vapor-Liquid-Equilibria in the Nitrogen + Carbon-Dioxide + Ethane System." Fluid Phase Equilibria **51**: 299-313.
- Chapman, N. R., J. F. Gettrust, et al. (2002). "High-resolution, deep-towed, multichannel seismic survey of deep-sea gas hydrates off western Canada." Geophysics **67**(4): 1038-1047.
- Chatterjee, S., G. R. Dickens, G Bhatnagar, W. G. Chapman, Brandon Dugan, G. T. Snyder, G. J. Hirasaki, Pore water sulfate, alkalinity, and carbon isotope profiles in shallow sediment above marine gas hydrate systems: A numerical modeling perspective, Journal of Geophysical Research, 116, B09103, doi: 10.1029/2011JB008290, 2011.
- Chatterjee, Sayantan, PhD Dissertation, 2012, Rice University, Houston, TX.
- Collett, T.S., K.A. Kvenvolden, and L.B. Magoon, *Characterization of Hydrocarbon-Gas within the Stratigraphic Interval of Gas-Hydrate Stability on the North Slope of Alaska, USA*. Applied Geochemistry, 1990. **5**(3): p. 279-287.
- Dameron, D.H., *Determination of the Acoustic Velocity in Tissues Using an Inhomogeneous-Media Model*. Ieee Transactions on Sonics and Ultrasonics, 1979. **26**(2): p. 69-74.
- Dameron, D.H., *An Inhomogeneous-Media Model for the Determination of Acoustic Parameters in Tissues*. Ieee Transactions on Sonics and Ultrasonics, 1980. **27**(5): p. 244-248.
- D'Hondt, S., et al., *Distributions of Microbial Activities in Deep Subseafloor Sediments*. Science (Washington, DC, United States), 2004. **306**(5705): p. 2216-2221.
- Dickens, G.R. and M.S. Quinbyhunt, *Methane Hydrate Stability in Seawater*. Geophysical Research Letters, 1994. **21**(19): p. 2115-2118.
- Dickens, G.R., et al., *Dissociation of Oceanic Methane Hydrate as a Cause of the Carbon-Isotope Excursion at the End of the Paleocene*. Paleoceanography, 1995. **10**(6): p. 965-971.
- Dickens, G.R., *Geochemical links between paleoceanography and marine sediment-hosted ore deposits (marine sediments, sediments)*. 1996, Univ. of Michigan: Ann Arbor, MI.
- Dickens, G.R., M.M. Castillo, and J.C.G. Walker, *A blast of gas in the latest Paleocene: Simulating first-order effects of massive dissociation of oceanic methane hydrate*. Geology, 1997. **25**(3): p. 259-262.

- Dickens, G. R. and M. S. QuinbyHunt (1997). "Methane hydrate stability in pore water: A simple theoretical approach for geophysical applications." *Journal of Geophysical Research-Solid Earth* **102**(B1): 773-783.
- Dickens, G. R. (1999). "Carbon cycle: The blast in the past." *Nature (London)* **401**(6755): 752-753, 755.
- Dickens, G., *On the fate of past gas: What happens to methane released from a bacterially mediated gas hydrate capacitor?* *Geochemistry Geophysics Geosystems*, 2001. **2**: p. -.
- Dickens, G.R., *Climate: A methane trigger for rapid warming? Methane Hydrates in Quaternary Climate change. The Clathrate Gun Hypothesis*, by James P. Kennett, Kevin G. Cannariato, Ingrid L. Hendy, and Richard J. Behl. *Science (Washington, DC, United States)*, 2003. **299**(5609): p. 1017.
- Dickens, G.R., *Rethinking the global carbon cycle with a large, dynamic and microbially mediated gas hydrate capacitor.* *Earth and Planetary Science Letters*, 2003. **213**(3-4): p. 169-183.
- Dickens, G.R., *Global change - Hydrocarbon-driven warming.* *Nature*, 2004. **429**(6991): p. 513-515.
- Dickens, G.R., *Methane hydrate and Abru.* *Geotimes*, 2004. **49**(11): p. 18-22.
- Dickens, G. (2008). Methane Release from Gas Hydrates during the Paleocene-Eocene Thermal Maximum: Current Perspective on the Issue. *Fire in the Ice*: 9.
- Dillon, W.P., M.W. Lee, and D.F. Coleman, *Identification of Marine Hydrates in-Situ and Their Distribution Off the Atlantic Coast of the United-States.* *International Conference on Natural Gas Hydrates*, 1994. **715**: p. 364-380.
- Egeberg, P. K. and G. R. Dickens (1999). "Thermodynamic and pore water halogen constraints on gas hydrate distribution at ODP Site 997 (Blake Ridge)." *Chemical Geology* **153**(1-4): 53-79.
- Fehn, U., G. T. Snyder, et al. (2007). "Iodine as a tracer of organic material: I-129 results from gas hydrate systems and fore arc fluids." *Journal of Geochemical Exploration* **95**(1-3): 66-80.
- Finley, P. and J. Krason (1986). Geological evolution and analysis of confirmed or suspected gas hydrate localities: Volume 9, Formation and stability of gas hydrates of the Middle America Trench, p. 261.
- Fischer, A.D., et al., *Dynamic triggering by strong-motion P and S waves: Evidence from the 1999 Chi-Chi, Taiwan, earthquake.* *Bulletin of the Seismological Society of America*, 2008. **98**(2): p. 580-592.
- Flemings, P.B., X.L. Liu, and W.J. Winters, *Critical pressure and multiphase flow in Blake Ridge gas hydrates.* *Geology*, 2003. **31**(12): p. 1057-1060.
- Freer, E.M., M.S. Selim, and E.D. Sloan, *Methane hydrate film growth kinetics.* *Fluid Phase Equilibria*, 2001. **185**(1-2): p. 65-75.
- Gu, G., G. R. Dickens, et al. (2011). "Abundant Early Palaeogene marine gas hydrates despite warm deep-ocean temperatures." *Nature Geoscience*

- 4(12): 848-851.
- Hadley, C., D. Peters, A. Vaughan, D. Bean, et al. Internl. Petroleum Techn. Conf., 12554. Gumusut - Kakap Project: Geohazard Characterisation and Impact on Field Development Plans, Kuala Lumpur, Malaysia, Dec. 2008.
- Hester, K.C., *et al.*, *Direct measurements of multi-component hydrates on the seafloor: Pathways to growth*. Fluid Phase Equilibria, 2007. **261**(1-2): p. 396-406.
- Hyndman, R. D., G. D. Spence, A Seismic Study of Methane Hydrate Marine Bottom Simulating Reflectors, J. GEOPHYS. RESEAR., VOL. 97, NO. B5, PP. 6683-6698, 1992, doi:10.1029/92JB00234.
- Jager, M.D., A.L. Ballard, and E.D. Sloan, *Comparison between experimental data and aqueous-phase fugacity model for hydrate prediction*. Fluid Phase Equilibria, 2005. **232**(1-2): p. 25-36.
- Jager, M.D., A.L. Ballard, and E.D. Sloan, *The next generation of hydrate prediction - II. Dedicated aqueous phase fugacity model for hydrate prediction*. Fluid Phase Equilibria, 2003. **211**(1): p. 85-107.
- Katz, M.E., *et al.*, *The source and fate of massive carbon input during the latest Paleocene thermal maximum*. Science (Washington, D. C.), 1999. **286**(5444): p. 1531-1533.
- Kvenvolden, K. A. (1988). "Methane Hydrate - a Major Reservoir of Carbon in the Shallow Geosphere." Chemical Geology **71**(1-3): 41-51.
- Kvenvolden, K. A. (1993). "Gas Hydrates - Geological Perspective and Global Change." Reviews of Geophysics **31**(2): 173-187.
- Kvenvolden, K.A., *Natural-Gas Hydrate Occurrence and Issues*. International Conference on Natural Gas Hydrates, 1994. **715**: p. 232-246.
- Kvenvolden, K., *Natural-Gas Hydrate Occurrence and Issues*. Sea Technology, 1995. **36**(9): p. 69-74.
- Kvenvolden, K.A., *A review of the geochemistry of methane in natural gas hydrate*. Organic Geochemistry, 1995. **23**(11-12): p. 997-1008.
- Kvenvolden, K.A., *Methane hydrate in the global organic carbon cycle*. Terra Nova, 2002. **14**(5): p. 302-306.
- Lake, L.W., *Enhanced Oil Recovery*. 1989, Austin: Prentice-Hall, Inc. 224.
- Lee, M. W., T. S. Collett, et al. (2012). "Anisotropic models to account for large borehole washouts to estimate gas hydrate saturations in the Gulf of Mexico Gas Hydrate Joint Industry Project Leg II Alaminos Canyon 21 B well." Marine and Petroleum Geology **34**(1): 85-95.
- Lee, M.W. and W.P. Dillon, *Amplitude blanking related to the pore-filling of gas hydrate in sediments*. Marine Geophysical Researches, 2001. **22**(2): p. 101-109.
- Lee, M.W., *et al.*, *Seismic Character of Gas Hydrates on the Southeastern United-States Continental-Margin*. Marine Geophysical Researches, 1994. **16**(3): p. 163-184.
- Lee, M.W., *et al.*, *Seismic velocities for hydrate-bearing sediments using*

- weighted equation*. Journal of Geophysical Research-Solid Earth, 1996. **101**(B9): p. 20347-20358.
- Lee, M.W., et al., *Method of Estimating the Amount of in-Situ Gas Hydrates in Deep Marine-Sediments*. Marine and Petroleum Geology, 1993. **10**(5): p. 493-506.
- Liu, X.L. and P.B. Flemings, *Passing gas through the hydrate stability zone at southern Hydrate Ridge, offshore Oregon*. Earth and Planetary Science Letters, 2006. **241**(1-2): p. 211-226.
- Liu, X.L. and P.B. Flemings, *Dynamic multiphase flow model of hydrate formation in marine sediments*. Journal of Geophysical Research-Solid Earth, 2007. **112**(B3): p. -.
- McConnell, D. R., Z. J. Zhang, et al. (2012). "Review of progress in evaluating gas hydrate drilling hazards." Marine and Petroleum Geology **34**(1): 209-223.
- Macdonald, I. R., N. L. Guinasso, et al. (1994). "Gas Hydrate That Breaches the Sea-Floor on the Continental-Slope of the Gulf-of-Mexico." Geology **22**(8): 699-702.
- Pagani, M., et al., *Arctic hydrology during global warming at the Palaeocene/Eocene thermal maximum*. Nature (London, United Kingdom), 2006. **442**(7103): p. 671-675.
- Paull, C. K., R. Matsumoto, et al. (2000). Proc. of ODP, v. 164, Sci. Res., doi: 10.2973/odp.proc.sr.164.2000.
- Reagan, M. T., G. J. Moridis, et al. (2011). "Contribution of oceanic gas hydrate dissociation to the formation of Arctic Ocean methane plumes." Journal of Geophysical Research-Oceans **116**.
- Riedel, M., G. D. Spence, et al. (2002). "Seismic investigations of a vent field associated with gas hydrates, offshore Vancouver Island." Journal of Geophysical Research-Solid Earth **107**(B9): 2200.
- Riedel, M. and U. Shankar (2012). "Combining impedance inversion and seismic similarity for robust gas hydrate concentration assessments - A case study from the Krishna-Godavari basin, East Coast of India." Marine and Petroleum Geology **36**(1): 35-49.
- Shelander, D., J. C. Dai, et al. (2012). "Estimating saturation of gas hydrates using conventional 3D seismic data, Gulf of Mexico Joint Industry Project Leg II." Marine and Petroleum Geology **34**(1): 96-110.
- Shipley, T.H., et al., *Seismic Evidence for Widespread Possible Gas Hydrate Horizons on Continental Slopes and Rises*. Aapg Bulletin-American Association of Petroleum Geologists, 1979. **63**(12): p. 2204-2213.
- Sloan, E.D., et al., *A Experimental-Method for the Measurement of 2 Phase Liquid Hydrocarbon-Hydrate Equilibrium*. Fluid Phase Equilibria, 1986. **29**: p. 233-240.
- Sloan, E.D. and P. Nasir, *Experimental Thermodynamics, Chromatography, and Transport Phenomena - a Collection of Papers in Honor of Kobayashi, Riki - Spring National Meeting of the*

- American-Institute-of-Chemical-Engineers - Houston, 29 March 1987 - Preface. Fluid Phase Equilibria, 1987. 36: p. U1-U1.*
- Sloan, E.D. and P. Nasir, *A Technical Biography of Professor Kobayashi Work. Fluid Phase Equilibria, 1987. 36: p. 1-31.*
- Sloan, E.D. and F. Fleyfel, *Hydrate Dissociation Enthalpy and Guest Size. Fluid Phase Equilibria, 1992. 76: p. 123-140.*
- Sloan, E.D. and F. Fleyfel, *Comments on - Hydrate Dissociation Enthalpy and Guest Size - Reply. Fluid Phase Equilibria, 1994. 96: p. 233-235.*
- Sloan, E.D., *Proceedings of the Seventh International Conference on Fluid Properties and Phase Equilibria for Chemical Process Design, Snowmass Village, Co, USA, June 18-23, 1995. Fluid Phase Equilibria, 1996. 116(1-2): p. R7-R7.*
- Sloan, E.D., *Proceedings of the Seventh International Conference on Fluid Properties and Phase Equilibria for Chemical Process Design, Snowmass Village, CO, USA, June 18-23, 1995 .2. Preface. Fluid Phase Equilibria, 1996. 117(1-2): p. R7-R7.*
- Sloan, E.D., *A changing hydrate paradigm - from apprehension to avoidance to risk management. Fluid Phase Equilibria, 2005. 228: p. 67-74.*
- Sloan, E.D., *A changing hydrate paradigm - from apprehension to avoidance to risk management. Fluid Phase Equilibria, 2005. 228: p. 67-74.*
- Sloan, E. D. and Koh, C. A. (2007). *Clathrate Hydrates of Natural Gases*, CRC Press.
- Sloan, D., *et al.*, *Four Critical Needs to Change the Hydrate Energy Paradigm from Assessment to Production: The 2007 Report to Congress by The U.S. Federal Methane Hydrate Advisory Committee. Proceedings of Offshore Technology Conference (OTC) 2008, 2008: p. 19519.*
- Sluijs, A., *et al.*, *Environmental environmental precursors to rapid light carbon injection at the Palaeocene/Eocene boundary. Nature (London, United Kingdom), 2007. 450(7173): p. 1218-1221.*
- Sluijs, A., *et al.*, *Subtropical Arctic Ocean temperatures during the Palaeocene/Eocene thermal maximum. Nature (London, United Kingdom), 2006. 441(7093): p. 610-613.*
- Torres, M. E., A. M. Trehu, *et al.* (2008). "Methane hydrate formation in turbidite sediments of northern Cascadia, IODP Expedition 311." *Earth and Planetary Science Letters* **271**(1-4): 170-180.
- Trehu, A. M., M. E. Torres, *et al.* (2004). "Three-dimensional distribution of gas hydrate beneath southern Hydrate Ridge: constraints from ODP Leg 204 (vol 222, pg 845, 2004)." *Earth and Planetary Science Letters* **227**(3-4): 557-558.
- Trehu, A.M., *et al.*, *Feeding methane vents and gas hydrate deposits at south*

- Hydrate Ridge*. Geophysical Research Letters, 2004. **31**(23): p. -.
- Turner, D.J., R.S. Cherry, and E.D. Sloan, *Sensitivity of methane hydrate phase equilibria to sediment pore size*. Fluid Phase Equilibria, 2005. **228**: p. 505-510.
- Uchida, T., et al., *Two-step formation of methane-propane mixed gas hydrates in a batch-type reactor*. Aiche Journal, 2004. **50**(2): p. 518-523.
- Walsh, M. R., S. H. Hancock, et al. (2009). "Preliminary report on the commercial viability of gas production from natural gas hydrates." Energy Economics **31**(5): 815-823.
- Winfrey, M. R. and J. G. Zeikus (1977). "Effect of Sulfate on Carbon and Electron Flow during Microbial Methanogenesis in Freshwater Sediments." Applied and Environmental Microbiology **33**(2): 275-281.
- Winters, W.J., et al., *Relation between gas hydrate and physical properties at the Mallik 2L-38 research well in the Mackenzie Delta*. Gas Hydrates: Challenges for the Future, 2000. **912**: p. 94-100.
- Winters, W.J., et al., *Physical properties and rock physics models of sediment containing natural and laboratory-formed methane gas hydrate*. American Mineralogist, 2004. **89**(8-9): p. 1221-1227.
- Winters, W.J., et al., *Physical properties of sediment containing methane gas hydrate*. Abstracts of Papers of the American Chemical Society, 2005. **229**: p. U593-U593.
- Winters, W.J., et al., *Methane gas hydrate effect on sediment acoustic and strength properties*. Journal of Petroleum Science and Engineering, 2007. **56**(1-3): p. 127-135.
- Wood, W.T., P.L. Stoffa, and T.H. Shipley, *Quantitative Detection of Methane Hydrate through High-Resolution Seismic Velocity Analysis*. Journal of Geophysical Research-Solid Earth, 1994. **99**(B5): p. 9681-9695.
- Xu, W. Y. and C. Ruppel (1999). "Predicting the occurrence, distribution, and evolution of methane gas hydrate in porous marine sediments." Journal of Geophysical Research-Solid Earth **104**(B3): 5081-5095.
- Yilmaz, O., S.M. Doherty (Seismic Data Processing), Society of Exploration, 1987.
- Yuan, J., Edwards, R.N., 2000. The assessment of marine gas hydrate through electrical remote sounding: hydrate without a BSR? Geophys. Res. Lett. **27**, 2397–2400.
- Zachos, J.C., G.R. Dickens, and R.E. Zeebe, *An early Cenozoic perspective on greenhouse warming and carbon-cycle dynamics*. Nature (London, United Kingdom), 2008. **451**(7176): p. 279-283.
- <http://www.naturalgas.org/overview/background.asp>
<http://www.ualberta.ca/~tayfun/eogrrc/Tarek-research.html>

List of Symbols

c_m^i ---- methane mass fraction in i -phase, $i=l, h, g$

$c_{m,eqb}^l$ ---- methane solubility at Base of GHSZ in *liquid*-phase

D_{sf}, T_{sf}, P_{sf} --- seafloor depth, temperature, and pressure, respectively

D_m --- diffusion coefficient (of methane) in pore water

$Da(z)$ --- In-situ Damkohler number at position z

$(\overline{Da})_0$ ---- In-situ Da number at mid point ($z=Lt_0/2$) when $T_{sf}=3C$

E --- Activation energy

L_t ---- thickness of Gas Hydrate Stability Zone (GHSZ)

L_ϕ ---- a characteristic length indicating the effect of compression

$K_{i,\phi_j/\phi_1}$ --- distribution coefficient, for i th-component in phase ϕ_j with respect to its concentration in phase ϕ_1

n_i the amount of species i in the system (unit: mol)

$N_{i\phi}$ --- dimensionless number, = L_t / L_ϕ

N_{ϕ_j} --- total amount of moles of all components in the j th-phase ϕ_j

p --- hydrostatic pressure

Pe_1 --- Peclet Number 1, $Pe_1 = U_{f, sed} L_t / D_m$

Pe_2 ---- Peclet number 2, $Pe_2 = U_{ext} L_t / D_m$

R --- universal gas constant, = 9.314 J/K/mol

S_h --- hydrate saturation

S_v --- vapor saturation

U_f, U_s --- net fluid flux and sediment flux, respectively

\tilde{U}_f, \tilde{U}_s --- net fluid flux and sediment flux, respectively

$U_{f, sed}, U_{ext}$ --- fluid flux due to sedimentation and upward external flow, respectively

V_h --- Total Hydrate Amount (per unit seafloor area)

V_{φ_j} --- volume of phase φ_j

x_{i, φ_j} --- molar fraction of species i in phase j

x_i^{wf} water-free molar fraction of species i

z, \tilde{z} --- vertical depth and normalized vertical depth, respectively

Greek Symbols

$\alpha, \tilde{\alpha}$ --- organic material concentration in sediment, and normalized value, respectively

α_0, β --- organic concentration at seafloor, and its normalized value, $\beta = \alpha_0 / c_{m, eqb}^l$

$\delta^{13}\text{C}$ --- isotope ratio of ^{13}C , normally relative to PDB

ϕ_0 --- porosity of sediments at seafloor

ϕ_∞ --- minimum porosity which can be achieved

$\tilde{\phi}$ --- normalized porosity

γ, η --- reduced porosity parameters, (in this work, we take $\gamma=9, \eta=6/9$)

λ --- methanogenesis rate constant

σ_e --- effective stress, $= \sigma_v - p$

σ_v --- overburden, caused by pressure difference between mineral and fluid densities

σ_ϕ --- characteristic constant for compaction, with the same unit as stress

ρ_f --- density of fluid

$\tilde{\rho}_h = \rho_h / \rho_f, \tilde{\rho}_g = \rho_g / \rho_f$ --- normalized densities of hydrate and gas, respectively

ω_i --- Volume Fraction of phase $i, \omega_i = S_i \phi$